MICROSOLVATION OF CHARGED AND NEUTRAL SPECIES: A THEORETICAL STUDY

By

ARUP KUMAR PATHAK

BHABHA ATOMIC REASERCH CENTRE

A thesis submitted to the
Board of Studies in Chemical Science Discipline

In partial fulfillment of requirements

For the Degree of

DOCTOR OF PHILOSOPHY

of

HOMI BHABHA NATIONAL INSTITUTE

September, 2009

Homi Bhabha National Institute

Recommendations of the Viva Voce Board

As members of the Viva Voce Board, we certify that we have read the dissertation prepared by **Arup Kumar Pathak** entitled **Microsolvation of Charged and Neutral Species: A Theoretical Study** and recommend that it may be accepted as fulfilling the dissertation requirement for the Degree of Doctor of Philosophy.

Chairman- Prof. S. K. Ghosh Date:

Convener- Prof. T. Mukherjee Date:

External Examiner- Prof. P. K. Chattaraj Date:

Member 1- Dr. D. K. Maity Date:

Member 2- Prof. P. D. Naik Date:

Member 3- Dr. T. K. Ghanty Date:

Member 4- Dr. C. Majumder Date:

Final approval and acceptance of this dissertation is contingent upon the candidate's submission of the final copies of the dissertation to HBNI.

We hereby certify that we have read this dissertation prepared under our direction and recommend that it may be accepted as fulfilling the dissertation requirement.

Guide – Prof. T. Mukherjee Date:

Co-guide – Dr. D. K. Maity Date:

STATEMENT BY AUTHOR

This dissertation has been submitted in partial fulfillment of requirements for an advanced degree at Homi Bhabha National Institute (HBNI) and is deposited in the Library to be made available to borrowers under rules of the HBNI.

Brief quotations from this dissertation are allowable without special permission, provided that accurate acknowledgement of source is made. Requests for permission for extended quotation from or reproduction of this manuscript in whole or in part may be granted by the Competent Authority of HBNI when in his or her judgment the proposed use of the material is in the interests of scholarship. In all other instances, however, permission must be obtained from the author.

Arup Kumar Pathak

DECLARATION

I, hereby declare that the investigation presented in the thesis has been carried out by me. The work is original and has not been submitted earlier as a whole or in part for a degree / diploma at this or any other Institution / University.

Arup Kumar Pathak

Dedicated to my Daughter, Wife and Grandparents

ACKNOWLEDGEMENTS

I wish to record my deep sense of gratitude and sincere thanks to my guide Prof. T. Mukherjee, and co-guide Prof. D. K. Maity of Bhabha Atomic Research Centre (BARC), for their unstinted inspiration, invaluable guidance, encouragement, keen interest, good wishes and valuable suggestions throughout my entire research tenure. I am grateful to them for critically reviewing this thesis.

It is my great privilege to acknowledge Prof. S. K. Ghosh and Prof. A. K. Samanta of Theoretical Chemistry Section, BARC for their valuable scientific suggestions during the course of this research work.

It is my great pleasure to thank Prof. S. K. Sarkar, Prof. P. N. Bajaj, Prof. D. K. Palit and Prof. H. Pal of Radiation & Photochemistry Division, BARC for their help and encouragement.

Members of Computer Centre, BARC is highly acknowledged for providing ANUPAM parallel computing facility and ready help over the years.

Chairman (Prof. S. K. Ghosh) and members (Prof. P. D. Naik, Prof. T. K. Ghanty, Dr. C. Majumder) of the doctorial committee are gratefully acknowledged for their critical review and suggestions during progress review and pre-synopsis viva-voce.

It is my pleasure to acknowledge the help rendered by all members of the RPCD and TCS, BARC at different times. I wish to thank my colleagues Dr. M. Kumbhakar, Dr. S. Nath, and Mr. P. K. Singh for their moral support, diversified help and several funs, which will always be remembered.

I wish to express my sincere gratitude and indebtedness to my grandparents, parents, parents-in-law, sister-in-law and other family members and all well wishers for their love and blessings on me.

Finally I would like to give credit and love to my wife Manika and daughter Anusha, for support and for bearing long separation from me while the progress of this work.

September, 2009

Arup Kumar Pathak

RPCD, BARC

CONTENTS

CHAPTER 2

Structure and Energetics of Water Embedded Anionic Clusters

CHAPTER 3

IR Spectra of Water Embedded Anionic Clusters

CHAPTER 4

Solubility of Halogen Gases in Water

CHAPTER 5

UV-Vis Spectra of Anionic Hydrated Clusters: Extrapolation to Bulk

CHAPTER 6

Structure, Energetics and Spectra of Ammonia Embedded Neutral Clusters

CHAPTER 7

Structure, Energetics and Spectra of CO_2 Embedded Anionic Clusters

SYNOPSIS

The process of solvation is an interaction of a solute with the solvent, which leads to stabilization of the solute species in the solution. Studies on solvation of charged and neutral chemical species (solutes) is one of the most important and attractive area of research. If a chemical species (solute) is immersed into a solvent medium (bulk), the network of solvent in the close vicinity of the solute gets rearranged to allow the solute going through the process of solvation. In the process of solvation, a few solvent molecules in the close vicinity of solute will interact instantaneously. Afterwards more and more solvent molecules from nearby surroundings will approach the solute and encapsulate the solute to solvate it. The process of solvation involves different types of intermolecular interactions namely ion-ion, hydrogen bonding, ion-dipole, and dipole-dipole attractions or van der Waals interactions. The nature of interactions depends on the nature of both solute (neutral or ionic) and solvent (ionic, polar or nonpolar). Studying the process of solvation of solutes in presence of a large number of solvent molecules (bulk) is termed as macroscopic solvation (see Fig. 1). On the other hand studying the solvation process at molecular level with only a few solvent molecules is known as microsolvation (see Fig. 1). The process of macro, micro and dual level solvation process is shown by a graphical model displayed in Fig.1.

Though solvation process at the macroscopic level is well studied but till today a little effort is given to understand the solvation process at molecular level. Average information about various interactions is obtained from macroscopic solvation study.

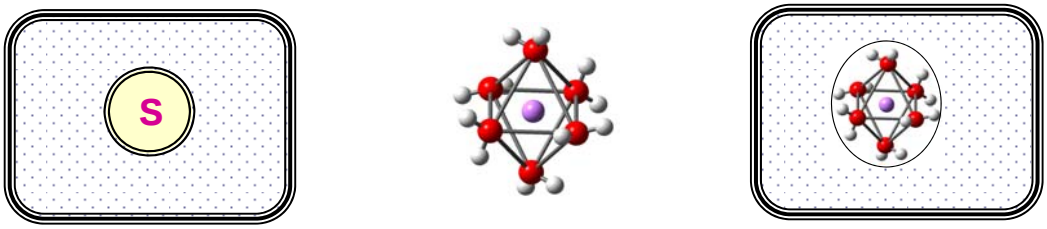

Fig. 1. Different models of solvations are displayed pictorially. In case of macroscopic solvation the solute 'S' is kept in solvent continuum. In microsolvation, the solute is encapsulated by a finite number of solvent molecules. In dual level solvation the microsolvated species is kept in the solvent continuum. In case of microscopic and dual level solvation, the central indigo colour ball refers to the solute and remaining balls refers to the solvent network (here water is considered as solvent).

Information about coordination number, thermodynamic parameters (e.g. free energy, enthalpy of solvation etc), bulk detachment energy of excess electron from a solute, UV-Vis spectra etc are obtained based on experiment carried out in bulk solution.[1-3] Many theoretical models are available to study macroscopic solvation of chemical species. Reaction field (SCRF) model due to Onsager –Krikwood is one of the simple and popular models to study macroscopic solvation.[4] In this model a spherical solute cavity is considered. Molecular shape cavity models like polarizable continuum model (PCM), conductor like screening model (COSMO) is also available to study the solvent effect at the macroscopic level.[4] There are two major advantages of continuum (implicit solvation) models. The first is a reduction in the system's number of degrees of freedom. The second advantage is that the continuum models provide a very accurate way to treat the strong, long-range electrostatic forces that dominate many solvation phenomena. The major drawback of these implicit solvation models is that explicit solvent effect is not taken into account. As a result, molecular level information cannot be extracted based on

studies carried out in bulk solution (macroscopic solvation) during the process of solvation. To understand different molecular level interactions responsible for solvation, one has to apply microsolvation model by adding solvent molecules one by one. The study on microsolvation of neutral and charged chemical species has been a subject of intense research both from experimental and theoretical points of view. This is not only because of the strong dependency of the properties on size and geometry of the solvated clusters of these species but also due to development of sophisticated experimental and theoretical techniques. These experiments are based on supersonic expansion and nozzle beam technique to produce finite size hetero clusters consisting of both solute and finite number solvent molecules. A number of solvent molecules is added to encapsulate the solute by bottom up approach. The hetero clusters are then monitored by various spectroscopic techniques (infrared, photoelectron etc). Molecular dynamics simulation based on model potential studies are also applied to understand microsolvation. But lack of accurate description on solute-solvent and solvent-solvent interaction, model Hamiltonian based studies are rarely used to study microsolvation. *First principles* based quantum chemical investigation is thus applied as major theoretical technique to study microsolvation. Experimental and theoretical investigations are carried out to study microsolvation both in hydrogen bonding solvent (water, ammonia etc)[5-13] and in non-hydrogen bonding solvent (carbon dioxide, argon etc).[14-15]

Positively charged ions have simple solvated structures compared to a negatively charged system as cation binds strongly with solvent molecules.[1] As anions are mass selectable, size selected gas-phase infrared (IR) cluster spectroscopy combined with first principle based theoretical studies have been successfully applied to explore the

molecular level interaction during the process of microhydration.[16-18] Indirect assignment on structure and growth motif is done based on IR spectra analysis of finite size clusters. Molecular cluster acts as an intermediate state between isolated gaseous molecule and condensed phase bulk system. Several efforts are being made to connect molecular cluster properties of a chemical species to its bulk properties. Size selected cluster study has been used to extract the bulk properties like detachment energies of an excess electron using simple extrapolation model based on the continuum model. [6,19] But this model fails to reproduce the bulk detachment energy in most of the cases.[6,20]

To understand the process of microsolvation, a detail study on structure and energetics of finite size cluster of various species in water, ammonia and carbon di oxide have been carried out. Solubility, IR, Photoelctron and UV-Vis spectral properties have also been predicted and compared with experimental findings whenever available. When only one solvent molecule is added to solvent, a few minimum energy structures are expected. With the increase in number of solvent molecules in solvated clusters, the number of minimum energy configurations with close in energy for each size solvated clusters are expected to increase. Thus weighted average properties are calculated for better predictability. It is well known that bromine gas is more soluble than chlorine gas in water but no theoretical understanding is available in literature. UV-Vis spectra of various species in aqueous solution are measured by experimental technique but no theoretical study is available. Bulk properties like solubility, bulk detachment energy of excess electron and aqueous UV-Vis spectra are also measured and compared with reported experimental values. Theoretical results on structures, energetics, spectral properties (vibrational, photoelectron) of clusters consisting of various solutes (both

neutral and anionic) and solvent molecules (water, ammonia and carbon dioxide) with different size have been presented and discussed in a systematic manner to understand the process of microsolvation. A general extrapolation model based on microscopic theory has also been developed for prediction of bulk detachment energy of excess electron from the finite size cluster data. The proposed thesis is to be submitted to the Homi Bhabha National Institute for the Doctor of Philosophy (PhD) degree. For convenience of presentation, different aspects of the present work have been discussed in eight different chapters of the thesis. Brief descriptions of the arrangements of different chapters in the thesis are given below.

Chapter 1: This is the introductory chapter of the proposed thesis and describes in brief the microsolvation and motivation of this work. A brief overview about the minimum energy search procedure, electron correlation, basis set, *ab initio* and DFT methods are discussed. A method based on Monte Carlo and simulated annealing for finding global optimized structures is also discussed.

Chapter 2: This chapter is dedicated to minimum energy structures and energy of hydrated clusters of various anionic and neutral chemical species in order to understand the process of microhydration. At present halogen dimer radical anions ($Cl_2^{\bullet-}$, $Br_2^{\bullet-}$ & $I_2^{\bullet-}$), carbonate radical anion ($CO_3^{\bullet-}$), carbonate anion (CO_3^{2-}), nitrate anion (NO_3^-) and halogen dimer (Cl_2, Br_2 & I_2) are taken to study microhydration. The growth motif of all the hydrated clusters is also followed.

Chapter 3: This chapter describes IR spectra of hydrated cluster of anionic solutes whose structures are discussed in chapter 1. Out of these systems, experimentally measured IR spectra are available for $Cl_2^{\bullet-}.nH_2O$ cluster. The IR spectra of $Cl_2^{\bullet-}.nH_2O$ cluster is presented in detail and compared with the reported experimental spectra. With the increase in number of solvent water molecules in hydrated clusters, the number of minimum energy configurations with close in energy for each size of hydrated clusters is expected to increase. Thus weighted average properties of clusters become more meaningful. Structures of hydrated clusters where solvent molecules are in the second shell i.e. not connected directly to the solute $Cl_2^{\bullet-}$, are also considered. Weighted average molecular properties are calculated based on the statistical population of different minimum energy configurations of a particular size of hydrated cluster at 100 K. Fourier transform to the dipole and velocity auto-correlation function is done to include dynamical contribution to the calculated IR spectra.

Chapter 4: This chapter is dedicated to discuss on bulk property, e.g. the solubility of halogen gas in water. It is well known that bromine gas is more soluble in water, than chlorine gas but no theoretical understanding is available in literature. Structures and properties of halogen gas (Cl_2, Br_2 & I_2) - water clusters are studied to understand the solubility order of halogen gases in water medium. It is observed that the halogen molecules remain as charge separated ion-pair in presence of solvent molecules. The extent of charge separation indeed explains the solubility order of the halogen gases in water.

Chapter 5: This chapter predicts the UV-Vis spectra of various radical anion systems ($Cl_2^{\bullet-}$, $Br_2^{\bullet-}$, $I_2^{\bullet-}$ & $CO_3^{\bullet-}$) in water and compare with the reported experimental UV-Vis spectra. It is also discussed that treating the solvent molecule explicitly is important (microhydration) to describe measured absorption profile as macrosolvation fails to describe reported absorption profile for such systems. Based on a few calculated low lying excited states, the UV-Vis spectra of these hydrated clusters are simulated. It is observed that UV-Vis spectra of certain hydrated cluster (e. g. $Cl_2^{\bullet-}.10H_2O$) is in excellent agreement with the measured aqueous phase spectra of that system.

Chapter 6: Up to chapter 5, discussions about microhydration have been given. This chapter describes about microsolvation of solute in a less polar medium like ammonia. Potassium atom is taken for such study. Structure, energy (solvation energy) and spectra are calculated for studying the microsolvation of potassium in ammoniated environment. This study is important with respect to the solvated electron problem. Structures having potassium–nitrogen interactions are more stable compared to those of hydrogen bonded structures. As several closely spaced minimum energy structures are obtained for larger clusters (n>3), weighted average energy parameters are also calculated based on the statistical population at 150 K.

Chapter 7: To understand the microsolvation of solutes, studies are carried out even in nonpolar medium like carbon dioxide. In this chapter, structure, energy and spectra of $I_2^{\bullet-}.nCO_2$ clusters (n=1-10) are reported. This study is important to follow photo recombination and dissociation dynamics in order to model complex chemical reaction.

In this system the conformers of a particular size of cluster is in very close in energy and have near equal statistical contribution. Monte Carlo based simulated annealing procedure is applied to find out the global minimum energy structures. Solvent stabilization and interaction energies are also calculated. It is observed that both the solvent stabilization as well as interaction energy continuously increases with the successive addition of solvent CO_2 units as in the case of more polar solvents like NH_3 or H_2O.

Chapter 8: Development of an extrapolation model based on microscopic theory to predict bulk detachment energy of excess electron from finite size cluster results is discussed in this chapter. A new relation connecting the size dependence of electron detachment energy of finite size hydrated anionic clusters is derived based on a microscopic theory. The relation is tested over a large number of different types of clusters and an excellent agreement with experimental results is observed. More importantly, an extrapolation is shown to provide a route to obtain the bulk property and again an excellent agreement with the experimental results is observed where existing empirical law fails completely.

References

1. Ohtaki, H.; Radani, T. *Chem. Rev.* **199**3, *93*, 1157.

2. Delahay, P. *Acc. Chem. Res.* **1982**, *15*, 40.

3. Nagarajan, V.; Fessenden, R. W. *J. Phys. Chem.***1985**, *89*, 2330.

4. Cramer, C. J.; Truhlar, D. G. *Chem. Rev.* **1999**, *99*, 2161.

5. Lehr, L.; Zannai, M. T.; Frischkorn,C.; Weinkauf, R.; Neumark, D. M. *Science*, **1999**, *284***,** 635.

6. Wang, X. B.; Yang, X.; Nicholas, J. B.; Wang, L. S. *Science*, **2001**, *294*, 1322.

7. Ayotte, P. G.; Weddle, H.; Kim, J.; Johnson, M. A. *J. Am. Chem. Soc.* **1998**, *120*, 12361.

8. Xantheas, S. S. *J. Am. Chem. Soc.* **1995**, *117*, 10373.

9. Chen, H-. Y.; Shew, W-S. J. Am. Chem. Soc.**2000**, *122*, 7534.

10. Masamura, M. *J. Chem. Phys.* **2003**, *118*, 6336

11. Majumdar, D.; Kim, J.; Kim, K. S. *J. Chem. Phys.* **2000**, *112*, 101.

12. Hertel, I. V., Huglin, C. N.; Psculz, C. P. *Phys. Rev. Lett*. **1991**, *67*, 1767.

13. Hashimoto, K.; Morokuma, K. *J. Am. Chem. Soc*. **1995**, *117*, 4151.

14. H. Gomez, T. R. Taylor, and D. M. Neumark, J. Chem. Phys. **2002**, *116*, 6111.

15. Greenblatt, B. J.; Zanni, M. T.; Neumark, D. M. *Science* **1997**, *276*, 1675.

16. Robertson, W. H.; Diken, E. G.; Price, E. A.; Shin, J. W.; Johnson, M. A. *Science* **2003**, *299*, 1367.

17. Weber, J. M.; Kelley, J. A.; Nielson, S. B.; Ayotte, P.; Johnson, M. A. *Science* **2000**, *287*, 2461.

18. Price, E. A.; Hammeer, N. I.; Johnson, M. A. *J. Phys. Chem. A* **2004**, *108,* 3910.

19. Barnett, R. N.; Landman, U.; Clevelend, C. L.; Jortnar, J. *J. Chem. Phys.* **1988**, *88*, 4429.

20. Zhan, C. G.; Zheng, F.; Dixon, D. A. *J. Chem. Phys.* **2003**, *119*, 781.

LIST OF FIGURES

LIST OF TABLES

Bulk vertical detachment ($\Delta E_{VDE}(\infty)$) and adiabatic detachment ($\Delta E_{ADE}(\infty)$) energy for $I^-.nH_2O$, $Br^-.nH_2O$, $Cl^-.nH_2O$, $NO_3^-.nH_2O$, $SO_4^{2-}.nH_2O$ and $C_2O_4^{2-}.nH_2O$ systems.

CHAPTER 1

Introduction

1.1. Microsolvation

The process of solvation is a dynamical interaction of a solute with the solvent, which leads to stabilization of the solute species in the solution. Studies on solvation of charged and neutral chemical species (solutes) is one of the most important and attractive area of research. If a chemical species (solute) is immersed into a solvent medium (bulk), its charge distribution interacts with that of the solvent. Due to that the network of solvent in the close proximity of the solute gets rearranged to allow the solute going through the process of solvation. In the process of solvation, a few solvent molecules in the close vicinity of the solute will interact instantaneously. Afterwards, more and more solvent molecules from nearby surroundings will approach the solute and encapsulate the solute to solvate it. The process of solvation involves different types of intermolecular interactions, namely, ion-ion, ion-dipole, hydrogen bonding and dipole-dipole attractions or van der Waals interactions. The nature of interactions depends on the nature of both solute (neutral or ionic) and solvent (ionic, polar or nonpolar). When the process of solvation of a solute in presence of large number of solvent molecules (i. e. in bulk) is studied, the solvation model refers to **macroscopic** solvation model (**continuum** model) (see Fig. 1). In this continuum model, rather than representing the charge distribution of the solvent explicitly, it is replaced by a continuous electric field that represents a

statistical average over all solvent degrees of freedom at thermal equilibrium. This field is usually called the **reaction field** in the regions of space occupied by the solute, since it is derived from the reaction of the solvent to the presence of the solute. On the other hand, the model used to study solvation process at molecular level is known as **microsolvation** (microscopic solvation) model (see Fig. 1). Microsolvation is studied by treating the effect of solvent molecules surrounding the solute in an explicit manner. In microsolvation, finite number of solvent molecules is added to encapsulate the solute usually in a bottom up approach to study what is going on at the molecular level during the process of solvation. The system consists of a finite number of solvent molecules and the solute, and is known as molecular **cluster** or microsolvated species. In **dual level** solvation model the microsolvated species is kept in the solvent continuum. The process of macro, microsolvation and dual level solvation process is shown by a graphical model displayed in Fig.1.

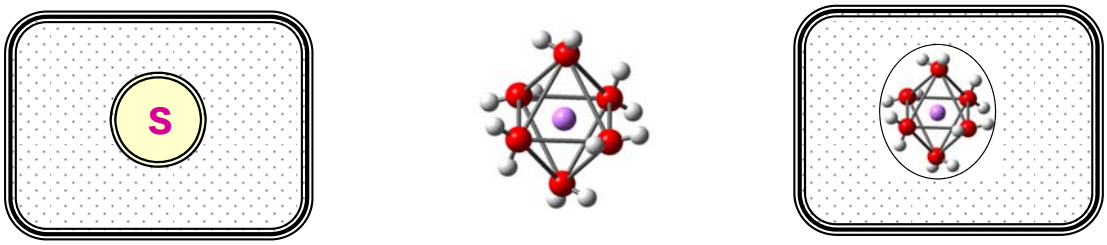

Fig. 1.1. Different models of solvation are displayed pictorially. In case of macroscopic solvation the solute 'S' is kept in the solvent continuum. In microsolvation, the solute is encapsulated by a finite number of solvent molecules. In dual level solvation the microsolvated species is kept in the solvent continuum. In case of microscopic and dual level solvation, the central violet colour ball refer to the solute and remaining balls refers to the solvent network (here, water is considered as the solvent).

1.2. Motivation

1.2.1. Macrosolvation versus Microsolvation

Though solvation process at the macroscopic level is well studied, only a little effort has been given to understand the solvation process at the molecular level. Average information about various interactions is obtained from macroscopic solvation study. Information about coordination number, thermodynamic parameters (e.g. free energy, enthalpy of solvation, etc), bulk detachment energy of excess electron from a solute, UV-Vis spectra, etc, is obtained based on experiments carried out in the bulk solution.[1-3] Many theoretical models are available to study macroscopic solvation of chemical species. Self consistent reaction field (SCRF) model due to Onsager –Kirkwood is one of the simple and popular models to study the macroscopic solvation.[4-5] In this model a spherical solute cavity is considered. Molecular shape cavity models like polarizable continuum model (PCM), conductor like screening model (CPCM) are also available to study the solvent effect at the macroscopic level.[6] There are two major advantages of continuum models (implicit solvation models). The first one is the reduction in the system's number of degrees of freedom. The second advantage is that the continuum models provide a very accurate way to treat the strong, long-range electrostatic forces that dominate many solvation phenomena. The major drawback of these implicit solvation models is that the explicit solvent effect is not taken into account. As a result, molecular level information cannot be extracted based on studies carried out in the bulk solution (macroscopic solvation) during the process of solvation. To understand different molecular level interactions responsible for solvation, one has to study the microsolvation by adding solvent molecules one by one following the bottom up approach. Studies on

clusters are helpful to investigate molecular level understanding about solute–solvent and solvent-solvent interactions. It also helps to understand how the properties of these solvated clusters evolve with the size and shape. Cluster study provides valuable insights into the structure and properties of the bulk as they are believed to resemble closely the solvation of solutes in the bulk phase. Recently, the study on microsolvation of neutral and charged chemical species has been a subject of intense research both from experimental and theoretical points of view. This is not only because of the strong dependency of the properties on size and geometry of the solvated clusters of these species, but also due to the development of sophisticated experimental and theoretical techniques. These experiments are based on supersonic expansion and nozzle beam technique to produce finite size hetero clusters consisting of both solute and solvent. A definite number of solvent molecules is added to encapsulate the solute by the bottom up approach. The hetero clusters are then monitored by various spectroscopic techniques (infrared, photoelectron spectroscopy etc).[7-10] Model potential based studies are reported to study microsolvation.[11-13] *First principle* based molecular structure calculations are also applied as one of the major theoretical techniques to study the microsolvation.[14-17] *Ab initio* molecular dynamics (AIMD) simulations are also applied for microsolvation study.[18-19] At present, only a few attempts are made to study microhydration based on AIMD due to the high computational cost.

1.2.2. Importance of the Cluster Study

Water is an excellent solvent having hydrogen bonding network. Most biological processes are unthinkable without water. So water is known as the solvent of life. While

bulk water and pure neutral water clusters have been studied extensively, water containing impurity molecules or ions (hetero clusters) is an equally important topic.[20] It is difficult to get pure water naturally, as always other substances are dissolved in it. Large number of atmospheric processes is believed to occur on water cluster and aerosol surface, but not to occur in the gas phase. One of the major sources of halogens, i. e. chlorine and bromine, in the atmosphere is also believed to be surface oxidation of marine aerosols and clusters of seawater.[20] Studies on hetero clusters also provide a convenient way to investigate atmospheric chemistry problems, e. g. ozone depletion. The water clusters can also "dissolve" numerous organic compounds and can be used as a medium for studies of aqueous organic reactions.[20] So microhydration of a solute is the most common and popular research area for the past few years. Other well known solvent having hydrogen bonded network is ammonia. Hydrogen bonded water network gets rearranges in order to solvate the solute during the process of microsolvation. The clusters of alkali metal atom and polar solvent molecules are studied at length, often from interests related to the solvated electron. Solvated electrons can form rather readily with the alkali metals because of the relatively low energy requirement for ionization. However, the detailed mechanism on the formation of the solvated electron in this medium with the alkali metal atom is not yet fully understood. Thus, solvated electron in polar solvents has been a subject of continued research. Studies on microsolvation of small chromophore are also carried out in non-polar and non-hydrogen bonded solvent medium like carbon dioxide, argon, etc. As carbon dioxide is a weakly interacting solvent, studies in this medium should help one to understand the dissociation and recombination dynamics in order to model complex chemical reactions. Many

experimental and theoretical investigations are carried out to study microsolvation both in hydrogen bonding solvent (water, ammonia, etc)[7-19] and in non-hydrogen bonding solvent (carbon dioxide, argon, etc).[13,21-22]

1.2.3. IR and PES Studies on Clusters

The electron distribution pattern of a solute plays the key role to control the structure of the solvent network around the solute during the solvation process. Positively charged ions have simple solvated structures compared to a negatively charged system as cation binds strongly with solvent molecules.[1] As anions are mass selectable, size selected gas-phase infrared (IR) cluster spectroscopy combined with first principle based theoretical studies have been successfully applied to explore the molecular level interaction during the process of microhydration.[7-8,20-26] Theoretical analysis of the observed IR band in the O-H stretching region of a particular cluster have yielded a understandable picture of how hydrogen bonded water networks are deformed when they attach to small solute anions. IR spectra of size selected cluster have been successfully applied to understand the geometry and growth motif of various chemical species during the process of microhydration. In this context, mostly spherical halide anions (F^-, Cl^-, Br^- and I^-) are studied.[7,8] Non spherical anions like OH^-, $O_2^{\bullet-}$, $Cl_2^{\bullet-}$, $NO^{\bullet-}$, SO_4^{2-}, etc, are also studied.[8,23-26] It is understood from the theoretical studies that the smaller solute – water cluster is stabilized by single (SHB) or double hydrogen bonding (DHB) and inter water hydrogen bonding (WHB). In larger clusters, the water network form cyclic arrangement to stabilize the particular cluster. Photoelectron spectroscopy of size-selected clusters with an excess electron is also successfully applied to provide indirect

insight about the electronic structure of the cluster.[27-29].In this context, many anionic systems are studied experimentally to understand microsolvation but very less theoretical attempts are available. [9,22,30-32]All the theoretical analysis on IR and PES spectra is based on a few most stable structures of the finite size clusters. But, with the increase in number of solvent water molecules in solvated clusters, the number of minimum energy configurations with close in energy for each size of clusters is expected to increase. Experimental observation on a particular size of cluster includes contribution from all possible minimum energy structures, which survive at that particular conditions of the experiment. Only average information is obtained from the experimental method. To predict a theoretical energetics and spectral properties of a microhydrated system, one has to take into account the contribution of all possible minimum energy structures for a particular size of the cluster, resulting in a weighted average energetics and spectral properties. However no such attempt has been reported in the literature. A part of the thesis is devoted to predict energetics and spectral properties based on a weighted average procedure. The weight factor is calculated following the free energy based Boltzmann population analysis at a finite temperature.

1.2.4. Connecting Cluster Properties to that of the Bulk

Molecular cluster acts as an intermediate state between isolated gaseous molecule and condense phase bulk system. Several efforts are being made to connect molecular cluster properties of a chemical species to its bulk properties. It is well known that in solution (bulk) many important properties of a chemical species are often widely different from those in the isolated gas phase. The structure and energetics of the cluster of a

chemical species may be different from those in the gas phase as well as the bulk. Bulk properties of a molecular system may emerge from the extrapolation of its clusters having sufficiently large size. Bulk properties of a solute in solution result from the combined effect of solute-solvent and solvent-solvent interactions. It cannot be obtained from the properties of the isolated solute species alone. To connect molecular properties of a chemical species to its bulk properties, one has to study clusters of sufficiently large size. Hence, studies on clusters help to understand how the properties of these solvated clusters evolve with the size and geometry. Size selected cluster study has been used to extract the bulk properties, like detachment energies of an excess electron using the empirical extrapolation model based on the continuum model.[9,33-34] But this model fails to reproduce bulk detachment energy in many cases.[9,35] The present thesis also covers an attempt to develop a formalism to extract bulk detachment energies of the solvated anion from the knowledge of the finite size hydrated cluster of that anion.

1.3. Theoretical Methodology

1.3.1. Geometry Search

The heart of the microsolvation study is the geometry of the microsolvated species (cluster). Many procedures are available to locate good minimum energy structure like conjugate gradient, steepest decent, Newton-Raphson, etc. At present pseudo Newton-Raphson (NR) method for geometry search along with Monte Carlo method based simulated annealing procedure for global minimum energy structure search procedure is discussed. The energy of a particular structure is calculated by self consistent field (SCF) method.

Newton –Raphson (NR) method expand the true function (energy) to second order around the current point x_0.

$$f(x) = f(x_0) + g(x - x_0) + \frac{1}{2} H(x - x_0)^2 \quad (1)$$

where, g is the gradient (force) and H is the Hessian. Requiring the force to be zero (in eq. 1) produces the following step,

$$(x - x_0) = -H^{-1} g \quad (2)$$

In the co-ordinate system (x) where the Hessian is diagonal, the NR step may be written as

$$\Delta x' = \sum_i \Delta x_i', \Delta x_i' = -\frac{f_i}{\varepsilon_i} \quad (3)$$

where f_i is the projection of the gradient (force) along the Hessian eigenvector with eigen value ε_i.

As the real function contains terms beyond the second order, the NR formula may be used iteratively for approaching towards the stationary point. Near minimum, all the Hessian eigenvalues are positive and the step direction is opposite to the gradient direction. If, one Hessian eigenvalue is negative, the step in this direction will be along the gradient and thus increase the function value. In this circumstances, the optimization may end up at a stationary point, which, having one negative Hessian eigenvalue, first order saddle point. If the stationary point has **n** negative Hessian eigenvalues, it is called $\mathbf{n}^{th}$ order saddle point in the potential energy surface. So, in general the NR method will attempt to converge on the nearest stationary point (either minimum or saddle point). Other problem is the use of inverse Hessian for control of the step size. If one of the

Hessian eigenvalue becomes close to zero, the step size goes to infinity (except f_i=0). The NR step is thus without bound, it may take the variables far outside the region where the second order Taylor expansion is valid. The latter region is often described by a "trust radius". Another problem is the computational aspect of calculating the Hessian.

The problem about controlling the step length and negative Hessian eigen value is solved by introducing a shift parameter λ . The choice of λ requires that the step length is equal to the trust radius (R), this is in essence the best step on a hypersphere with radius R. This is known as the quadratic approximation (QA) method.

$$|\Delta x'|^2 = \sum_i \left(\frac{f_i}{\varepsilon_i - \lambda}\right)^2 = R \qquad (4)$$

This may again have multiple solutions, but by choosing the lowest λ values the minimization step is selected. The maximum step size R is allowed to change dynamically during the optimization. If for example the actual energy change between two steps agrees well with that predicted from the second order Taylor expansion, the R for the next step may be increased and *vice versa*.

The problem regarding calculating the Hessian is solved by the *updating* scheme. The idea is to start off with an approximation to the Hessian, maybe just a unit matrix. Then updating the Hessian is used in each optimization step using a suitable scheme due to Broyden-Fletcher-Goldfarb-Shanno (BFGS). NR methods with updating Hessian scheme is known as pseudo Newton-Raphson method. Quasi Newton-Raphson based algorithm has been adopted to search for the minimum energy structure in each of these hydrated clusters with various initial structures designed systematically following the bottom-up approach. This procedure involves the calculation of a multi-dimensional

potential energy surface for these clusters and finding a minimum on the surface. The key issue in this search procedure is to guess a good initial geometry of the cluster, which might converge during the calculation to a local or the global minimum. It is to be noted that the adopted procedure for geometry search cannot guarantee to locate the global minimum. Thus, **Monte Carlo** based **simulated annealing** procedures have also been applied with the effective fragment solvent molecules to find out the global minimum structure of different size molecular clusters.[36] In this method, molecular coordinates are displaced by a random amount and the energy of the system has been evaluated at the new structure. The new structure with lower energy is accepted while structures with higher energies have been accepted at a probability determined by the Boltzmann factor. Random structures are generated by carrying out Monte-Carlo steps at a temperature range of 2000 K to 100 K for more than 8000 steps.[36]

In molecular electronic structure methods the energy of a system is calculated using the self consistent field (SCF) method. For calculation of the energy system many methods are available. Among them the simplest *ab initio* method is Hartree-Fock (HF), which is an electron uncorrelated method.

In all the SCF method the density matrix (P) is guessed initially and is defined for restricted HF case [37]

$$P_{\lambda\sigma} = 2 \sum_{i}^{occupied} \chi_{\lambda i} \chi_{\sigma i} \qquad (5)$$

where the coefficient (χ) comes from the linear combination of the basis set (φ_i)

$$\phi_j = \sum_{i=1}^{N} \chi_{ij} \varphi_i \qquad (6)$$

For open shell HF i. e. unrestricted HF (UHF) two sets of density matrix is defined, one for α and other for β electrons.

$$P^{\alpha}_{\lambda\sigma} = \sum_{i}^{\alpha-occupied} \chi^{\alpha}_{\lambda i}\chi^{\alpha}_{\sigma i} \ , \ P^{\beta}_{\lambda\sigma} = \sum_{i}^{\beta-occupied} \chi^{\beta}_{\lambda i}\chi^{\beta}_{\sigma i} \qquad (7)$$

1.3.2. Electron Correlation

Energies calculated by the HF method are typically in error by 0.5 % to 1% of the total energy.[38] Though an absolute basis this is not too much, it is of the order of the chemical bond energy. So, to study the clusters having weak interaction one need to improve on the HF energy. The motions of electrons are correlated with each other and this is called **electron correlation**. The electron correlation energy is the difference between the exact non-relativistic energy and HF energy of the system (clusters). The wave function in HF method is single determinant, not capable of considering the correlation of the electron motion. To include the electron correlation energy several *ab initio* post HF multi-determinant methods are constructed, namely, second order Moller-Plesset perturbation theory (MP2), Configuration interaction (CI), Coupled cluster (CC) etc. It is well known that all these methods are costly ones and some time it is impossible to calculate the geometry by applying these methods. Density functional theory (DFT) is developed to improve the time requirement over the *ab initio* correlated methods like MP2, CC, etc.

1.3.3. Density Functional Theory

The electronic wave function of an N electron system depends upon 3N spatial and N spin coordinated. Since the Hamiltonian contains only one and two electron spatial

terms, the energy can be written in terms of only six spatial coordinates. This has prompted the search for a function which has fewer variables than the wave function and also can be used to calculate the energy of the systems. Unfortunately, no convenient method like the variational principle is developed to determine the density matrix without first constructing the wave function. Hohenberg and Kohn (HK) shows that the ground state wave function, energy and other molecular electronic properties are uniquely calculated from the electron density ρ(x,y,z), which is a function of only three variables. The ground state energy E_0 is a function of ρ and can be writen as, $E_0 = [\rho(x,y,z)]$, where the square bracket denotes the functional relation. But HK principle does not show how to calculate E_0 from ρ or hoe to find ρ without first calculating the wave function. In order to solve this problem **Kohn and Sham** (KS) proposed a self consistent method. They showed that the ground state electronic energy would be given by, [37]

$$E_0 = -\frac{1}{2}\sum_{i=1}^{N}\langle \chi_i(1) \mid \nabla_1^2 \mid \chi_i(1)\rangle - \sum_{\alpha}\int \frac{z_\alpha \rho(1)}{r_{1\alpha}} d\nu_1 + \frac{1}{2}\iint \frac{\rho(1)\rho(2)}{r_{12}} d\nu_1 d\nu_2 + E_{xc}[\rho] \qquad (8)$$

Where, the KS orbital χ_i are found by the procedure discussed below and the exchange – correlation energy, $E_{xc}[\rho]$ is a function of ρ. The symbols $\chi_i(1)$ and ρ(1) indicates that χ_i and ρ are taken as function of the spatial coordinates of electron 1. Kohn and Sham also showed that the exact ground state ρ could be found from the expression given below,

$$\rho = \sum_{i=1}^{N} \mid \chi_i \mid^2 \qquad (9)$$

KS orbitals are found by solving the one electron equations,

$$h_i^{KS}(1)\chi_i(1) = \varepsilon_i(1)\chi_i(1) \qquad (10)$$

where the KS operator h^{KS} is given by,

$$h^{KS} = -\frac{1}{2}\nabla_1^2 - \sum_{\alpha}\frac{z_\alpha}{r_{1\alpha}} + \int\frac{\rho(2)}{r_{12}}dr_2 + V_{xc} \tag{11}$$

And the exchange-correlation potential V_{xc}, is found by the functional derivative of E_{xc}

$$V_{xc} = \delta E_{xc}[\rho]/\delta\rho \tag{12}$$

In DFT the most important part is to derive the functional form of the exchange-correlation functional. The hybrid density functional, namely B3LYP (Becke's three parameter exchange and Lee-Yang-Parr correlation functional), BHHLYP (50% Slater and 50 % Hartree-Fock exchange and correlation due to Lee-Yang-Parr) etc are the most popular. They are derived by the adiabatic connection method (ACM), where the fictitious non interacting system connects to the real system i. e. fully interacting systems. So these functionals are called hybrid functionals.[37]

1.3.4. Basis Set

Basis set is the mathematical functions to represent the wavefunctions of electrons of an atom. The basis sets having proper 'cusp' at the nuclear center are closely resemble the hydrogenic orbitals. The functional form of such basis set is

$$\varphi_i = Ax^i y^j z^k e^{-\varsigma(x^2+y^2+z^2)^{1/2}} \tag{13}$$

where A is normalization constant, ζ is an exponent and depends on the atomic number, and i, j, and k are non-negative integers that indicate the nature of the orbital in a Cartesian sense. They are known as Slater type orbitals (STOs). It is very difficult to evaluate multicentered four-index integrals with STOs. So, to overcome this problem,

Boyd proposed the use of Gaussian type orbitals (GTOs). The general functional form of a GTO in atom-centered Cartesian coordinate is,

$$\varphi_i = Ax^i y^j z^k e^{-\alpha(x^2+y^2+z^2)} \quad (14)$$

where A is the normalization constant, α is an exponent controlling the width of the GTO, and i, j, and k are non-negative integers that indicate the nature of the orbital in a Cartesian sense. [37] As the GTOs do not have proper 'cusp' at the nuclear centre, Boyd suggested that the combination of several GTOs with fixed combination coefficients will mimic the STOs. When a basis functions is defined as a linear combination of GTOs , is known as contracted GTOs (CGTOs) and the individual GTOs from which it is formed is known as primitive Gaussians. A CGTOs of the from 6-311+G(d) means that 6 primitives for the core, 3, 1, 1 primitives for the triply split valence orbital and the diffuse and polarizations functions are represented by + and d symbol, respectively. For these type of CGTOs the exponent and contraction coefficients are determined by uncorrelated HF method. When the exponent and contraction coefficients are variationally optimized not only for HF but also for the electron correlated method, the basis is known as 'correlated consistent polarized valence' (cc-pVDZ, cc-pVTZ etc) basis set. If they are augmented with extra set of diffuse functions, they are called as aug-cc-pVDZ, etc.

1.4. Scope of the Present Thesis

To understand the process of microsolvation, a detailed study on the structure and energetics of finite size cluster of various chemical species in water, ammonia and carbon dioxide solvents have been carried out. Both close and open shell chemical species are considered for investigation. At present halogen dimer radical anions ($Cl_2^{\bullet-}$, $Br_2^{\bullet-}$ & $I_2^{\bullet-}$),

carbonate radical anion ($CO_3^{\bullet-}$), nitrate anion (NO_3^-), and multiply charged anion e.g. carbonate anion (CO_3^{2-}) and halogen dimer (Cl_2, Br_2 & I_2) are taken to study microhydration due to their chemical importance as well as progressive complexity. Potassium atom and iodine dimer radical anion ($I_2^{\bullet-}$) are also taken to study the process of microsolvation in ammonia and carbon dioxide solvents, respectively. Solubility, IR, Photoelectron and UV-Vis spectral properties have also been predicted and compared with experimental findings whenever available. When only one solvent molecule is added to solvent, a few minimum energy structures are expected. With the increase in number of solvent molecules in solvated clusters, the number of minimum energy configurations with close in energy for each size solvated clusters are expected to increase. Experimental observation on a particular size of cluster includes contribution from all possible minimum energy structures, which survive at that particular condition of the experiment. Average information is obtained from the experimental method. Thus weighted average properties are calculated for better predictability. Fourier transform to the dipole and velocity auto-correlation function is also done to include dynamical contribution to the calculated IR spectra and compared to the weighted average IR spectra.

It is well known that bromine gas is more soluble than chlorine gas in water but no theoretical understanding is available in the literature. UV-Vis spectra in aqueous solution of $Cl_2^{\bullet-}$, $Br_2^{\bullet-}$, $I_2^{\bullet-}$ &, $CO_3^{\bullet-}$ radical anionic species, and specific one electron oxidants are measured by experimental techniques. But theoretical attempt to generate their absorption profiles is not available. A major part of the thesis (chapters 4, 5 & 8) is dedicated to study bulk properties like solubility, aqueous UV-Vis spectra and bulk detachment energy of excess electron. They are also systematically compared with

reported experimental findings. Theoretical results on structures, energetics, spectral properties (vibrational, photoelectron) of clusters consisting of various solutes (both neutral and anionic) and solvent molecules (water, ammonia and carbon dioxide) with different size have been presented in chapters 2, 3, 4, 6 & 7 and discussed in a systematic manner to understand the process of microsolvation. A general extrapolation model based on a microscopic theory has also been developed for prediction of bulk detachment energy of excess electron from finite size cluster data and is reported in chapter 8.

CHAPTER 2

Structure and Energetics of Water Embedded Anionic Clusters

2.1. Introduction

Lately, hydrogen bonded water clusters encapsulating charged solutes have been a subject of intense research both by theoretical and experimental researchers.[1-3, 7-10,14-15,18-19,23-35]. When a charged solute is added into a solvent water pool, preexisting hydrogen bonded water network in solvent breaks up to accommodate the solute and a new hydrogen bonded water network forms surrounding the solute. This process of hydration with an anionic solute is rather complex compared to that of a cationic species as cation binds strongly with the solvent water molecules.[1] A delicate balance between water-anion and water-water interactions determines the structure of hydrated cluster of the anion. Studies on finite size hydrated clusters are important because of the strong dependency of their properties on their size and structure and to understand the growth motif of solvent molecules surrounding the solute. Recently, with the advent of supersonic expansions and nozzle beam techniques as well as sophisticated theoretical techniques, solvation in small as well as large size hetero clusters has been amenable to experimental and theoretical observations. A number of experimental, theoritical and simulation studies have been carried out to understand the structural, energetics, spectroscopic and dynamic aspects of hydration at molecular level on small negatively charged ions.[7-10,14-15,18-19,23-35] Among the simplest of the anionic systems studied by experimental and theoretical techniques is the

hydrated halide series, $X^-.nH_2O$, (X=Cl, Br, I).[7-8,14] Beyond these simple halide anions, the next complex hydrated clusters investigated involve diatomic singly charged anions of the type $Y^-.nH_2O$, where Y refers to OH,[8,15] O_2,[23] NO[25].

In this chapter, both open shell systems like, halogen dimer radical anions, $X_2^{\bullet-}$ ($Cl_2^{\bullet-}$, $Br_2^{\bullet-}$ & $I_2^{\bullet-}$), carbonate radical anion ($CO_3^{\bullet-}$) and close shell systems like, carbonate anion (CO_3^{2-}), nitrate anion (NO_3^-) are taken to understand the process of microhydration. The study on the evolution of hydration motifs when a second halogen atom, $X^\bullet$ is added to X^- to form $X_2^{\bullet-}$ ($Cl_2^{\bullet-}$, $Br_2^{\bullet-}$ & $I_2^{\bullet-}$) diatomic species should provide information on binary ion-molecule interaction with extended electron distribution. Study on $CO_3^{\bullet-}$ radical anion is also a subject of numerous investigations not only due to its role as terminal ion in atmospheric chemistry but also due to its rich and varied photophysical properties. Interest in oxidative chemistry of carbonate radical anion, $CO_3^{\bullet-}$ has significantly grown within the last decade due to its important role in inflammatory processes. It is also reported that carbonate radical anion is produced in the physiological system during xanthine oxidase turnover. Xanthine oxidase is generally recognized as the key enzyme in purine catabolism.[39] Such study will help to enhance our understanding on molecular level interactions between solvent water molecules and negatively charged ions in aqueous solution. Investigations on hydrated clusters of these radical anions are also useful to radiation chemistry studies in water medium. In aqueous solution, hydroxyl radical ($^\bullet$OH) reacts with X^- (X=Cl, Br & I) to form a transient species, which has a strong optical absorption in the visible region. This absorption maxima is assigned to the halogen dimer radical anion species, $X_2^{\bullet-}$(X=Cl, Br & I), a specific one electron oxidation species. Similarly in aqueous solution, hydroxyl radical ($^\bullet$OH) reacts with

CO_3^{2-} or HCO_3^- anion to form a transient species, which has a broad and moderately strong absorption in the visible region. This absorption maximum is assigned to the carbonate radical anion species, $CO_3^{\bullet-}$, again a specific one electron oxidising species. Nitrate anion (NO_3^-) is one of the most abundant species in acidic wastes as well as in the atmosphere.[40] It is known as the so-called terminal anion in the series of atmospheric reactions involving nitrogen and thus its study is of particular importance. The process of hydration involving nitrate anion in the atmosphere is very important, as water is present in the atmosphere in relatively large concentrations.

Structure and energetics of $Cl_2^{\bullet-}.nH_2O$ (n=1-5), $NO_3^-.nH_2O$ (n=1-5) and $CO_3^{\bullet-}.H_2O$ cluster is reported in literature.[24,32,41] But no report is available on higher clusters and on other systems in this series. In what follows, structural (growth motif) and energetics aspects of X. $n$$H_2O$ (X= $Cl_2^{\bullet-}$, $Br_2^{\bullet-}$, $I_2^{\bullet-}$, $CO_3^{\bullet-}$, NO_3^- and CO_3^{2-}) clusters are presented in a systematic manner in this chapter.

2.2. Theoretical Approach

All the calculations have been carried out applying hybrid density functional, namely, Becke's half-and-half (BHH) non-local exchange and Lee-Yang-Parr (LYP) non-local correlation functionals (BHHLYP) and Becke's three parameter non-local exchange (B3) and Lee-Yang-Parr (LYP) non-local correlation functionals (B3LYP) with triple split valence, 6-311++G(d,p) set of basis function. This BHHLYP hybrid functional includes 50% Hartree-Fock exchange, 50% Slater exchange and the additional correlation effects of the LYP functional.[42] It is reported in the literature that BHHLYP functional performs well to describe such open shell doublet systems like halogen dimer radical

anions ($Cl_2^{\bullet-}$, $Br_2^{\bullet-}$ & $I_2^{\bullet-}$).[43-44] Quasi Newton Raphson based algorithm has been applied to carry out geometry optimization for each of these molecular clusters with various initial thought structures to find out the most stable one. This procedure involves the calculation of a multi-dimensional potential energy surface for the anionic molecular cluster and finding a minimum on the surface. The key issue in this search procedure is to guess a good starting geometry of the cluster, which might converge during the calculation to a local or the global minimum. In the present calculation, several possible starting geometries are generated systematically based on different possible three-dimensional structures. In the *first* case, initial structures are considered where all the solvent water molecules are at a distance of ionic hydrogen bonding with either of the two I atoms and far from another solvent molecule to have any inter solvent hydrogen bonding interaction. In the *second* case, guess structures are considered where all the solvent molecules are at a distance of ionic hydrogen bonding with either of the two I atoms and also at a distance to have an inter water hydrogen bonding interaction. In the *third* case, a few solvent water molecules are considered at a distance of ionic hydrogen bonding with either of the two iodine atoms and far from another solvent water molecule to have any inter water hydrogen bonding interaction. Rest of the solvent water molecules are considered at a distance of ionic hydrogen bonding with either of the two I atoms and also at a distance where inter water hydrogen bonding interaction can exist. No symmetry restriction has been imposed in the adopted optimization procedure. However, it is to be noted that the adopted procedure for geometry optimization cannot guarantee to locate the global minimum energy structure especially for the higher hydrated clusters. Hessian calculations have been performed for all the optimized minimum energy structures to

check the nature of the equilibrium geometry and to generate the IR spectrum. Geometry of small size hydrated clusters are also calculated incorporating correction due to basis set superposition error (BSSE) following counterpoise method.[45] Population (P_i) of the conformers of each size clusters has been calculated based on free energy change (ΔG_i) at 150 K (T) following Boltzmann distribution i. e. $P_i = \text{Exp}(-\Delta G_i/kT)$. The weighted average properties (A_w) is constructed as $A_w = \sum_i P_i A_i$. All electronic structure calculations have been carried out adopting GAMESS program system on a LINUX cluster platform.[46] MOLDEN program systems have been used for visualization of molecular geometry.[47] Triple split Gaussian type basis sets for Br and I atoms are obtained from the Extensible Computational Chemistry Environment Basis Set Database, Pacific Northwest Laboratory.

2.3. Results and Discussion

2.3.1.1. Structure of X.*n*H_2O (X= $Cl_2^{\bullet-}$, $Br_2^{\bullet-}$ & $I_2^{\bullet-}$) Clusters

To choose a suitable level of theoretical method for these calculations, geometrical parameters of mono-, di and tri-hydrated clusters of $Cl_2^{\bullet-}$, $Br_2^{\bullet-}$ & $I_2^{\bullet-}$ are carried out following 30 correlated density functionals (hybrid, pure and meta generalized gradient approximation density functionals). The calculated geometrical parameters are compared to that of at second-order Moller–Plesset perturbation (MP2) theory adopting 6-311++G(d,p) basis functions (I atom treated by 6-311 basis set). It is observed that Becke's half-and-half (BHH) non-local exchange and Lee–Yang–Parr (LYP) non-local correlation functionals (BHHLYP) perform well to describe these clusters producing

geometrical parameters close to MP2 values. So, BHHLYP functional is used for geometry search throughout.

Several minimum energy structures are obtained for $I_2^{\bullet-}.nH_2O$ (n=1-8) clusters, on full geometry optimization. All the stable conformers for each size hydrated cluster are displayed in Fig. 2.1. Fig. 2.1-I shows the structure of monohydrate cluster ($I_2^{\bullet-}.H_2O$) consisting symmetrical double hydrogen bonding (DHB) arrangement where two I atoms and two H-atoms of the H_2O molecule are connected by H-bonding of distance ~2 Å. It is worthmentioning that all possible combinations of initial geometry for optimization converged on the same structure. Two minimum energy structures are obtained for the di-hydrate ($I_2^{\bullet-}.2H_2O$) cluster. Structure II-A having one DHB, one single hydrogen bonding (SHB) and one inter water H-bonding (WHB) arrangements is calculated to be more stable compared to the structure II-B having two symmetrical DHB arrangements by 1.42 kcal/mol. It appears that structure II-A is formed when H-bonded water dimer is connected to two I atoms of $I_2^{\bullet-}$ system by three free H atoms *via* H-bonding. But the initial guess structure of II-A is the one where two water molecules are connected *via* one WHB arrangement and two SHB arrangements. II-B is obtained from the initial guess where a water molecule is added to the structure I from opposite side of H_2O making another DHB arrangement. It is worth mentioning that structure II-B is also obtained from a initial guess where two water molecules approach the $I_2^{\bullet-}$ moiety from two sides of I-I axis. Structure II-B is planar having the dihedral angle, O-I-I-O as 180^o. The energy for a WHB and SHB in such system is calculated to be 7.0 and 6.6 kcal/mol, respectively whereas the H-bonding energy in neutral water dimer is ~6.0 kcal/mol. Thus, a particular minimum energy structure is obtained on compromise between the formation of inter

water H-bonding network among solvent H_2O molecules and ionic hydrogen bond formation between solvent H_2O molecule and I atom.

Four minimum energy structures predicted for tri-hydrate cluster, $I_2^{\bullet-}.3H_2O$ are displayed in Fig. 2.1-III(A-D). Initial guess structures are considered based on the optimized minimum energy structures observed in case of di-hydrate cluster, $I_2^{\bullet-}.2H_2O$. Geometry optimization leads to two different minimum energy structures when the initial guess structure is designed based on structure II-A adding the third H_2O forming symmetrical DHB with two I atoms. When the third H_2O is kept at a close distance from one of the H_2O molecules (r_{OO} ~ 3.5 Å), structure III-A is obtained. On the other hand when the said distance, r_{OO} is more than 3.5 Å in the initial geometry, structure III-B is obtained. The initial guess for structure III-C consists of three symmetrical DHB arrangements. In this particular optimized structure, all the three H_2O molecules are directly connected to I atoms without any inter H_2O interaction. Structure III-D, having two DHB and one SHB arrangements from axial side of $I_2^{\bullet-}$ moiety is the least stable conformer for the tri-hydrate cluster. The surface structure III-A having three H_2O molecules connected by inter H_2O H-bonding network (WHB arrangements) is the most stable one and has the shortest I-I bond distance among the different conformers of $I_2^{\bullet-}.3H_2O$ cluster. The calculated dihedral angle, δ(O-I-I-O) in the structure III-C is 120^o.

As expected, the number of possible conformers increases with the increase in the number of solvent water molecules. Initial guess structures are considered with a bottom-up approach based on the predicted stable structures from the smaller size hydrated clusters. Thus the initial guess structures for $I_2^{\bullet-}.4H_2O$ cluster is designed based on the predicted minimum energy structures of $I_2^{\bullet-}.\ nH_2O$ (n=1-3), keeping different numbers of

symmetrical DHB, SHB or WHB arrangements. Seven different structures having no imaginary frequency are obtained for $I_2^{\bullet-}.4H_2O$ cluster and are displayed in Fig. 2.1-IV(A-G). Once again, the surface structure, IV-A where four H_2O molecules form a H-bond cyclic network using one of its H atoms and the other H atoms are connected to I atoms is the most stable one. Structure IV-A consists of four WHB and four SHB arrangements. The least stable structure, IV-G, has two symmetrical double H-bonding (DHB) and two axial single H-bonding (SHB) arrangements with no inter water H-bonding (WHB). Structure IV-E has four symmetrical DHB keeping the angle between two successive O-I-I planes as 90^o. Structure IV-F with three DHB and one axial SHB arrangement is less stable than IV-A by 15.18 kcal/mol. Rest of the conformers have at least one DHB arrangement with different number of H_2O systems in inter water H-bonding networks. It is clearly observed that the most stable structure has the maximum number of WHB arrangements and the relative stability of the conformers decreases with the decrease in the number of WHB arrangements.

Similarly, the initial guess structures for penta-hydrate ($I_2^{\bullet-}.5H_2O$) cluster is designed based on the predicted minimum energy structures of $I_2^{\bullet-}.nH_2O$ (n=1-4), keeping different numbers of symmetrical DHB, SHB or WHB arrangements. Geometry optimization with various initial guess structures for the penta-hydrate cluster, $I_2^{\bullet-}.5H_2O$ yields seven minimum energy structures, having no imaginary frequency and the structures are displayed in Fig. 2.1-V(A-G). The most stable structure, V-A is the one where one solvent H_2O molecule adds to the most stable structure of the tetra-hydrate cluster, $I_2^{\bullet-}.4H_2O$ (IV-A) from the other side of H-bond network forming double hydrogen bonding between two I atoms and two H-atoms of H_2O. Structure V-B is 4.47

kcal/mol less stable than V-A. It is obtained from an initial guess where two water molecules forming two SHB and one WHB arrangements is added opposite to the H-bonded network of structure III-A. Conformers V-C and V-D are having at least two DHB arrangements. Structure V-E has five symmetrical DHB arrangements keeping the angle between the successive O-I-I planes as 72^{o}. Conformer V-F having comparable stability with structure V-E has four DHB and one axial SHB arrangements. The least stable structure (~19 kcal/mol less stable compared to V-A), V-G has three symmetrical DHB and two axial SHB arrangements.

Seven minimum energy structures displayed in Fig. 2.1-VI(A-G) are obtained for the hexa-hydrate cluster, $I_2^{\bullet-}.6H_2O$. The most stable structure, VI-A has five SHB and five WHB arrangements. Structure VI-G, having no WHB arrangement is the least stable conformer (~22 kcal/mol less stable compared to V-A). It is interesting to mention that structure VI-B, having exactly the same number of WHB and SHB arrangements as of VI-A is 0.33 kcal/mol less stable than VI-A. Both structures contained one H-bonded water cyclic tetramer. Structure VI-C, where two I atoms are in between two H-bonded water trimer networks, is less stable than the structure VI-A by ~1.3 kcal/mol though it has more number of inter water H-bonds. Four H_2O units form a hydrogen bonded tetramer network in case of structure VI-D. Remaining two H_2O units are linked to the solute atoms by symmetrical DHB arrangement and at a distance to have no interaction with each other or with any other H_2O units. Structure VI-E, having six SHB, four WHB arrangements but no DHB arrangement is 4.14 kcal/mol less stable than VI-A. Structure VI-F has one H_2O with a symmetrical DHB, five SHB and four WHB arrangements. The least stable structure, VI-G has four symmetrical DHB and two SHB from the both sides

of I-I axis and having the least I-I distance among all the conformers for $I_2^{\bullet-}.6H_2O$ cluster. None of these solvent H_2O molecules are connected to each other suggesting this structure to be a first hydration shell structure for the solute $I_2^{\bullet-}$. At present no structure is included where one or more H_2O reside in the second solvation shell (I..H distance > 4 Å) of the anion.

Various possible initial guess structures of $I_2^{\bullet-}.7H_2O$ clusters are taken up for full geometry optimization based on the knowledge of predicted structures in hexa-hydrate cluster, $I_2^{\bullet-}.6H_2O$. Seven conformers are obtained with real frequencies based on full geometry optimization followed by Hessian calculations and are displayed in Fig. 2.1-VII(A-G). Unlike the smaller clusters, the energy of these conformers is very closely spaced as in the case of $I_2^{\bullet-}.6H_2O$ cluster (within ~10 kcal/mol). Structure VII-A having one cyclic H-bonded tetramer is the most stable structure for $I_2^{\bullet-}.7H_2O$ cluster. Two I atoms are in between inter water H-bonded cyclic tetramer and trimer water networks in structure VII-B which is 3.1 kcal/mol less stable compared to the most stable conformer. It has seven SHB and seven WHB arrangements. All H_2O molecules are directly attached to the $I_2^{\bullet-}$ moiety for the structure VII(A-E). At least one H_2O unit is present in the structures VII(F-G) which is not directly linked to any of the I atoms of the solute dimer radical anion (I..H distance > 4 Å). Another interesting fact observed is that solvent H_2O units are connected with each other by inter water hydrogen bonding in each structure. This shows the completion of the first hydration shell in the hexa-hydrate cluster itself.

Situation becomes much more complicated when one more H_2O is added to $I_2^{\bullet-}.7H_2O$ cluster. Initial guess structures taken for geometry optimization in case of octa-hydrate cluster, $I_2^{\bullet-}.8H_2O$ are based on the knowledge of predicted structures for $I_2^{\bullet-}.7H_2O$

cluster. Nine conformers are obtained with all real frequencies based on full geometry optimization followed by Hessian calculations. The optimized structures are displayed in Fig. 2.1-VIII(A-I). One can see from Fig. 2.1-VIIIA that the anion moiety is sandwiched between the two cyclic water tetramers in the most stable conformer. Structure VIII-B making one cyclic water tetramer is less stable than the most stable conformer by 0.67 kcal/mol. Structure VIII (A-C, E-F) has at least one cyclic water tetramer. The least stable conformer (~10 kcal/mol less stable compared to VIII-A), (see Fig. 2.1-VIII(I)) has two H_2O cyclic trimers and two DHB arrangements.

It is noticed that several minimum energy conformations with a small energy difference can exist for the hydrated cluster, $I_2^{\bullet-}.n$H2O (n=3-8). It is clear from the figure that the $I_2^{\bullet-}.nH_2O$ clusters are stabilized by double hydrogen bonding (DHB), single hydrogen bonding (SHB) and inter water hydrogen bonding (WHB). Conformation having H-bonded water network (WHB arrangements) are more stable over the other structures where H_2O units are connected to the anion moiety independently either by SHB or DHB for a particular size of the cluster. H-bonded water network, having two, three or four H_2O units, are present in different conformers of these clusters. Hydrated cluster having cyclic water network units is the most stable conformer for each size cluster. Hydrated $I_2^{\bullet-}.nH_2O$ clusters of size n=4-8 contain at least one four member water ring (see Fig. 2.1). In each case, the distance between the two I atoms is ~ 3.3 Å, the distance between I and H-bonded H atoms is 2.3-2.8 Å (SHB and DHB bond) and the distance between O and H atoms in inter water network is 1.9-2.1 Å (WHB bond).

Structures of microhydrated species, $Cl_2^{\bullet-}.nH_2O$ and $Br_2^{\bullet-}.nH_2O$ are also calculated. Similar minimum energy structures are also observed for $Cl_2^{\bullet-}.nH_2O$ and

$Br_2^{\bullet-}.nH_2O$ hydrated cluster. For $Cl_2^{\bullet-}.nH_2O$ cluster, in each case, the distance between the two Cl atoms is ~ 2. 6 Å, the distance between Cl and H-bonded H atoms is 2.3-2.8 Å (SHB and DHB bond) and the distance between O and H atoms in inter water network is 1.9-2.1 Å (WHB bond). For $Br_2^{\bullet-}.nH_2O$ cluster, in each case, the distance between the two Br atoms is ~ 2. 8 Å, the distance between Br and H-bonded H atoms is 2.3-2.8 Å (SHB and DHB bond) and the distance between O and H atoms in inter water network is 1.9-2.1 Å (WHB bond).

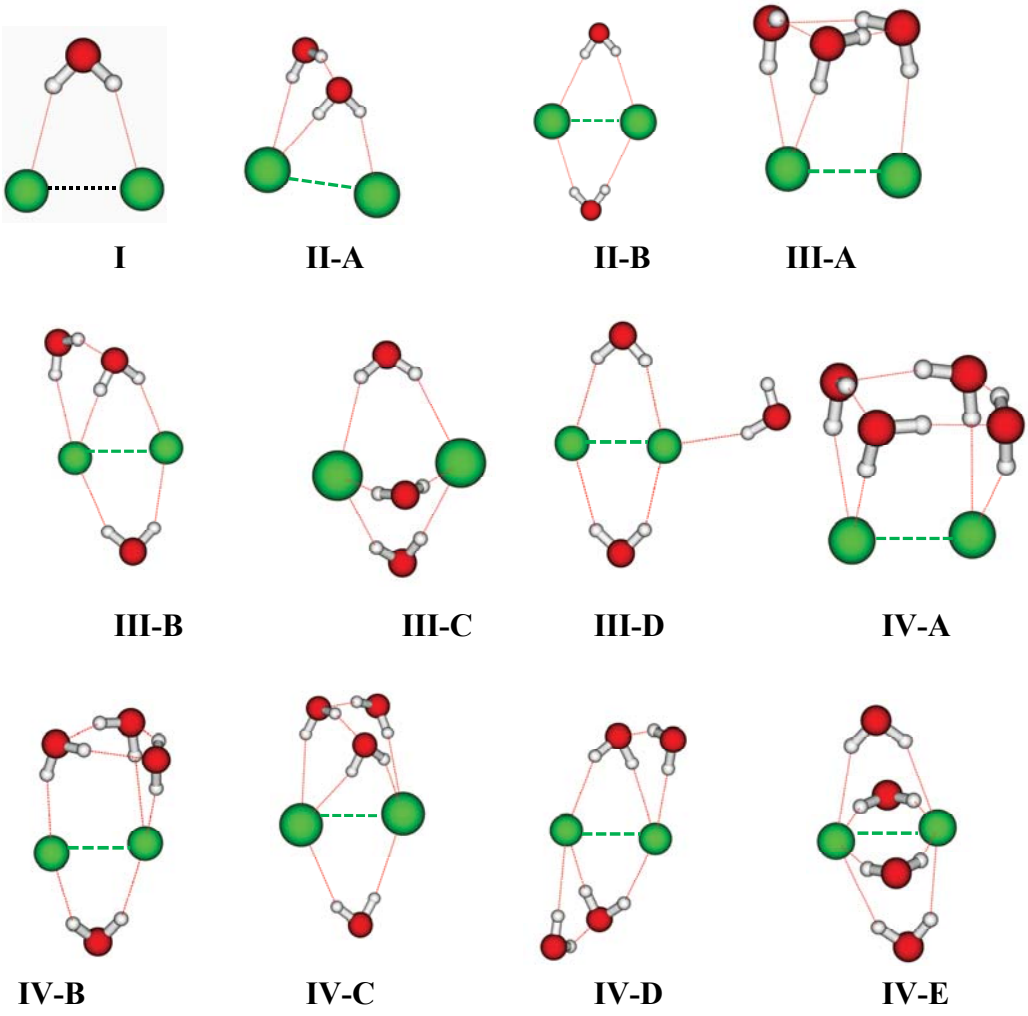

Fig. 2.1 (Contd.)

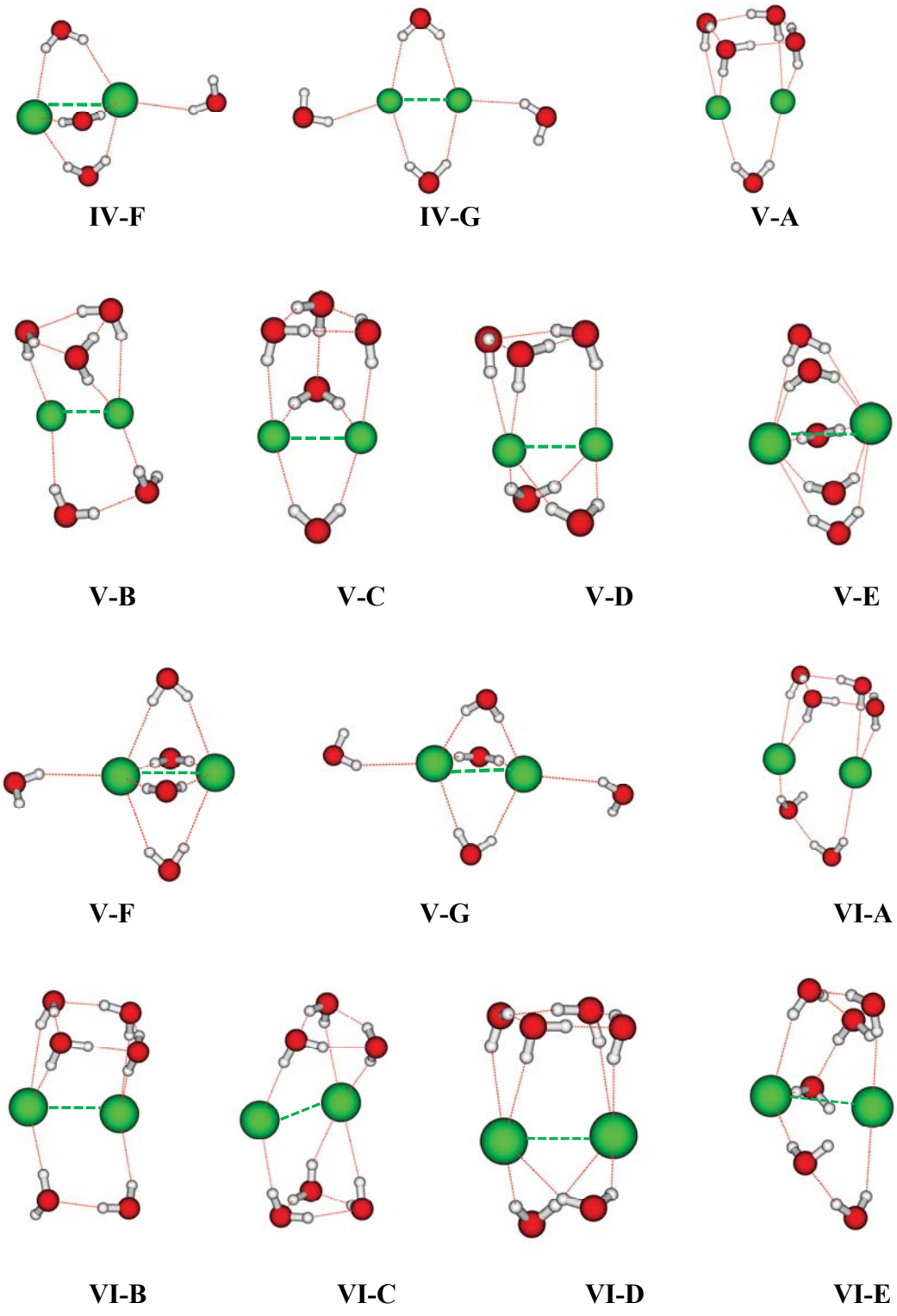

Fig. 2.1 (Contd.)

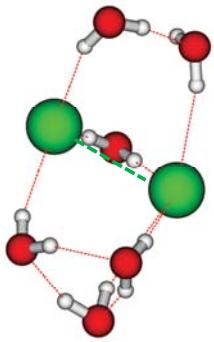

VI-F

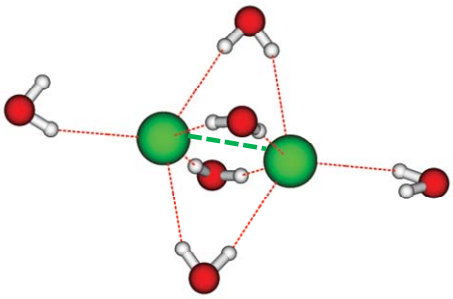

VI-G

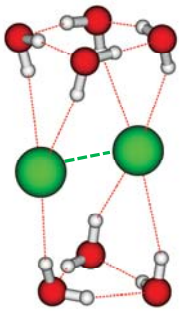

VII-A

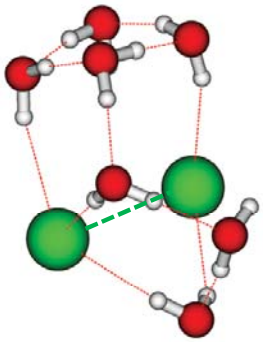

VII-B

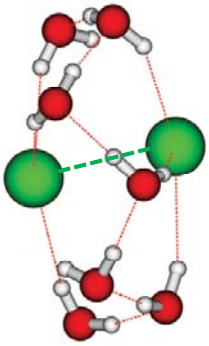

VII-C

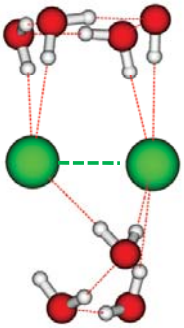

VII-D

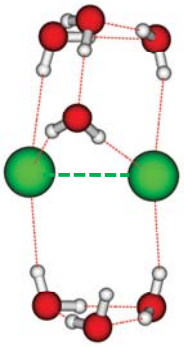

VII-E

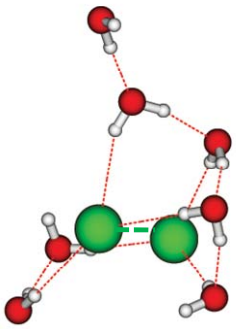

VII-F

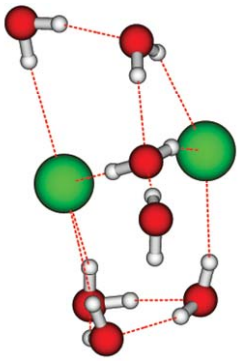

VII-G

Fig. 2.1 (Contd.)

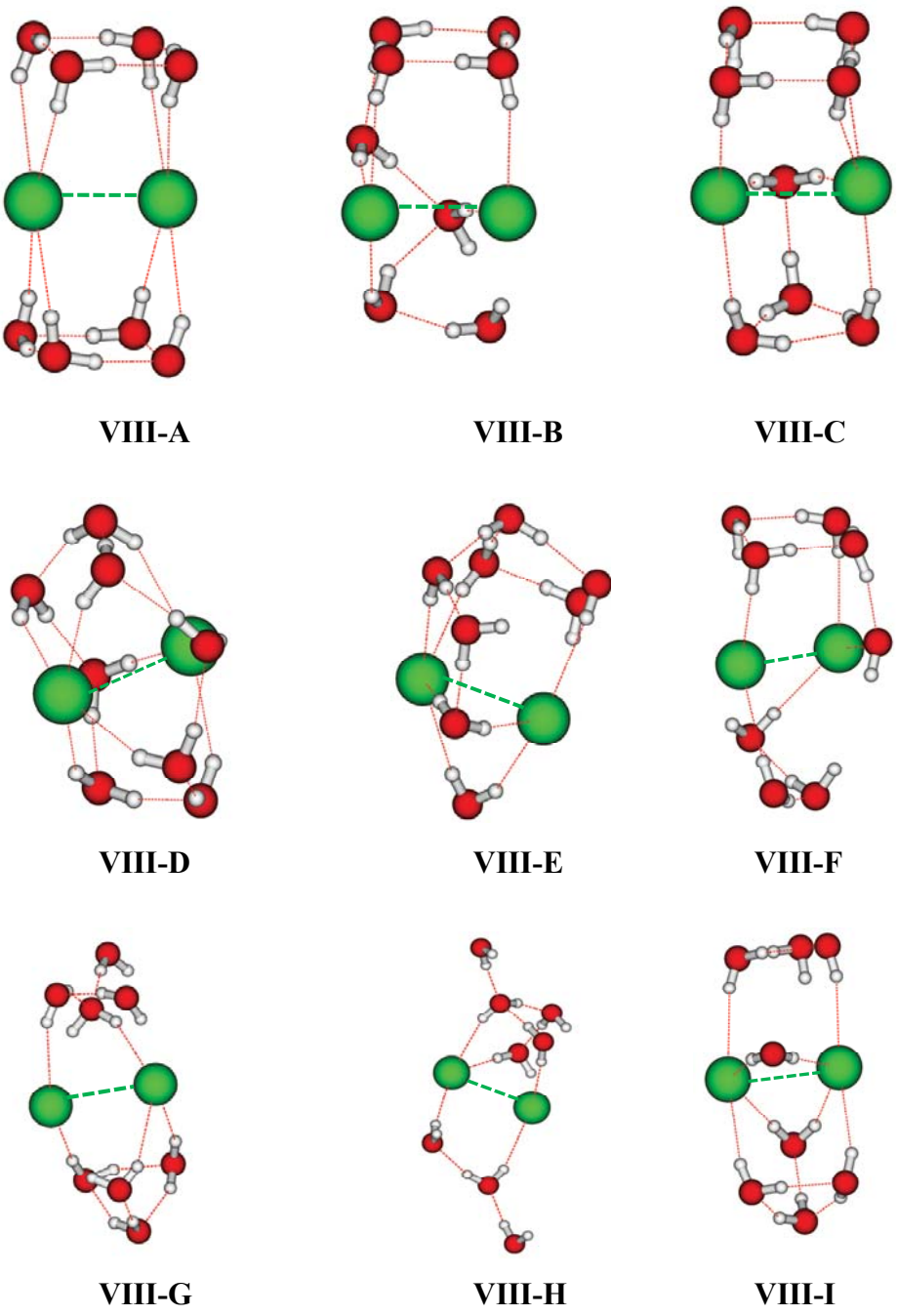

Fig. 2.1. Fully optimized minimum energy structures at BHHLYP/6-311++G(d,p) level of theory for (I) $I_2^{\bullet-}.H_2O$, (II) $I_2^{\bullet-}.2H_2O$, (III) $I_2^{\bullet-}.3H_2O$, (IV) $I_2^{\bullet-}.4H_2O$, (V) $I_2^{\bullet-}.5H_2O$, (VI) $I_2^{\bullet-}.6H_2O$, (VII) $I_2^{\bullet-}.7H_2O$, and (VIII) $I_2^{\bullet-}.8H_2O$ clusters. I atoms are shown by the largest green colour spheres, the smallest spheres refer to H atoms and the rest (red in colour) corresponds to O atoms in each structure shown in the figure. Marked alphabets in upper case are used to refer different minimum energy conformers for each hydrated cluster size arranged in order of stability showing 'A' as the most stable one.

To see the effect of hydration on the distribution of the excess electron in iodine dimer radical anion, $I_2^{\bullet-}$, Mulliken atomic spin (α–β) population over different atoms is calculated in the hydrated cluster, $I_2^{\bullet-}.nH_2O$ clusters (*n*=0-8). It is clearly observed that the odd electron spin is localized over the two I atoms only. Results suggest that the spin distribution of the odd electron does not change significantly on successive addition of solvent H_2O molecules in $I_2^{\bullet-}.nH_2O$ clusters (*n*=1-8). The nature of σ type *hemi* bond (*2c-3e*) between two I atoms in $I_2^{\bullet-}$ remains the same even after addition of successive water molecules. This observation is true for $Cl_2^{\bullet-}.nH_2O$ and $Br_2^{\bullet-}.nH_2O$ systems too.

2.3.1.2. Structure of X.*n*H_2O (X= NO_3^- and $CO_3^{\bullet-}$) Clusters

In the previous section, structures of diatomic anionic systems are discussed. In this section, structure of hydrated clusters of carbonate radical anion ($CO_3^{\bullet-}$) and nitrate anion (NO_3^-) is reported. To choose a suitable level of theoretical method for geometry search in these systems, geometrical parameters of mono-, di and tri-hydrated clusters of NO_3^- and $CO_3^{\bullet-}$ are carried out following 30 correlated density functionals (hybrid, pure and meta generalized gradient approximation density functionals). The caculated geometrical parameters are compared to that at MP2 theory adopting 6-311++G(d,p) basis functions. It is observed that Becke's three parameter non-local exchange (B3) and Lee-Yang-Parr (LYP) non-local correlation functionals (B3LYP) performs well to describe these clusters producing geometrical parameters close to MP2 results. Various possible initial structures of $NO_3^-.nH_2O$ and $CO_3^{\bullet-}.nH_2O$ clusters (*n*=1-8) are considered for geometry optimization and a number of minimum energy structures (conformers) are obtained for each size cluster as expected.

Different minimum energy structures obtained on full geometry optimization of each size hydrated cluster of nitrate anion, $NO_3^-.nH_2O$ (n=1-8) are displayed in Fig. 2.2. Two stable minimum energy structures are obtained on full geometry optimization of the monohydrate cluster, NO_3^--H_2O as shown in Fig. 2.2-I(A-B). In contrast to the earlier reported structure,[15] the most stable structure has a symmetric double-hydrogen-bonding (DHB) arrangement where two O atoms from NO_3^- group and two H-atoms of the solvent H_2O molecule are connected by H-bonding of length 2.06 Å. Calculated NO bond distances are 1.25 and 1.27 Å, respectively, for the spectator and H-bonded bonds. Structure I-B having one single hydrogen bonding (SHB) between one oxygen atom of the nitrate anion and H atom of the solvent H_2O molecule is less stable than the structure I-A by 2.78 kcal/mol. The calculated H-bond distance is 1.83 Å and so this SHB should be stronger than each DHB of structure I-A. Again, NO bond distances are 1.25 and 1.27 Å, respectively for the spectator and H-bonded bonds.

Three minimum energy structures are predicted for the di-hydrate cluster, $NO_3^-.2H_2O$ and displayed in Fig. 2.2-II(A-C). The structures are very close in energy with a difference in relative stability of < 2 kcal/mol. Structures II-A and II-C have two double-hydrogen-bonding (DHB) arrangements and both the solvent H_2O units are attached to the same two O atoms of NO_3^- in case of the less stable structure II-C. In case of II-C, none of the solvent H_2O units is in the NO_3^- plane, structure II-A is planar though. Structure II-B has two single hydrogen bonding (SHB) and one inter water hydrogen bonding (WHB) arrangements.

Five minimum energy structures displayed in Fig. 2.2-III(A-E) are predicted for tri-hydrate cluster, $NO_3^-.3H_2O$. Structure III-A is the most stable one having a cyclic three-member water network attached to two oxygen atoms of NO_3^- moiety. This particular structure consisting of three SHB and three WHB arrangements is more stable than the least stable structure III-E having two SHB, one DHB and one WHB arrangements by only ~1 kcal/mol. Structure III-B consisting of a cyclic three-member water network attached to all the three oxygen atoms is less stable than the structure III-A by 0.26 kcal/mol. Symmetric structure III-C having three DHB arrangements is 0.39 kcal/mol less stable compared to the most stable one. Structure III-D consisting of three SHB and two WHB arrangements is less stable by 0.66 kcal/mol compared to the structure III-A. Based on the optimized structures up to $NO_3^-.nH_2O$ (n=1-3), it is observed that the average energy of a single SHB and WHB arrangements are 7-11 kcal/mol and 5-8 kcal/mol, respectively. So, a balance between water-NO_3^- and water-water interactions decides the structure of hydrated anion clusters, $NO_3^-.nH_2O$.

As the number of solvent water molecules increases, a large number of minimum energy configurations are expected for a particular size of hydrated cluster. The initial structures for larger hydrated clusters are considered with a bottom-up approach based on the predicted stable structures from the smaller size hydrated clusters. Thus the initial guess structures for $NO_3^-.4H_2O$ cluster are considered based on the predicted minimum energy structures of $NO_3^-.nH_2O$ clusters (n=1-3), keeping a different number of symmetrical DHB, SHB and WHB arrangements. Six stable minimum energy structures are obtained for $NO_3^-.4H_2O$ cluster. The optimized structures are displayed in Fig. 2.2-

IV(A-F). Structure IV-A is more stable over the least stable conformer, IV-F by 5.16 kcal/mol. Structure IV-A consists of a four-member cyclic water network with four SHB and four WHB arrangements. But the structure IV-F consists of four SHB and two WHB arrangements. Structures IV-B and IV-C consist of one cyclic three member water network and one DHB water arrangement. Structure IV-D has one DHB, three SHB and two WHB arrangements. As one can see from the figure, structure IV-E has two DHB, two SHB and one WHB arrangements. At present no structure for $NO_3^-.4H_2O$ cluster is obtained where all the four solvent water units are in DHB arrangements.

Geometry optimization followed by Hessian calculations with various initial guess structures for the penta-hydrate cluster, $NO_3^-.5H_2O$ yields nine minimum energy structures having no imaginary frequency and the structures are displayed in Fig. 2.2-V(A-I). The most stable structure, V-A consists of one DHB arrangement and one cyclic four-member water network. Overall, four SHB, four WHB and one DHB arrangements are present in structure V-A. Structure V-B consisting one five-member water network is less stable than the most stable conformer by 2.29 kcal/mol. Structure V-I is the least stable conformer which is less stable than the most stable conformer, V-A by 8.30 kcal/mol. Structure V-I consists of one DHB, five SHB and two WHB arrangements. Structures V-D, V-E and V-F have one cyclic three member water network. Remaining conformers have different number of DHB, SHB and WHB arrangements. As can be seen from Table I, structures V-(C-I) are very close in energy (< 2.42 kcal/mol).

Nine different minimum energy structures displayed in Fig. 2.2-VI(A-I) having all real frequency, are obtained for the $NO_3^-.6H_2O$ cluster. The most stable structure of $NO_3^-.6H_2O$ cluster (VI-A) has one DHB and one cyclic five member water network

arrangements. In total, it has one DHB, four SHB and five WHB arrangements. This structure is more stable than the least stable structure VI-I by 11.03 kcal/mol. Structure VI-I has six SHB and three WHB arrangements. Structure VI-B having two DHB and one cyclic four-member water network arrangements is less stable than the structure VI-A by 1.90 kcal/mol. Structures VI-D and VI-E both have two cyclic three member water networks and structure VI-F has one cyclic three member water network arrangement. These are two interior 3D structures in which the solute is surrounded by two H-bonded solvent water networks. In case of the minimum energy structure VI-G, a solvent water molecule is not directly connected to NO_3^- moiety, though all the six water molecules were kept directly connected to the NO_3^- moiety in the initial guess structure. Structure VI-G has one DHB, four SHB and two WHB arrangements.

Ten minimum energy configurations are predicted for $NO_3^-.7H_2O$ cluster and the final optimized structures are displayed in Fig. 2.2-VII(A-J). Hessian calculations do not produce any normal mode having imaginary frequency for these structures. This confirms that the predicted minimum energy configurations correspond to true equilibrium structures of $NO_3^-.7H_2O$ cluster. The most stable structure, VII-A has a cyclic five member water network arrangement and the solute anion, NO_3^- resides at the surface. Similar geometrical arrangements keeping the solute at the surface are also observed in case of structures VII(B-E) and VII(H-J). Interior structures in which the solute is surrounded by solvent water units are predicted for two minimum energy configurations, VII(F-G).

On full geometry optimization of $NO_3^-.8H_2O$ cluster, twelve minimum energy structures are predicted and the final optimized structures are displayed in Fig. 2.2-VIII(A-L). None of these structures yields imaginary frequency on Hessian calculations suggesting these minimum energy configurations as true equilibrium structures. As in case of the hepta- hydrated cluster, the most stable structure has a cyclic five member water network arrangement keeping the solute anion at the surface. Similar geometrical arrangements, keeping the solute at the surface, are also observed in the remaining of structures except for the structures VIII-H and VIII-K. In these two cases, NO_3^- is trapped inside H-bonded solvent water networks.

In all the minimum energy configurations of $NO_3^-.nH_2O$ cluster, NO bond distance is calculated in the range of 1.25-1.27 Å. The calculated distance between O of NO_3^- and H-bonded H atoms is 1.8-2.3 Å and the distance between O and H atoms in inter water network (WHB) is 1.8-2.0 Å. In all the structures, the calculated SHB distance is shorter than that of DHB distance. Structure having cyclic inter water H-bonding network is more stable over other structures in a particular size of hydrated cluster. It is observed that more than three solvent water molecules cannot reside in a DHB arrangement in these hydrated clusters. It is also observed that more than five water molecules cannot stay in the cyclic water network. Most of the minimum energy configurations in $NO_3^-.nH_2O$ cluster show surface structure in which the solute resides at the surface of the solvent water network. In case of large size hydrated clusters,

$NO_3^-.nH_2O$ (n ≥ 6), a few equilibrium geometries are predicted showing interior structure in which the solute resides inside the solvent water network. However, surface structures are observed to be more stable than corresponding interior structures.

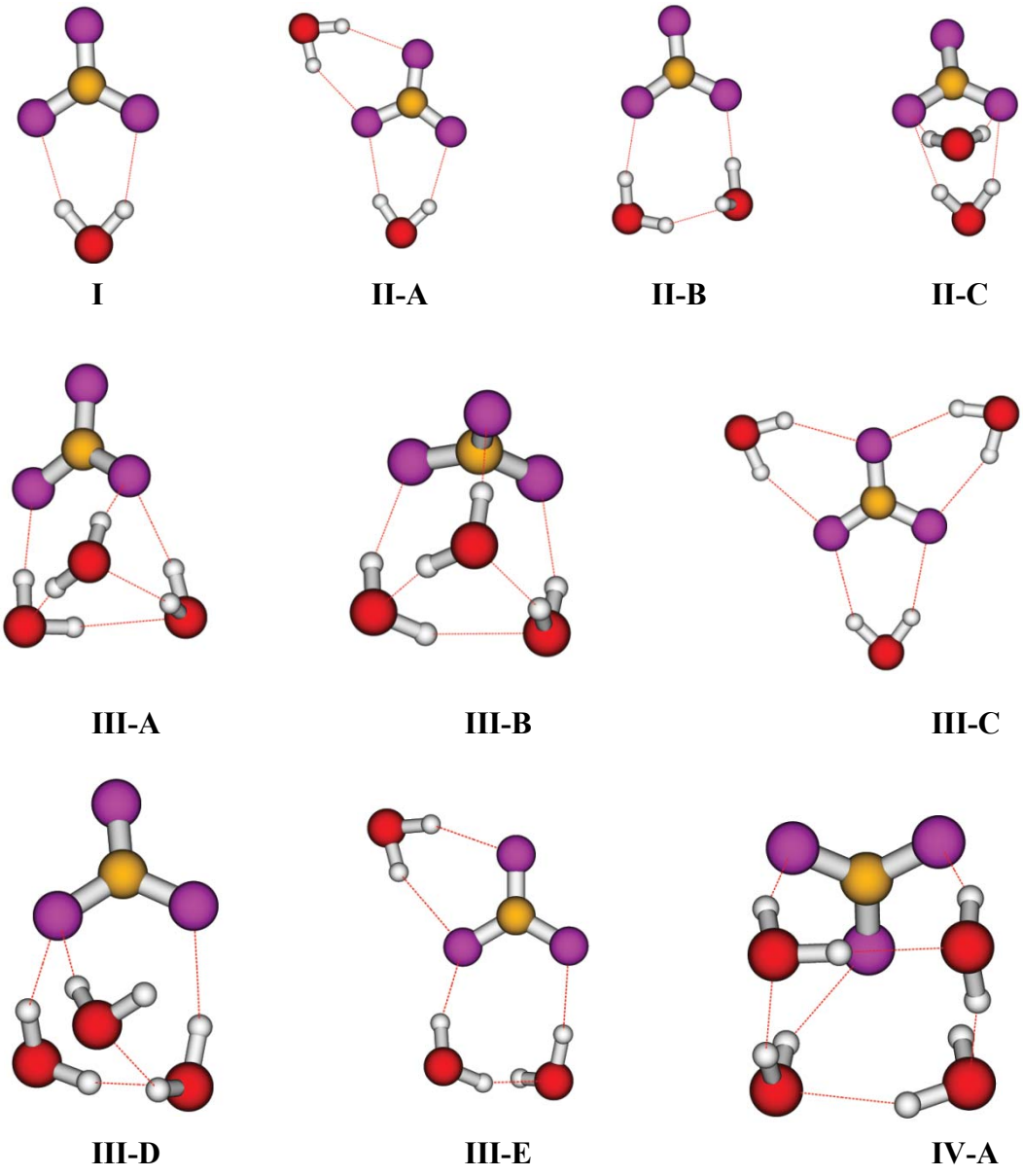

Fig. 2.2 (Contd.)

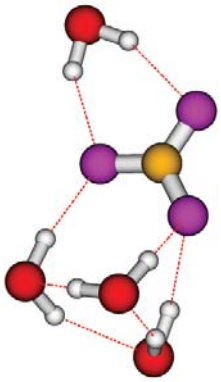

IV-B

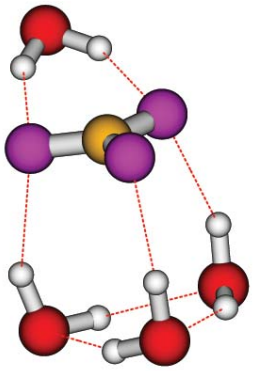

IV-C

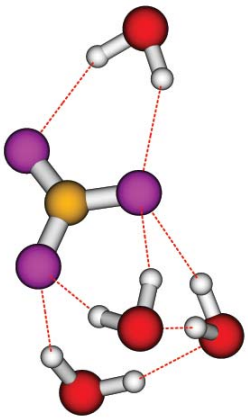

IV-D

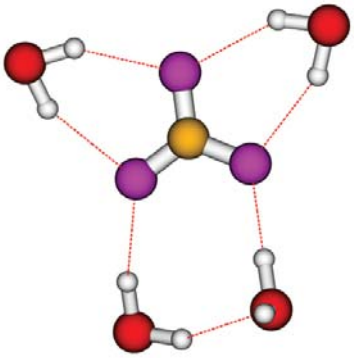

IV-E

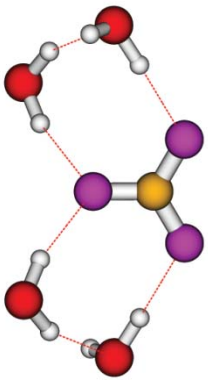

IV-F

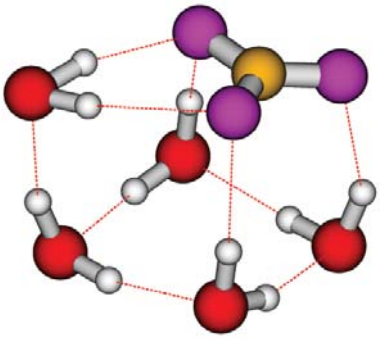

V-A

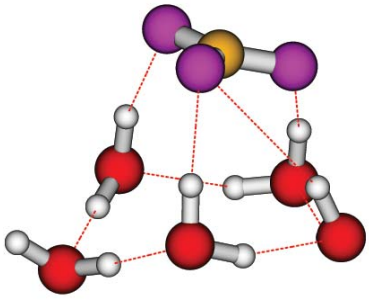

V-B

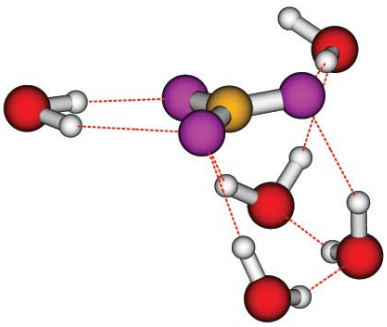

V-C

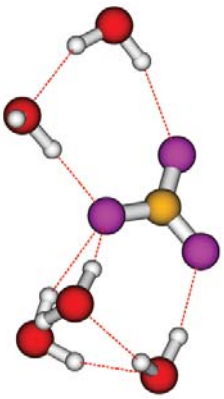

V-D

Fig. 2.2 (Contd.)

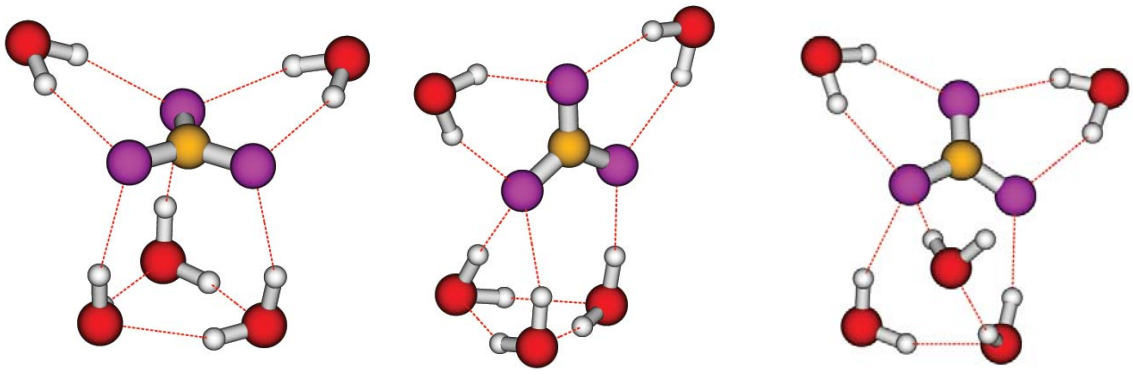

V-E **V-F** **V-G**

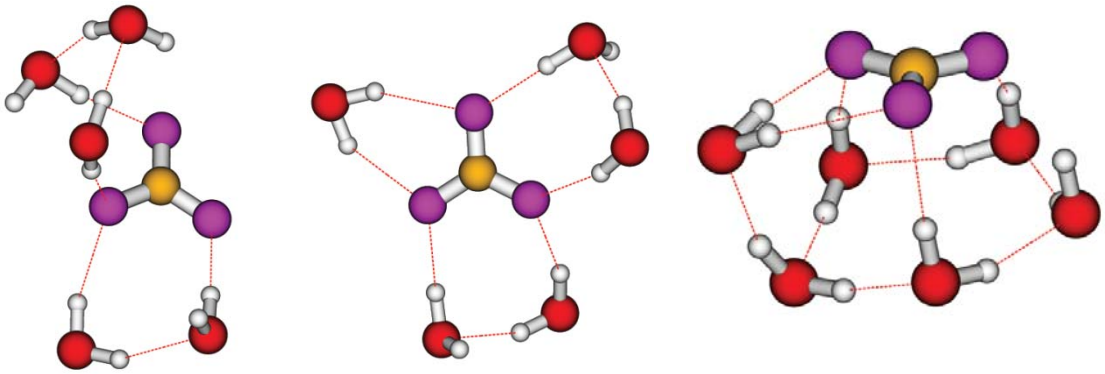

V-H **V-I** **VI-A**

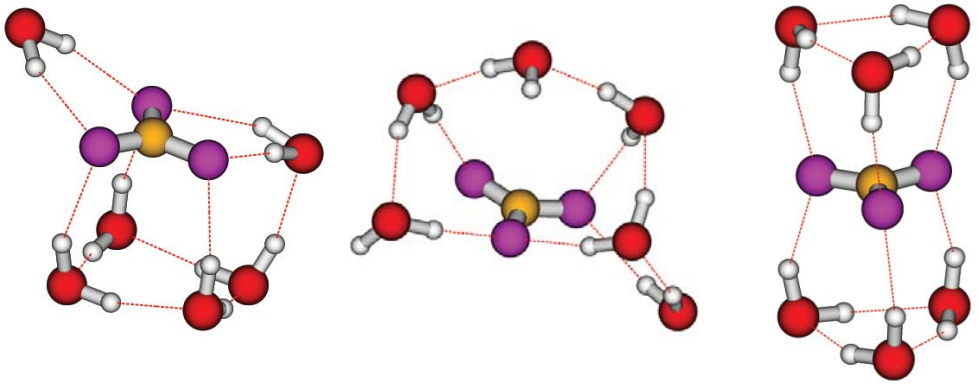

VI-B **VI-C** **VI-D**

Fig. 2.2 (Contd.)

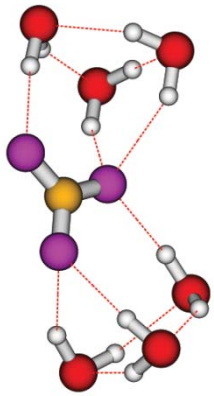

VI-E

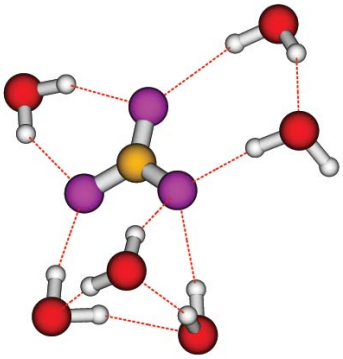

VI-F

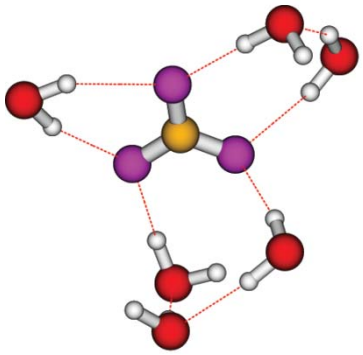

VI-G

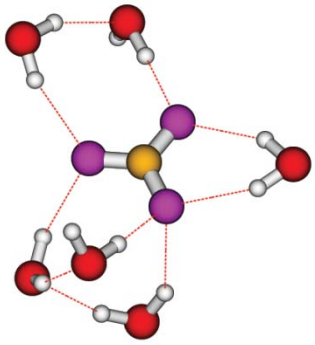

VI-H

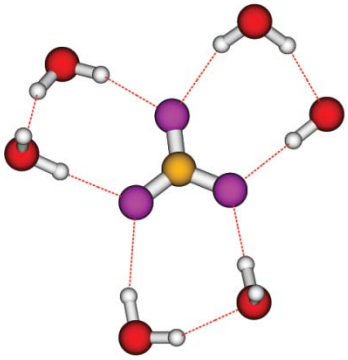

VI-I

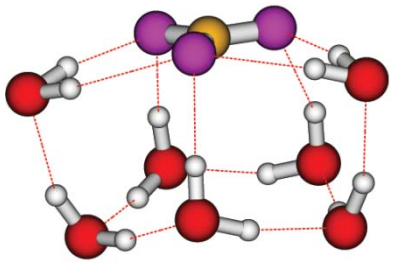

VII-A

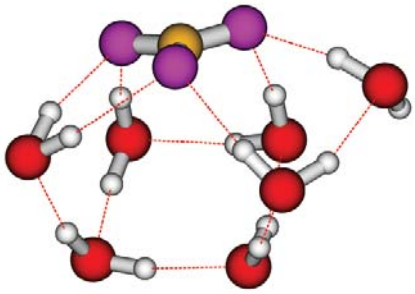

VII-B

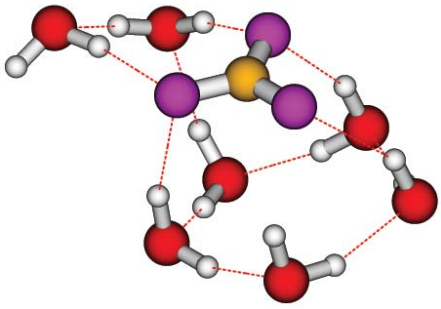

VII-C

Fig. 2.2 (Contd.)

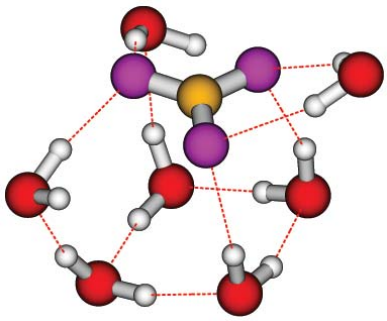

VII-D

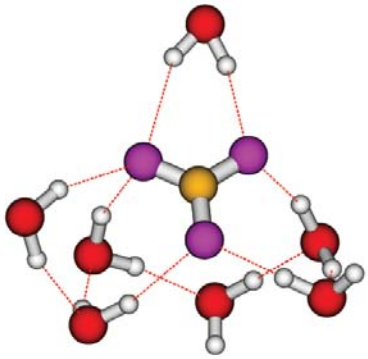

VII-E

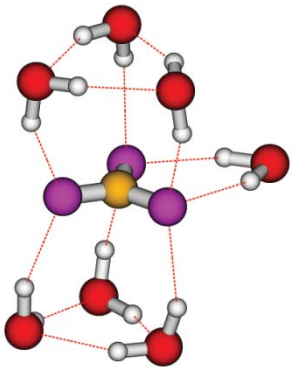

VII-F

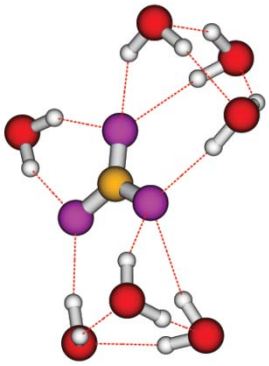

VII-G

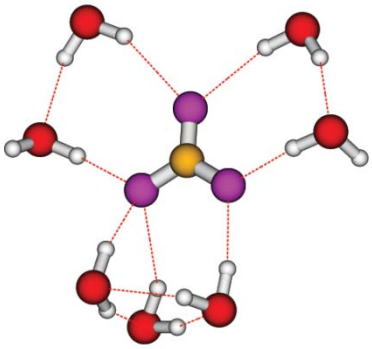

VII-H

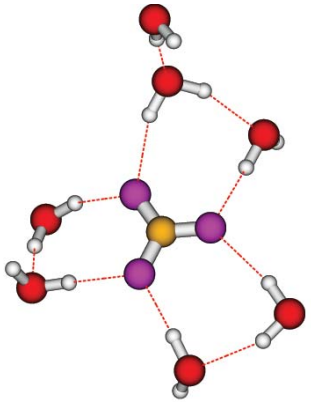

VII-I

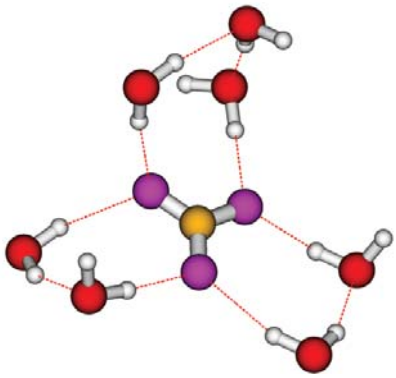

VII-J

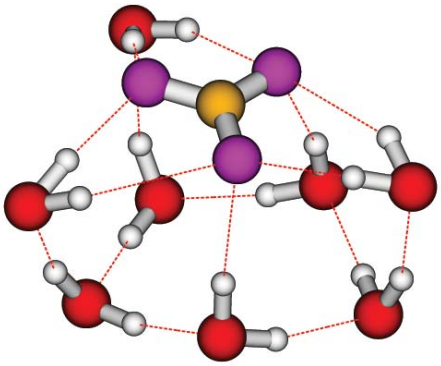

VIII-A

Fig. 2.2 (Contd.)

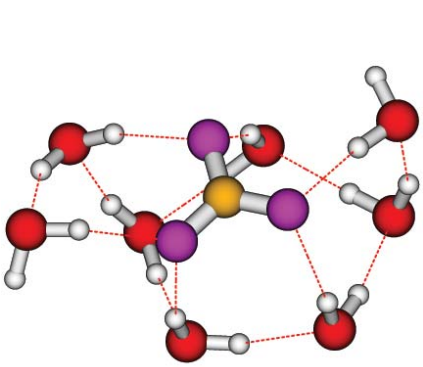

VIII-B

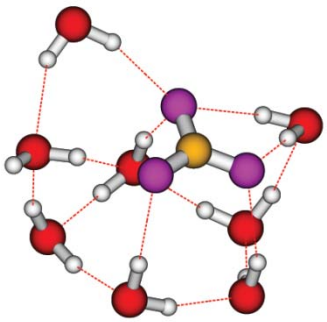

VIII-C

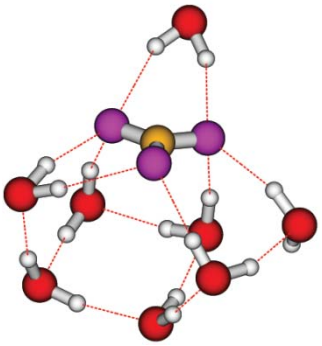

VIII-D

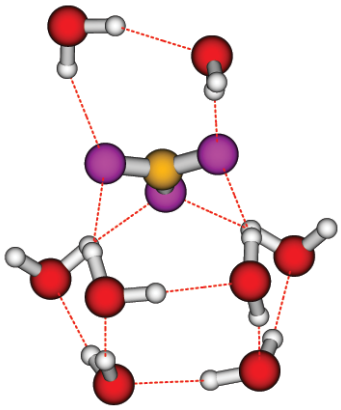

VIII-E

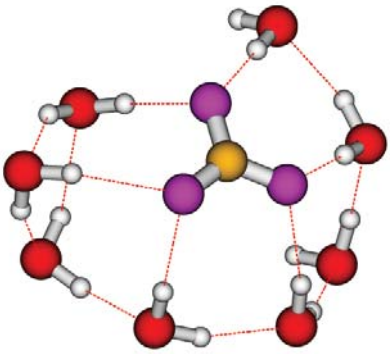

VIII-F

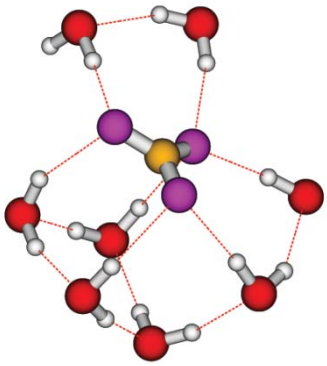

VIII-G

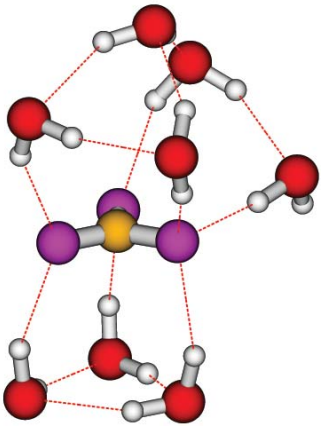

VIII-H

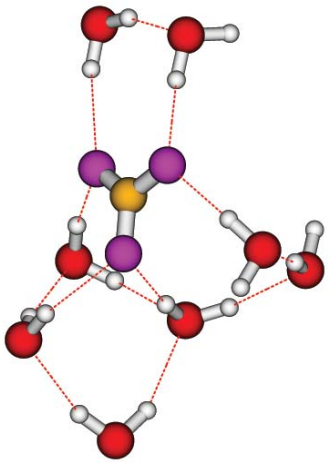

VIII-I

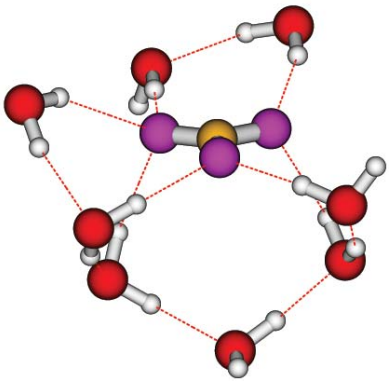

VIII-J

Fig. 2.2 (Contd.)

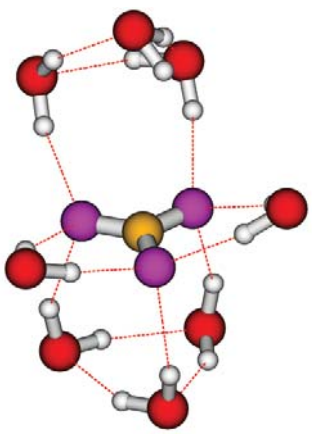

VIII-K

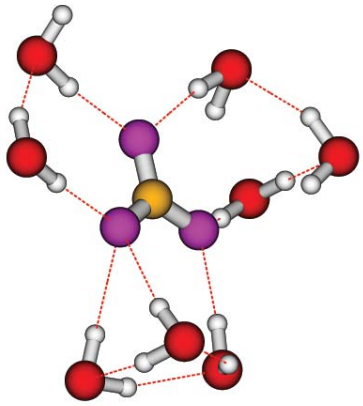

VIII-L

Fig.2.2. Fully optimized minimum energy structures at B3LYP/6-311++G(d,p) level of theory for (I) $NO_3^-.H_2O$, (II) $NO_3^-.2H_2O$, (III) $NO_3^-.3H_2O$, (IV) $NO_3^-.4H_2O$, (V) $NO_3^-.5H_2O$, (VI) $NO_3^-.6H_2O$, (VII) $NO_3^-.7H_2O$ and (VIII) $NO_3^-.8H_2O$. N atoms are shown by the yellow colour spheres, the smallest spheres refer to H atoms and the rest corresponds to O atoms in each structure shown in the figure. Pink colour spheres refer to the nitrate O atoms and rest (red in colour) for water O atoms. Marked alphabets in upper case are used to refer different minimum energy conformers for each hydrated cluster size arranged in order of stability showing 'A' as the most stable one.

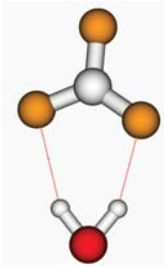

A

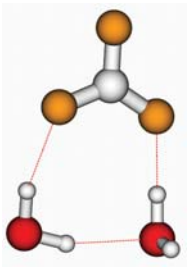

B

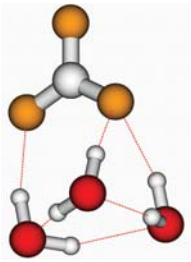

C

Fig.2.3 (Contd.)

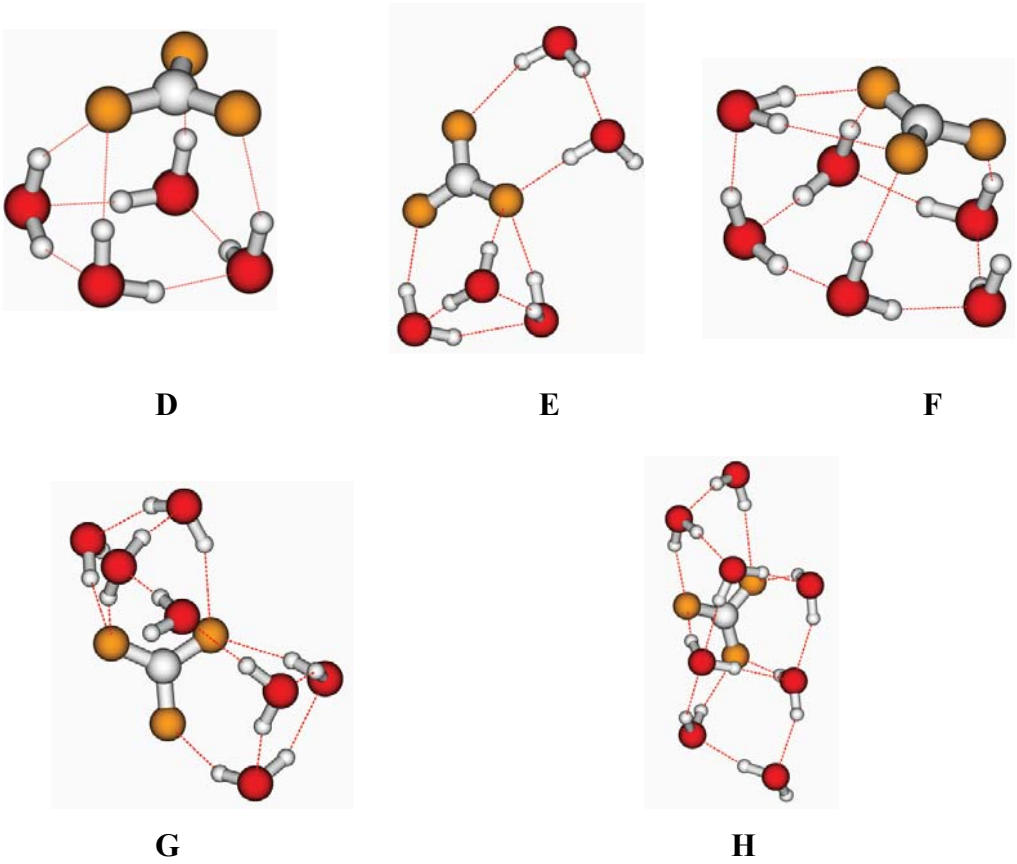

Fig.2.3. Fully optimized most stable structures at B3LYP/6-311++G(d,p) level of theory for (A) $CO_3^{\bullet-}.H_2O$, (B) $CO_3^{\bullet-}.2H_2O$, (C) $CO_3^{\bullet-}.3H_2O$, (D) $CO_3^{\bullet-}.4H_2O$, (E) $CO_3^{\bullet-}.5H_2O$, (F) $CO_3^{\bullet-}.6H_2O$, (G) $CO_3^{\bullet-}.7H_2O$ and (H) $CO_3^{\bullet-}.8H_2O$. C atoms are shown by the grey colour spheres, the smallest spheres refer to H atoms and the rest correspond to O atoms in each structure shown in the figure. Yellow colour spheres refer to the carbonate O atoms and rest (red in colour) for water O atoms.

The structures of the various conformations of $CO_3^{\bullet-}.nH_2O$ clusters are very similar to that of $NO_3^-.nH_2O$ clusters. So, only the most stable structures of $CO_3^{\bullet-}.nH_2O$ clusters are displayed in Fig. 2.3. The $CO_3^{\bullet-}.nH_2O$ clusters are stabilized by double hydrogen bonding (DHB), single hydrogen bonding (SHB) as well as inter water hydrogen bonding (WHB). H-bonded water network having two, three, four or five H_2O units are present in different conformers of these clusters. Surface structures are preferred upto tetra- hydrated cluster keeping the solute anion at the surface of the solute water

clusters. Hydrated cluster having cyclic water network units, is the most stable conformer for each size cluster (see Fig. 2.3). In each case, the distance between the C and O atoms of carbonate moiety ($CO_3^{\bullet-}$) is ~ 1.3 Å. The calculated distance between O (of $CO_3^{\bullet-}$) and H-bonded H atoms is 1.8-2.2 Å (SHB and DHB bond) and the distance between O and H atoms in the inter water network is 1.9-2.1 Å (WHB bond).

2.3.1.3. Structure of $CO_3^{2-}.nH_2O$ Clusters

In the previous two sections, structures of singly anionic species are discussed. It is also interesting to study structure of microhydrated polyatomic species with doubly negative charge like carbonate anion (CO_3^{2-}). On full geometry optimization at B3LYP/6-311++G(d.p) level of theory, different minimum energy structures are obtained for each size of hydrated carbonate dianion cluster, $CO_3^{2-}.nH_2O$ (n=1-6). It is observed that the structures of conformers of each size of $CO_3^{2-}.nH_2O$ cluster are very close to those obtained for $NO_3^-.nH_2O$ and $CO_3^{\bullet-}.nH_2O$ clusters. The most stable structure for each size of hydrated cluster, $CO_3^{2-}.nH_2O$ is displayed in Fig. 2.4. It is clear from the figure that $CO_3^{2-}.nH_2O$ clusters are stabilized by double hydrogen bonding (DHB), single hydrogen bonding (SHB) as well as inter water hydrogen bonding (WHB). H-bonded water network having two or three, H_2O units are present in the different conformers of these clusters. But structures with cyclic water network is not the most stable structures for n=3-5 in contrast to the other hydrated clusters of $Cl_2^{\bullet-}$, $Br_2^{\bullet-}$, $I_2^{\bullet-}$, $CO_3^{\bullet-}$ and NO_3^-. For n=6, the most stable structure has one cyclic water network. No structure with four of higher member water network is found. In each case, the distance between the C and O atoms of the carbonate moiety (CO_3^{2-}) is ~ 1.3 Å. The calculated distance between O (of

CO_3^{2-}) and H-bonded H atoms is 1.7-2.1 Å (SHB and DHB bond) and the distance between O and H atoms in inter water network is 1.7-2.1 Å (WHB bond).

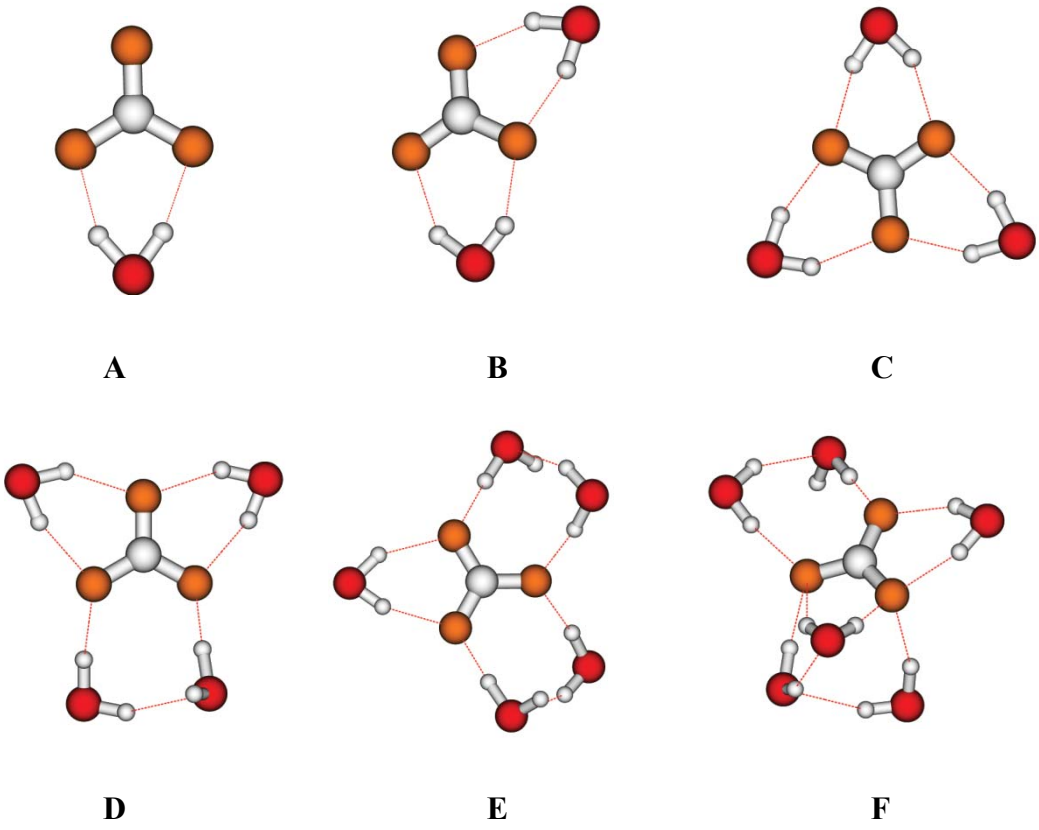

Fig.2.4. Fully optimized most stable structures at B3LYP/6-311++G(d,p) level of theory for (A) $CO_3^{2-}.H_2O$, (B) $CO_3^{2-}.2H_2O$, (C) $CO_3^{2-}.3H_2O$, (D) $CO_3^{2-}.4H_2O$, (E) $CO_3^{2-}.5H_2O$, and (F) $CO_3^{2-}.6H_2O$. C atoms are shown by the grey colour spheres, the smallest spheres refer to H atoms and the rest correspond to O atoms in each structure shown in the figure. Yellow colour spheres refer to the carbonate O atoms and rest (red in colour) for water O atoms.

It is to be noted that the geometry of small size hydrated clusters, X. $n$$H_2O$ (n=1-3; X= $Cl_2^{\bullet-}$, $Br_2^{\bullet-}$, $I_2^{\bullet-}$, $CO_3^{\bullet-}$, NO_3^- and CO_3^{2-}) are also calculated incorporating correction due to basis set superposition error (BSSE) following counterpoise method.[45]

However, these calculations do not lead to any significant change in the structural parameters of these hydrated clusters.

2.3.2. Solvent Stabilization and Interaction Energy

The stabilzation energy of $I_2^{\bullet-}.nH_2O$ clusters can be expressed as

$$E^{solv} = E_{I_2^-.nH_2O} - (nE_{H_2O} + E_{I_2^-}),$$

where $E_{I_2^-.nH_2O}$, E_{H_2O} and $E_{I_2^-}$ refer to the total energy of the cluster $I_2^{\bullet-}.nH_2O$, the energy of a single H_2O molecule and the energy of the bare $I_2^{\bullet-}$ system, respectively. Thus, E^{solv} essentially refers to the total interaction energy of the solute with *n* solvent H_2O units around it in the hydrated cluster of size *n*. A number of minimum energy configurations are obtained in these hydrated clusters and it is increasing with the size (*n*) of the cluster. It is understood that at a particular temperature there will be a statistical contribution of the conformers of a particular size to the overall property. So the weighted average solvent stabilization energy (E_w^{solv}) values are calculated and provided in Table 1. The plot for the variation of E_w^{solv} *vs*. *n* is shown in Fig. 2.5(a). The weight factor of a conformer within a particular size (*n*) of the cluster is calculated based on the Boltzmann statistical population of the conformer at 150 K. It is observed that E_w^{solv} varies linearly with *n*, the number of water molecules in the hydrated clusters and the variation of E_w^{solv} is best fitted as

E_w^{solv} = -0.83 + 11.25 *n*,

When, E_w^{solv} is expressed in kcal/mol and *n* is the number of water molecules. This linear fitted plot has correlation coefficient ~ 0.999 promising the power of prediction of

solvation energy for larger hydrated clusters. The slope of the best-fitted linear equation suggests that the solvation energy per solvent water unit is 11.25 kcal/mol. In other words, on an average each additional H-bond provides a solvent stabilzation of 5.6 kcal/mol at large *n* limit, assuming each additional solvent water molecule increases the number of H-bonds by two. However, this assumption is valid for very large size (*n*) of cluster. It is worthwhile to mention that basis set superposition error (BSSE) calculated for mono- and di- hydrated clusters following counterpoise method [45] is less than 10%.

It is to be noted that the stabilzation energy for the hydrated cluster, $I_2^{\bullet-}.nH_2O$ calculated by discrete model corresponds to the internal energy of the molecular clusters. The stabilzation energy of the clusters (E_w^{solv} or E^{solv}) naturally increases with the increase in the number of solvent molecules accounting ion-solvent interaction as well as inter water H-bonding interaction. However, stabilzation energy has the status of free energy in case of the continuum model. One can see form Fig. 2.5 that stabilzation energy profiles do not indicate closing of any geometrical shell. Thus, it does not provide any information on the hydration number of $I_2^{\bullet-}$.

To estimate the energy of interaction between the solute dimer radical anion, $I_2^{\bullet-}$ and the water cluster, $(H_2O)_n$, a quantity, interaction energy (E^{int}) in $I_2^{\bullet-}.nH_2O$ clusters can be defined as

$$E^{\text{int}} = E_{I_2^-.nH_2O} - (E_{(H_2O)_n} + E_{I_2^-}),$$

where, $E_{I_2^-.nH_2O}$, $E_{(H_2O)_n}$ and $E_{I_2^-}$ refer to the energy of the cluster $I_2^{\bullet-}.nH_2O$, the energy of $(H_2O)_n$ system and the energy of $I_2^{\bullet-}$ system, respectively. The energy of the $(H_2O)_n$ system is calculated by removing iodine part from the optimized geometry of that

Table 2.1. Weighted average energy values for $I_2^{\bullet-}.nH_2O$ clusters (n=1-8) at BHHLYP/6-311++G(d,p) level of theory (for I atom split valence 6-311 basis set is used).

$I_2^{\bullet-}.nH_2O$[#]	Weighted average solvation energy, E_w^{solv} (kcal/mol)	Weighted average interaction energy, E_w^{int} (kcal/mol)	Weighted average vertical detachment energy, VDE_w (eV)
n=1 (1)	10.69	10.88	4.51
n=2 (2)	20.33	20.37	4.92
n=3 (4)	32.43	24.52	5.03
n=4 (7)	46.9	27.7	5.14
n=5 (7)	56.43	34.87	5.45
n=6 (7)	64.33	40.6	5.66
n=7 (7)	77.31	43.77	5.77
n=8 (9)	89.97	45.47	5.85

[#] Values in the parentheses are the number of minimum energy structures for each size of clusters.

hydrated cluster followed by single point energy calculation at the same level of theory. $E_{I_2^-}$ is also evaluated in the same way, i.e., by removing the water part of the optimized structure followed by the single point energy calculation. Weighted average interaction energy, E_w^{int} is also calculated for all the hydrated clusters and the results are tabulated in Table 2.1. The plot of E_w^{int} *vs*. n is displayed in Fig. 2.5(b) showing the geometrical shell closing at n=4 and n=8. The geometrical shell closing is due to the formation of respective one and two H-bonded water tetramers surrounding the solute. Thus, though the stabilzation energy profiles show a linear increment in energy with the successive addition of solvent H_2O units for $I_2^{\bullet-}.nH_2O$ (n=1-8) clusters, the interaction energy

profiles show saturation behaviour with the successive addition of solvent H_2O units for $I_2^{\bullet-}.nH_2O$ (n =1-8) clusters.

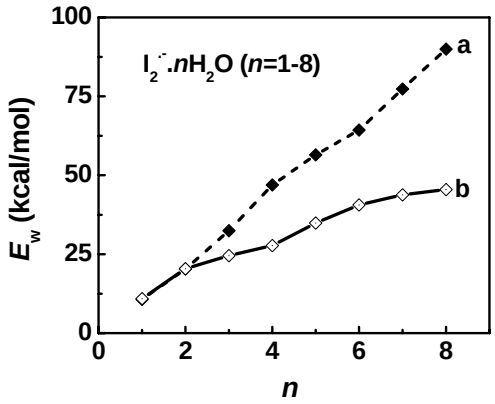

Fig. 2.5. Plot of calculated weighted average (a) solvent stabilization energy (E_w^{solv}) and (b) interaction energy (E_w^{int}) in kcal/mol *vs*. number of water molecules (n) in $I_2^{\bullet-}.nH_2O$ (n=1-8) cluster at BHHLYP/6-311++G(d,p) level of theory. To estimate E_w^{solv} and E_w^{int} the weight factor is calculated based on the statistical population of all the conformers of each size cluster at 150 K.

The variation of weighted average solvation energy and weighted average interaction energy with the size of the cluster is similar for all other hydrated cluster, X.nH_2O (X= $Cl_2^{\bullet-}$, $Br_2^{\bullet-}$, $CO_3^{\bullet-}$, NO_3^- and CO_3^{2-}).

2.3.3. Vertical Detachment Energy

Vertical detachment energy (VDE) of the hydrated clusters, $I_2^{\bullet-}.nH_2O$ can be defined by the relation:

$$VDE = E[I_2^{\bullet-}.nH_2O] - E^s[I_2.nH_2O]$$

Where, E[$I_2^{\bullet-}$.$n$$H_2O$] is the energy of the optimized $I_2^{\bullet-}$.$n$$H_2O$ cluster and E^s[I_2.$n$$H_2O$] is the single point energy of the I_2.$n$$H_2O$ obtained by removing the extra electron from the optimized $I_2^{\bullet-}$.$n$$H_2O$ cluster. VDE is the energy required to remove an electron from the anionic hydrated clusters. It is clearly observed that the conformer that has higher interaction energy, E^{int} has higher VDE in each size (n) cluster. The weighted average VDE (VDE_w) is also calculated based on the statistical population of different conformers for each size (n) cluster and displayed in Table 2.1. Fig. 2.6-I displays the plot of VDE_w *vs*. n showing the similar nature of shell closing at n=4 and n=8 as in case of E_w^{int} plot. It is worthwhile to mention that the variation of weighted average vertical detachment energy with the size of the cluster is similar for all other hydrated cluster, X. $n$$H_2O$ (X= $Cl_2^{\bullet-}$, $Br_2^{\bullet-}$, $CO_3^{\bullet-}$, NO_3^- and CO_3^{2-}).

As it is discussed, the plot of interaction energy (E^{int}) and vertical detachment energy (VDE) *vs*. number of water molecules (n) in these hydrated clusters ($I_2^{\bullet-}$.$n$$H_2O$) behave in a similar way. So it is interesting to test if there is any direct correlation between these two energy terms. For $I_2^{\bullet-}$.$n$$H_2O$ clusters (n=1-8), weighted average interaction energy, E_w^{int} is related to the statistical weighted average vertical detachment energy, VDE_w by a simple linear relation,

$$E_w^{\text{int}} = -4.64 + 1.13\ VDE_w$$

Where, both E_w^{int} and VDE_w are expressed in eV. The best fit linear plot with the graphical data points are shown in Fig. 2.6-II(a).

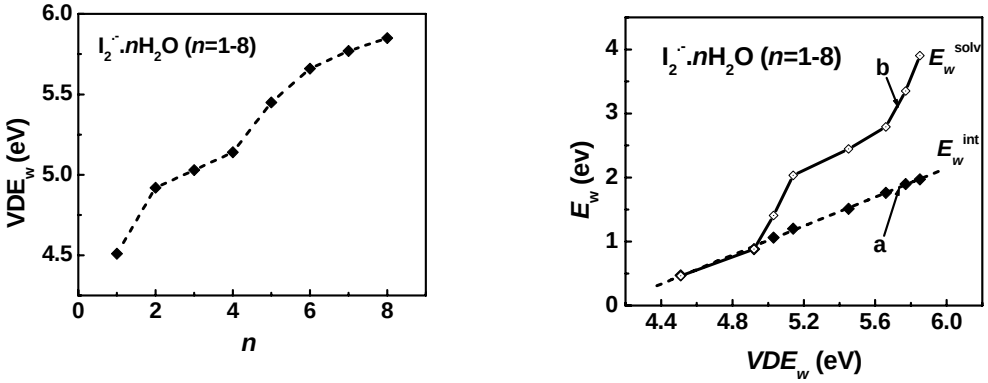

I **II**

Fig. 2.6. (I) Plot of calculated weighted average vertical detachment energy (VDE_w) in eV *vs*. number of water molecules (*n*) in $I_2^{\bullet-}.nH_2O$ (*n*=1-8) cluster at BHHLYP/6-311++G(d,p) level of theory (II) Plot of calculated weighted average (a) interaction, E_w^{int} in eV *vs*. weighted in eV for the hydrated cluster, $I_2^{\bullet-}.nH_2O$ ($n \leq 8$) showing a linear relationship and (b) solvation energy, E_w^{solv} in eV *vs*. weighted average vertical detachment energy (VDE_w) in eV for the hydrated cluster, $I_2^{\bullet-}.nH_2O$ ($n \leq 8$).

Plot of the weighted average stabilzation energy, E_w^{solv} in eV *vs*. the weighted average vertical detachment energy (VDE_w) in eV for the hydrated cluster, $I_2^{\bullet-}.nH_2O$ ($n \leq 8$) is displayed in Fig. 2.6-II(b). No simple relation is observed between calculated E_w^{solv} and VDE_w. It is worthwhile to mention that VDE is a measurable quantity following photoelectron spectroscopy and based on the above simple linear relation, E^{int} for a hydrated cluster can be extracted. $I_2^{\bullet-}.(CO_2)_n$ and $I_2^{\bullet-}.(OCS)_n$ systems are well studied following photoelectron spectroscopy and measured VDE values for different cluster size are reported in the literature.[48-49]

The variation of the weighted average vertical detachment interaction energy with the size of the cluster is similar for all other hydrated clusters, X. $n$$H_2O$ (X= $Cl_2^{\bullet-}$, $Br_2^{\bullet-}$, $CO_3^{\bullet-}$, NO_3^- and CO_3^{2-}).

2.4. Conclusions

Minimum energy structures of X. $n$$H_2O$ (X= $Cl_2^{\bullet-}$, $Br_2^{\bullet-}$ & $I_2^{\bullet-}$) are calculated applying BHHLYP functional and minimum energy structures of X. $n$$H_2O$ (X=$CO_3^{\bullet-}$, NO_3^- & CO_3^{2-}) are optimized applying B3LYP functional with a triple split valence 6-311++G(d,p) basis function (I is treated by 6-311 basis set). It is observed that all the hydrated clusters are stabilized by double hydrogen bonding (DHB), single hydrogen bonding (SHB) as well as inter water hydrogen bonding (WHB). Hydrated cluster having cyclic water network units is the most stable conformer for each size of the cluster, except CO_3^{2-}. $n$$H_2O$, where structure with SHB and DHB interaction is the most preferred one for n<6. Up to four solvent H_2O units can reside around the solute in a cyclic inter-water hydrogen bonded network for X. $n$$H_2O$ (X= $Cl_2^{\bullet-}$, $Br_2^{\bullet-}$ & $I_2^{\bullet-}$) cluster. On the other hand a maximum of five H_2O units can reside around the solute in a cyclic inter-water hydrogen bonded network for X. $n$$H_2O$ (X=$CO_3^{\bullet-}$, NO_3^- & CO_3^{2-}) cluster. The weighted average interaction and solvent stabilization energy are calculated for all the clusters. It is observed that the solvent stabilization energy continuously increases with the successive addition of solvent H_2O units and is much larger than the interaction energy for larger hydrated clusters. The calculated weighted average vertical detachment energy (VDE) is also reported for all the clusters. Energy of interaction and vertical detachment energy profiles show stepwise saturation indicating geometrical shell closing

in the hydrated clusters. A linear correlation is also obtained between the weighted interaction and the vertical detachment energy. Population of the conformers of each size of clusters has been calculated based on free energy change (ΔG) at 150 K following Boltzmann distribution.

CHAPTER 3

IR Spectra of Water Embedded Anionic Clusters

3.1. Introduction

Recently, size selected gas-phase infrared (IR) cluster spectroscopy combined with first principle based theoretical studies are being successfully applied to explore the molecular level interaction during the process of microhydration. Theoretical analysis of the observed IR band in the O-H stretching region of water of a particular cluster have yielded an understandable picture of how hydrogen bonding water networks are deformed when they attach to small solute anions.[7-8,23] IR spectra of size selected cluster are being widely applied to understand the geometry and growth motif of various chemical species during the process of microhydration. In this context, mostly spherical halide anions (F^-, Cl^-, Br^- and I^-) are studied.[7-8] Microhydration of diatomic and polyatomic species like OH^-, O_2^-, $NO^{\bullet-}$, SO_4^{2-}, etc are also studied based on IR spectroscopy.[8,15,23,25-26] It is understood from the studies that the smaller size solute – water cluster is stabilized by single (SHB) or double hydrogen bonding (DHB) and inter water hydrogen bonding (WHB). In the larger cluster the water network form cyclic arrangement to stabilize a particular cluster.

In this chapter, IR spectra of halogen dimer radical anions ($Cl_2^{\bullet-}$, $Br_2^{\bullet-}$ & $I_2^{\bullet-}$), carbonate radical anion ($CO_3^{\bullet-}$), nitrate anion (NO_3^-) and carbonate anion (CO_3^{2-}) systems have been studied by *first principle* based electronic structure methods to

generate IR spectra. Such study should help to enhance our understanding on molecular level interactions between solvent water molecules and negatively charged ions in the aqueous solution. The IR studies on size selected hydrated anion clusters also play a critical role to follow the evolution of molecular properties with the number of solvent water molecules present in the cluster and to bridge the gap between the monohydrated cluster to the ion (I^-) in bulk aqueous solution, I^-(aq). Recently IR spectra of $Cl_2^{\bullet-}.nH_2O$ (n=1-5) is reported based on size selected cluster spectroscopy by Johnson and coworkers.[24] In this chapter, theoretical IR spectra of $Cl_2^{\bullet-}.nH_2O$ are reported in detail and compared with the experimental ones. Weighted average IR spectra is calculated based on the statistical population of different minimum energy configurations of a particular size hydrated cluster at 100 K. Fourier transform to the dipole auto-correlation function is also carried out to include dynamical contribution to the calculated IR spectra.

3.2. Theoretical Approach

Vibrational analysis is performed at the same level of theory as for geometry search discussed in chapter 2 to generate IR spectra following harmonic approximations. Frequency of different normal modes of a few small hydrated clusters is also calculated by taking anharmonic nature of vibration using vibrational self-consistent field (VSCF) method. With the increase in number of solvent water molecules in hydrated clusters, the number of minimum energy configurations with close in energy for hydrated clusters of each size is expected to increase. Experimental IR spectrum of particular size of cluster includes contribution from all possible minimum energy structures, which are survived at that particular experimental condition. Thus weighted average properties of clusters

become more meaningful. At present, weighted average IR spectra for different clusters is calculated and compared with the available experimental spectra. Population (P_i) of the conformers of each size clusters has been calculated based on free energy change (ΔG_i) at a particular temperture (T) following Boltzmann distribution i. e. $P_i = Exp(-\Delta G_i/kT)$. The weighted average IR spectra is constructed as IR(weighted average) = $\sum_i P_i IR_i$. *Ab initio* molecular dynamics simulations, namely Car-Parrinello molecular dynamics (CPMD) simulations have also been carried out for different time durations at different tempetures.[50] These simulations have been carried out using the BLYP functional with fictitious electron mass of 600 a.u. and an integration step of Δt = 5 au (0.12 fs). The core-valence interaction was described by a norm-conserving Trouiller-Martins pseudopotential.[51] Valence wave functions were expanded in a plane wave basis set with an energy cutoff value of 120 Ry, which is greater than the normally used value of 90 Ry. Poisson solver using the Tuckerman method on the reciprocal space have been applied.[52]. A Nose-Hoover thermostat[53] has been attached to every degree of freedom to ensure proper thermalization over the CPMD trajectory. During the simulations, the clusters have been kept at the center of an isolated cubic box of fixed side length (12Å for $Cl_2^{\bullet-}.3H_2O$, 14Å for $Cl_2^{\bullet-}.4H_2O$ and16Å for $Cl_2^{\bullet-}.5H_2O$). On the basis of the CPMD simulations, time correlation functions have been generated. The Fourier transform of dipole moment and velocity autocorrelation functions (FT-DACF/FT-VACF) have been carried out to include dynamical contribution to the IR spectra. The IR absorption spectrum can be computed from FT-DACF[54]

$$I(\omega) = \frac{h\beta}{(2\pi)^2}\omega^2 \int dt e^{-i\omega t} < \mu(0).\mu(t) >$$

Here, the symbols are used to denote intensity (I), frequency (ω), Plank constant ($\hbar$) inverse of Boltzmann constant multiplied by temperature (β) $1/kT$), time (t), and dipole moment (μ).

3.3. Results and Discussion

The clusters, X. $n$$H_2O$ (X= $Cl_2^{\bullet-}$, $Br_2^{\bullet-}$, $I_2^{\bullet-}$, $CO_3^{\bullet-}$, NO_3^- and CO_3^{2-}) are stabilized by the SHB, DHB and WHB interactions as discussed in Chapter 2. Due to these interactions it is expected that bands due to O-H stretching and bending modes of H_2O in the hydrated clusters of X get shifted compared to that of free water molecule. Based on the literature data on the stretching frequency of H_2O (ν_{sym} = 3657 cm^{-1}, ν_{asym} = 3756 cm^{-1}) and the present calculated values (ν_{sym} = 3983 cm^{-1}, ν_{asym} = 4087 cm^{-1}) at BHHLYP/6-311++G(d,p) level, the scaling factor is taken as 0.92 to account for the anharmonic nature of vibration. At B3LYP level the scaling factor is found to be 0.96 to account for the anharmonic nature of vibration.

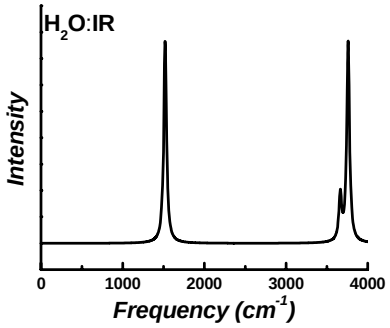

Fig. 3.1. Calculated scaled IR spectra at BHHLYP/6-311++G(d,p) level free H_2O molecule. The scaling factor is taken as 0.92 to account for the anharmonic nature of stretching vibrations. Lorentzian line shape has been applied with peak half-width of 10 cm^{-1}.

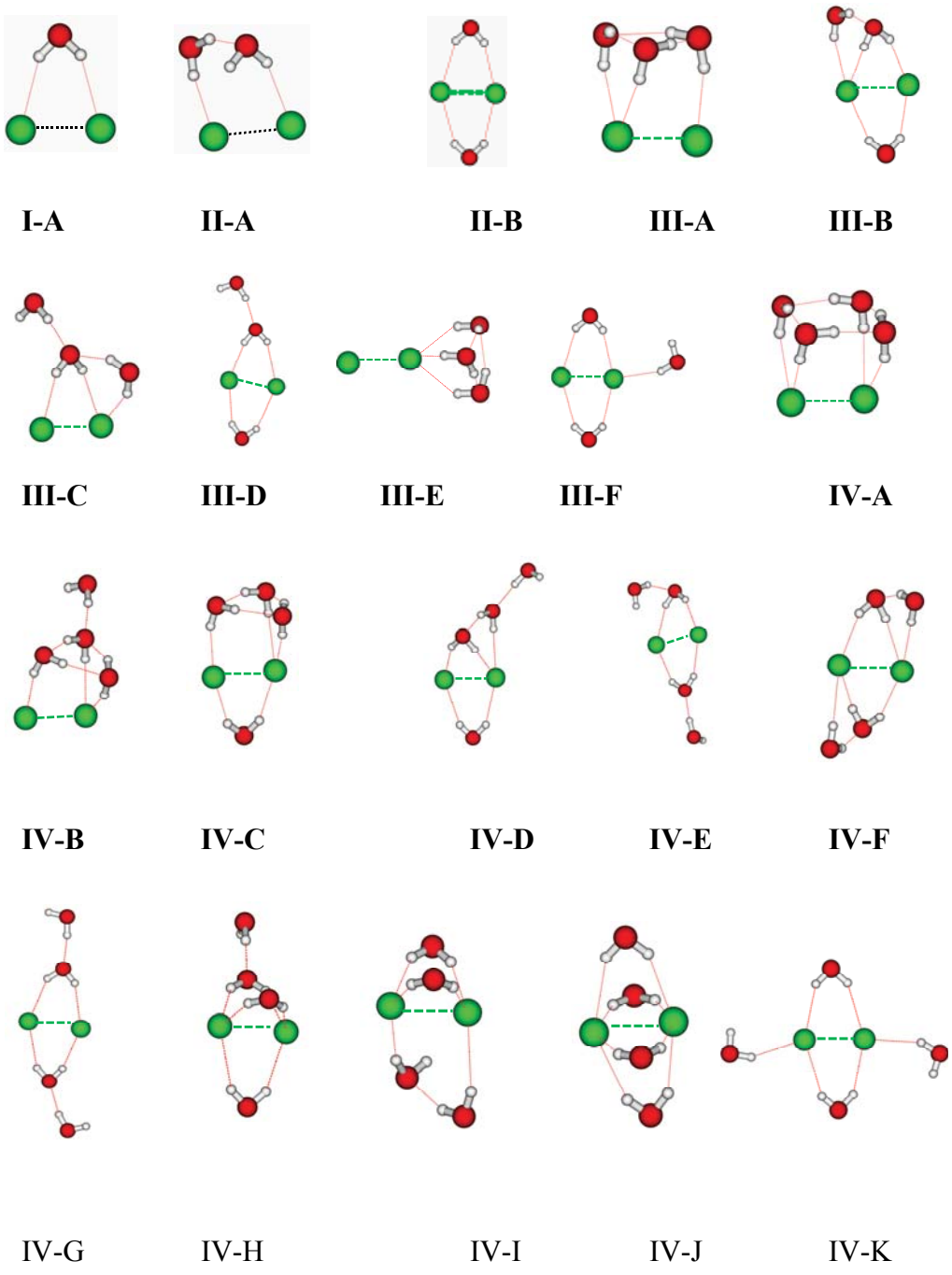
I-A
II-A
II-B
III-A
III-B
III-C
III-D
III-E
III-F
IV-A
IV-B
IV-C
IV-D
IV-E
IV-F
IV-G
IV-H
IV-I
IV-J
IV-K

Fig. 3.2 (Contd.)

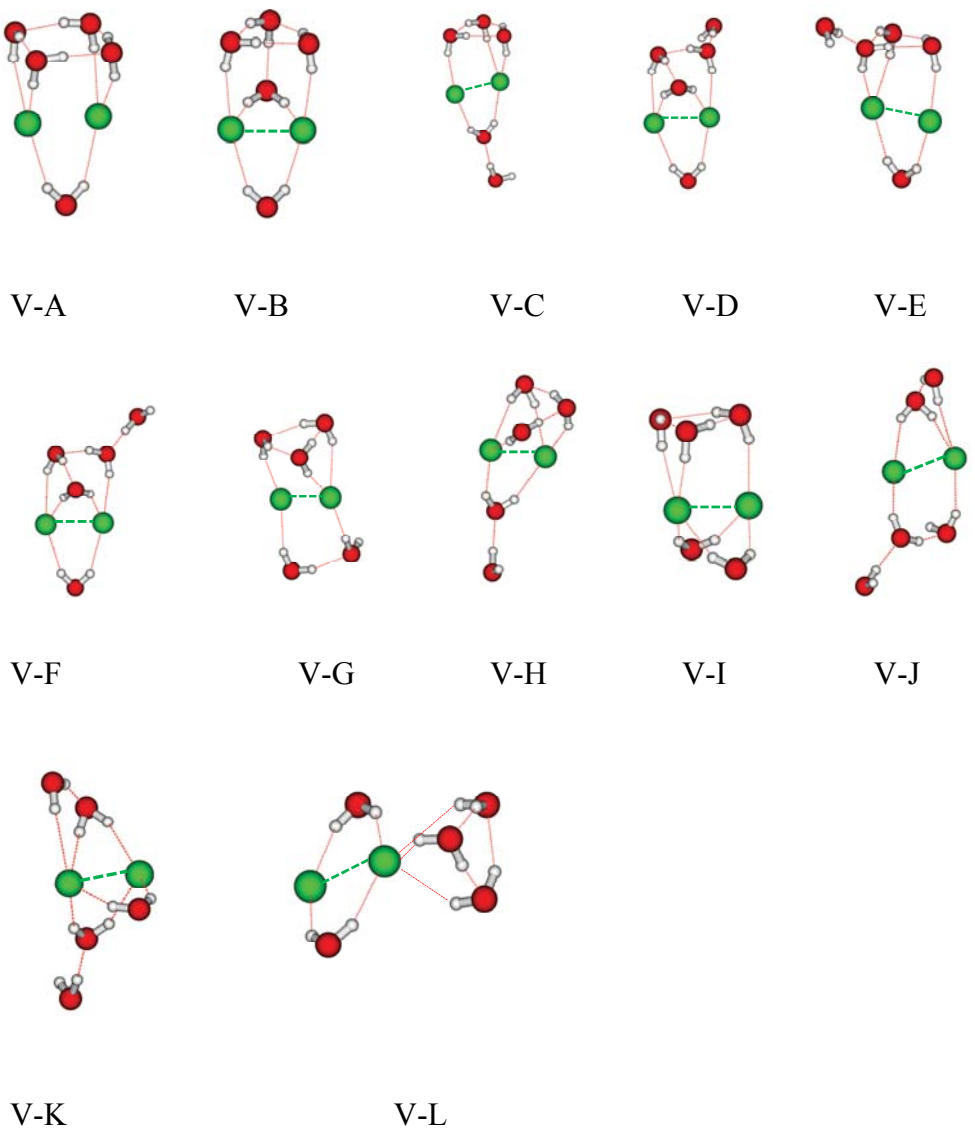

Fig. 3.2. Fully optimized minimum energy structures at BHHLYP/6-311++G(d,p) level of theory for (I) $Cl_2^{\bullet-}.H_2O$, (II) $Cl_2^{\bullet-}.2H_2O$, (III) $Cl_2^{\bullet-}.3H_2O$, (IV) $Cl_2^{\bullet-}.4H_2O$ and (V) $Cl_2^{\bullet-}.5H_2O$ clusters. Marked alphabets in the upper case are used to refer different minimum energy conformers for each size of the hydrated cluster arranged in order of stability showing 'A' as the most stable one. Cl atoms are shown by the largest green color spheres, the smallest spheres refer to H atoms and the rest (red in color) corresponds to O atoms in each structure shown in the figure. In each case, the distance between the two Cl atoms is ~ 2.6 Å, the distance between Cl and H-bonded H atoms is 2.3-2.8 Å and the distance between O and H atoms in inter water network is ~ 2.0 Å.

Cluster experiments are carried out under NVE ensemble condition and the precise value of the low temperature is not known. However, as these molecular clusters are stable only in the low temperature, the experimental condition is such that the temperature is kept below 200K. To choose a suitable method for the calculation of IR spectra of $Cl_2^{\bullet-}.nH_2O$ clusters, weighted average IR spectra is generated at MP2, B3LYP and BHHLYP level of theory at various temperature (T= 75 K to 200 K) with 6-311++G(d,p) basis set. It is observed that the calculated IR spectrum at BHHLYP level of theory at 100K is very close to the experimentally recorded spectrum. So, BHHLYP functional is used to generate IR spectra for all the $Cl_2^{\bullet-}.nH_2O$ clusters. The minimum energy structures (including the second hydration shell) of $Cl_2^{\bullet-}.nH_2O$ (n=1-5) clusters are displayed in Fig. 3.2. $Cl_2^{\bullet-}.nH_2O$ clusters are stabilized by double hydrogen bonding (DHB), single hydrogen bonding (SHB) and inter water hydrogen bonding (WHB) as discussed in Chapter 2. Due to these interactions, it is expected that IR bands due to stretching (O-H) and bending modes of H_2O in the hydrated clusters get shifted compared to that of the free water molecule. For mono- and di-hydrated cluster, one and two minimum energy structures have been found, respectively. The calculated scaled IR spectra of $Cl_2^{\bullet-}.nH_2O$ (n=1 and 2) cluster is also shown in Fig. 3.3. It is reported that for mono- and di-hydrate cluster (n=1 and 2), the experimental IR spectra [24]corresponding to the symmetric structure having one and two DHB, respectively (see Fig.3.2-1A and II-B).

First principles CPMD simulations are also carried out for 1.2 ps at 100K to generate the dipole autocorrelation function (DACF) for $Cl_2^{\bullet-}.3H_2O$. The Fourier transform to DACF (FT-DACF) is carried out to generate IR spectra. The IR spectrum for $Cl_2^{\bullet-}.3H_2O$ cluster based on FT-DACF is displayed in Fig.3.4 (I). It is clear from the

figure that the FT-DACF IR spectrum is far off from the experimental spectrum.[24] It is worthwhile to mention that for this open shell system, IR spectra generated applying FT of velocity autocorrelation function (FT-VACF) has a poorer match than that by FT-DACF procedure.

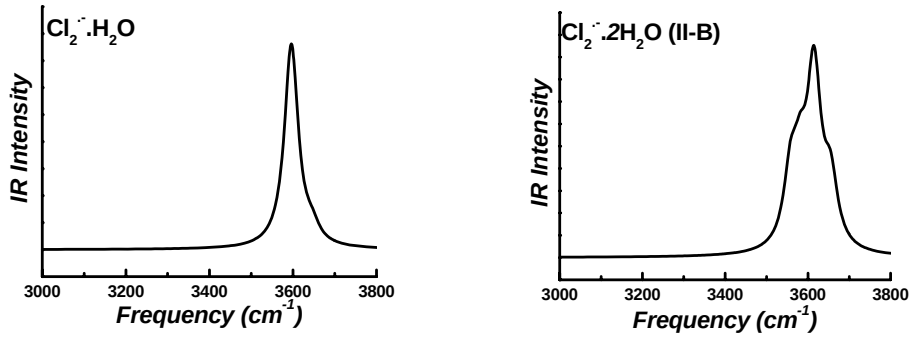

A **B**

Fig. 3.3. Calculated scaled IR spectra at BHHLYP/6-311++G(d,p) level for (A) $Cl_2^{\bullet-}.H_2O$ and (B) $Cl_2^{\bullet-}.2H_2O$. The scaling factor is taken as 0.92 to account for the anharmonic nature of stretching vibrations. Lorentzian line shape has been applied with peak half-width of 20 cm^{-1}.

For $Cl_2^{\bullet-}.3H_2O$, $Cl_2^{\bullet-}.4H_2O$ and $Cl_2^{\bullet-}.5H_2O$ clusters, 10, 15 and 24 minimum energy structures have been found at BHHLYP/6-311++G(d,p) level, respectively. The structures which have population of >1% are considered (displayed in Fig. 3.2) and their population is shown in Table 3. 1. Frequency is also calculated by taking the anharmonic nature of vibration using vibrational self-consistent field (VSCF) method. As the VSCF calculation is found to be very costly method for this open shell system, an appropriate scaling is carried out of the normal mode to include the anharmonic nature of vibrations. Based on the anhamonic calculation, it is also found that different modes have different anharmonicity. So different scaling is carried out in the regions having energy range of

3350-3500 cm^{-1} (scaling factor ~0.93) and 3500-3650 cm^{-1} (scaling factor ~0.90). The actual scaling factor is obtained by comparing the harmonic frequency with the experimentally observed spectrum. As large number of minimum energy structures are found, weighted average IR spectra are calculated which can be best comparable to the experimental spectra. The weight factor is calculated based on Boltzmann population at 100K. The weight factor is also calculated at a temperature range from 75K to 200K as the cluster experiment (NVE ensemble) is carried out in this low temperature range. The calculated IR spectra ~100K for all this three systems are close to the experimental spectra. So, based on this scaling factor, weighted average scaled IR spectra are calculated at 100K for $Cl_2^{\bullet-}.nH_2O$ (n=3-5) and are shown in Fig. 3.4(II) along with the experimental spectrum. An excellent agreement with experimental results is observed.

Table 3.1. Population (P_i) of the conformers of clusters of each size have been calculated based on free energy change at 100 K (T) following Boltzmann distribution. Structures are shown in Fig. 3.2.

Structure	III-A	III-B	III-C	III-D	III-E	III-F	IV-A	IV-B	IV-C	IV-D
Population (P_i)	0.54	0.04	0.08	0.09	0.22	0.03	0.53	0.17	0.11	0.03
Structure	IV-E	IV-F	IV-G	IV-H	IV-I	IV-J	IV-K	V-A	V-B	V-C
Population (P_i)	0.01	0.03	0.05	0.02	0.02	0.02	0.01	0.15	0.11	0.24
Structure	V-D	V-E	V-F	V-G	V-H	V-I	V-J	V-K	V-L	
Population (P_i)	0.04	0.05	0.03	0.20	0.04	0.04	0.03	0.02	0.05	

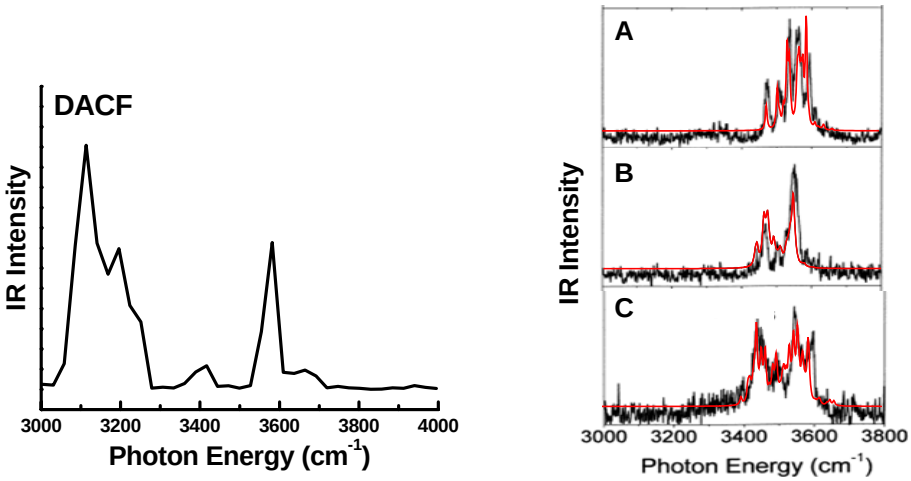

I **II**

Fig. 3.4. (I) FT-DACF IR spectra of $Cl_2^{\bullet-}.3H_2O$ at 100K. (II) Weighted average scaled IR spectra (red line) of (A) $Cl_2^{\bullet-}.3H_2O$, (B) $Cl_2^{\bullet-}.4H_2O$ and (C) $Cl_2^{\bullet-}.5H_2O$ at BHHLYP/6-311++G(d,p) level of theory. The black line denotes the experimental IR spectra and is reproduced from ref.24 with the permission from the American Chemical Society. The weight factor is calculated based on Boltzmann population at 100K. Lorentzian line shape has been applied with peak half-width of 5 cm^{-1} for $Cl_2^{\bullet-}.3H_2O$ and $Cl_2^{\bullet-}.5H_2O$ and 10 cm^{-1} for $Cl_2^{\bullet-}.4H_2O$.

IR spectra of X. nH_2O (X= $Br_2^{\bullet-}$ and $I_2^{\bullet-}$) clusters are calculated at BHHLYP/6-311++G(d,p) and X. nH_2O (X= $CO_3^{\bullet-}$, NO_3^- and CO_3^{2-}) clusters are calculated at B3LYP/6-311++G(d,p) level of theory. Weighted average IR spectra based on Boltzmann population factor is also generated for all the systems. It is observed that the clustering makes the shifting of O-H stretching mode of water in a similar fashion for all the halogen dimer radical anion system, X. nH_2O (X= $Cl_2^{\bullet-}$, $Br_2^{\bullet-}$ and $I_2^{\bullet-}$). The weighted average IR spectra for X. $5H_2O$ (X= $CO_3^{\bullet-}$, NO_3^- and CO_3^{2-}) clusters is shown in Fig. 3.5 (A-C), respectively as a representative result. However, the calculated IR spectra for

these systems, X. nH$_2$O (X= $Br_2^{\bullet-}$, $I_2^{\bullet-}$, $CO_3^{\bullet-}$, NO_3^- and CO_3^{2-}) cannot be validated due to unavailability of experimentally measured IR spectra.

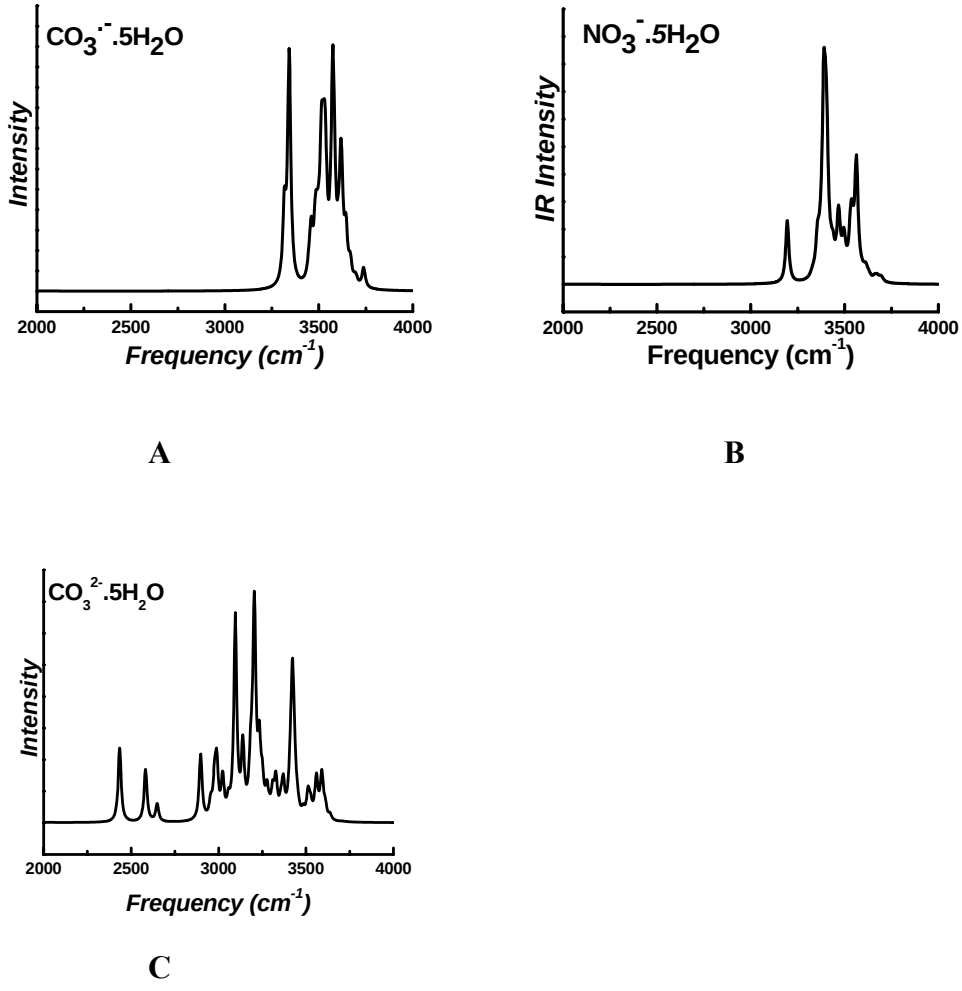

Fig. 3.5. Weighted average scaled IR spectra for (A) $CO_3^{\bullet-}$. 5H$_2$O, (B) NO_3^-. 5H$_2$O and (C) CO_3^{2-}. 5H$_2$O at B3LYP/6-311++G(d,p) level of theory. The weight factor is calculated based on Boltzmann population at 100K. Lorentzian line shape has been applied with peak half-width of 10 cm^{-1}.

It is observed that the IR spectra of each clusters, X. nH$_2$O (X= $Cl_2^{\bullet-}$, $Br_2^{\bullet-}$, $I_2^{\bullet-}$, $CO_3^{\bullet-}$, NO_3^- and CO_3^{2-}) are characterized by large shift of O-H (~300 cm^{-1}) stretching

mode compared to the free water mode. But stretching mode of X. nH_2O (X= $Cl_2^{\bullet-}$, $Br_2^{\bullet-}$, $I_2^{\bullet-}$, $CO_3^{\bullet-}$ & NO_3^-) clusters always remains far beyond of 3000 cm^{-1} except CO_3^{2-} system, where at least one stretching mode appeared below 3000 cm^{-1}. On the other hand the bending mode of water molecule remains unaffected in all the cases.

3.4. Conclusions

The IR spectra of $Cl_2^{\bullet-}.nH_2O$ (n=1-5) clusters are studied at BHHLYP/6-311++G(d,p) level of theory. It is observed that the hydrated clusters are stabilized by double hydrogen bonding (DHB), single hydrogen bonding (SHB) and inter water hydrogen bonding (WHB). Due to these interactions, bands due to stretching (O-H) hydrated clusters get shifted compared to that of the free water molecule. The IR spectra of $Cl_2^{\bullet-}.nH_2O$ (n=1-5) clusters is characterized by large shift of O-H (~300 cm^{-1}) stretching mode compared to the free water mode. But stretching mode remains always far beyond of 3000 cm^{-1}. On the other hand, the bending mode of water molecule remains unaffected. This observation is also true for other systems ($Br_2^{\bullet-}$, $I_2^{\bullet-}$, $CO_3^{\bullet-}$ and NO_3^-) except CO_3^{2-} system, where at least one stretching mode appears below 3000 cm^{-1}. It is observed that the FT-DACF IR spectrum is far off from the experimentally reported spectrum. On other hand an excellent agreement of weighted average scaled IR spectrum of $Cl_2^{\bullet-}.nH_2O$ (n=3-5) clusters at 100K with experimentally measured spectrum is observed.

CHAPTER 4

Solubility of Halogen Gases in Water

4.1. Introduction

Molecular cluster acts as an intermediate state between isolated gaseous molecule and condensed phase bulk system. It is well known that in solution (bulk) many important properties of neutral and charged chemical species are often widely different from that in the isolated gas phase. The structure and energetics of the cluster of a chemical species may be different from both the gas phase as well as the bulk. Bulk properties of a solute in solution result from the combined effect of solute-solvent and solvent-solvent interactions. It cannot be obtained from the properties of the isolated solute species alone. Several efforts are being made to connect molecular cluster properties of a chemical species to its bulk properties.[9,33-35]

Halogen molecules, X_2 (X=Cl, Br & I) provided one of the early model systems for understanding solvent effects on molecular spectra because they are apparently simple molecules whose spectral bands shift substantially in different solvents. The halogens also act as a popular model system for studying nearest neighbour effects on spectroscopy with the advent of molecular beam studies of dimers and small clusters. However, a very little effort has been put to study microhydration of X_2 (X=Cl & Br) systems.[55-57] The molecular interaction between a neutral solute and solvent water molecules as well as the hydrogen bonding interactions among the solvent water

molecules can be examined in such studies, which will also provide information on the evolution of hydration motifs of X_2 systems in water. It is also known that gaseous bromine is much more soluble than gaseous chlorine in water. But no information is available on the order of solubility of iodine in the gas phase. As these species have zero dipole moment, one has to apply an explicit solvation model to study the solvent effect rather than taking a continuum model like Onsager's reaction field model.[4] At present, various possible minimum energy configurations of $X_2.nH_2O$ cluster (X=Cl, Br and I; n=1-8), bonding characteristics and energy parameters (both solvent stabilization and interaction) are reported following *first principle* based electronic structure theory to predict the solubility order of halogen gases in water.

4.2. Theoretical Approach

To decide a suitable level of theoretical method for calculations, geometrical parameters of mono- and di- hydrated clusters of Cl_2 and Br_2 are calculated following correlated hybrid density functionals (B3LYP and BHHLYP) and second-order Moller-Plesset perturbation (MP2) theory adopting triple spit Gaussian type basis functions. It is observed that Becke's half-and-half (BHH) non-local exchange and Lee-Yang-Parr (LYP) non-local correlation functionals (BHHLYP) perform well to describe these clusters producing geometrical parameters and polarizability close to MP2 values. Geometry optimization on all the hydrated clusters has been carried out at BHHLYP level of theory to locate minimum energy structures followed by single point energy calculation applying second order Moller-Plesset perturbation theory (MP2) for improvement in energy of the systems. Triple split valence basis function due to Pople

including polarized and diffuse functions has been adopted for all calculations. Newton Raphson based algorithm has been applied to carry out geometry optimization for each of these molecular clusters with various initial guess structures to find out the most stable configuration without any symmetry restriction. Triple split Gaussian type basis sets for Br and I atoms are obtained from the Extensible Computational Chemistry Environment Basis Set Database, Pacific Northwest Laboratory.

4.3. Results and Discussion

4.3.1. Structure

Solvent H_2O molecules are added to Cl_2, Br_2 and I_2 species by various different possible ways and full geometry optimization is carried out at BHHLYP/6-311++G(d,p) level (6-311 basis set is used for I) of theory followed by single point energy calculation at second order Moller-Plesset perturbation theory (MP2) with the same set of basis functions. Optimized structures of the most stable configurations for each size hydrated cluster of Cl_2, Br_2 and I_2 systems are displayed in Fig. 4.1. Structures corresponding to IA, IB and IC are the most stable structures of the monohydrate clusters, $Cl_2.H_2O$, $Br_2.H_2O$ and $I_2.H_2O$. For all the structures, O atom from H_2O molecule is connected to one of the halogen atoms ($r_{O..X}$~2.5 Å). Most favoured structures for the di-hydrated cluster of Cl_2, Br_2 and I_2 systems are shown as IIA, IIB and IIC, respectively in Fig. 4.1. It is clearly observed that only one H_2O molecule is in the close vicinity of halogen moiety in the di-hydrated clusters except for $Br_2.2H_2O$ cluster, where both the water molecules are in the close vicinity of Br_2. It is to be noted that the initial guess structures for di-hydrated clusters were considered, where one H_2O molecule attached to one of the

halogen atoms (Cl, Br or I) through O site and the other H_2O is connected to X_2 *via* H atom without any inter water H bonding. Structures of the most stable configurations of tri-hydrated cluster of Cl_2, Br_2 and I_2 are very similar in nature and are displayed in Fig. 4.1 as IIIA, IIIB and III-C, respectively. Two solvent water molecules are in close proximity and connected by H-bonds in these tri-hydrate clusters. The initial guess structures were considered where all the three solvent H_2O units were directly linked to halogen atoms. In case of tetra-hydrated cluster, planar cyclic H-bonded structures (see Fig.4.1 IVA, IVB and IVC) are obtained as the most stable geometries. One can see that only two solvent water molecules are directly connected to the halogen atoms and the remaining two acts as both H-bond donor and acceptor in this minimum energy structure. In case of penta-hydrated clusters, the most favored structures are also planar where H atom of one H_2O is approached to one halogen (Cl, Br or I) atom and O atom of another H_2O is approached to other halogen atom and both these H_2O units are linked with two other solvent H_2O molecules *via* H-bond. The fifth solvent unit is connected to the halogen atom (which is already connected by a H_2O unit through H atom) through its O atom in case of $Cl_2.5H_2O$, $Br_2.5H_2O$ systems and through one of its H atoms in $I_2.5H_2O$ system as shown in Fig. 4.1 (VA, VB and VC). It is to be noted that in all these three cases the initial structure for optimization was similar. The most stable structure for hexa-hydrated cluster, $Cl_2.6H_2O$ is calculated to have a surface structure with a three dimensional water network formed by six H_2O molecules *via* inter water H-bonding as displayed in Fig. 4.1-VIA. The minimum energy structure of $Br_2.6H_2O$ and $I_2.6H_2O$ cluster (see Fig.4.1-VIB and 1-VIC) is similar to that of $Cl_2.6H_2O$ cluster. In case of hepta-hydrated cluster, Cl_2 system behaves in a different manner compared to that of Br_2

and I_2 systems. The most stable structures of $Cl_2.7H_2O$, $Br_2.7H_2O$ and $I_2.7H_2O$ are shown in Fig. 4.1-(VIIA, VIIB and VIIC). In $Cl_2.7H_2O$ cluster, the solvent water units are separated from Cl_2 moiety by a distance of ~ 4.0 Å. The most favoured structure of $Br_2.7H_2O$ is the one where the three dimensional network surrounds only one Br atom (see Fig. 4.1-VIIB). On the other hand, the most stable structure of $I_2.7H_2O$ cluster is the one where I_2 unit is surrounded by cyclic three dimensional water network formed by seven H_2O molecules *via* inter water H-bond as shown in Fig.4.1-VIIC. All H_2O molecules act as both H-bond donor and acceptor in this hepta-hydrated cluster except two, which were directly attached to the I_2 moiety. The most stable structure of $Cl_2.8H_2O$ cluster is displayed in Fig. 4.1-VIIIA. It is clearly seen that Cl_2 moiety is directly attached to only one water molecule as the monohydrated system, $Cl_2.H_2O$ and staying away (> 4 Å) from the seven member water network. The most stable structure of $Br_2.8H_2O$ cluster (see Fig. 4.1-VIIIB) is rather different from that of $Br_2.7H_2O$ cluster (see Fig. 4.1-VIIB). In the present case, all water molecules act simultaneously as hydrogen bond donor and accepter except the water molecule which is directly attached to the bromine moiety by H-end. Minimum energy structure of $I_2.8H_2O$ cluster is very similar to the same from hepta- hydrated cluster, $I_2.7H_2O$. All eight water molecules form a cyclic network, which is connected to iodine molecule from one side of I_2 making a surface structure as shown in Fig.4.1-VIIIC.

All $X_2.nH_2O$ (X=Cl, Br & I; n=1-8) clusters are stabilized by X…O, X…H and inter water hydrogen bonding interactions. The inter water hydrogen bonding energy (~6-7 kcal/mol) is greater than the both X…O and X…H interaction energy (~3-5 kcal/mol). Thus, the larger clusters prefer to form strong inter water hydrogen bonded network.

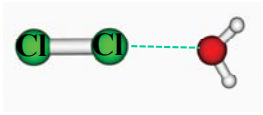

IA

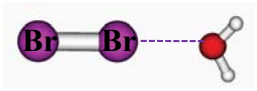

IB

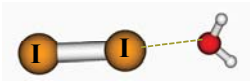

IC

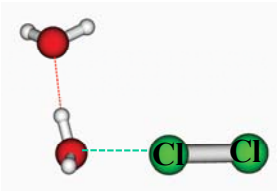

IIA

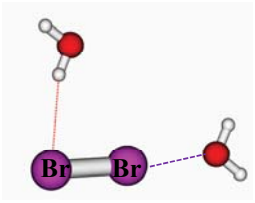

IIB

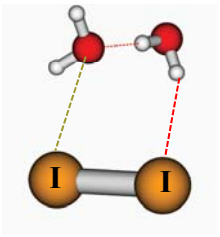

IIC

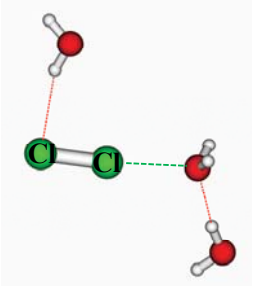

IIIA

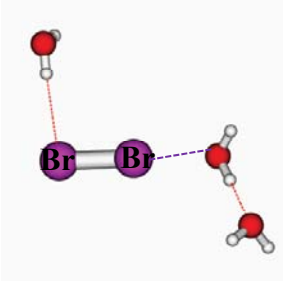

IIIB

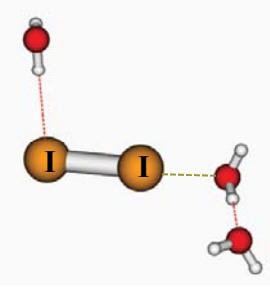

IIIC

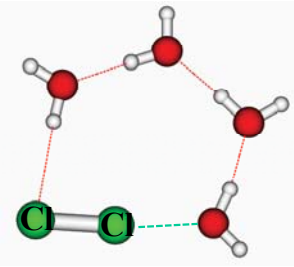

IVA

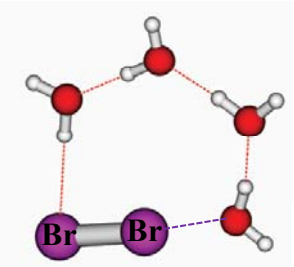

IVB

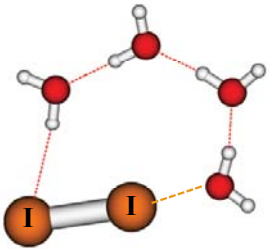

IVC

Fig. 4.1, (Contd.)

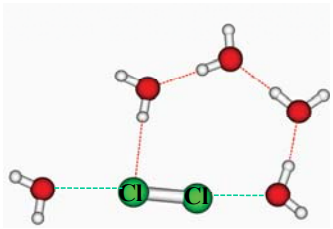

VA

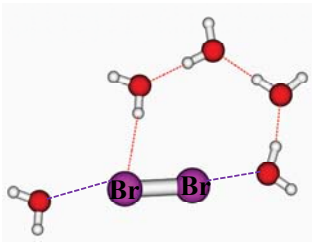

VB

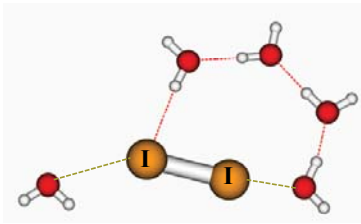

VC

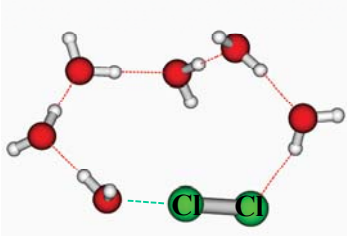

VIA

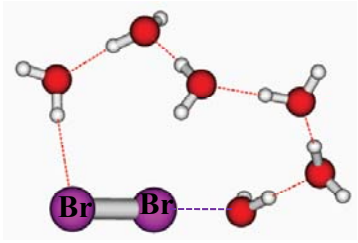

VIB

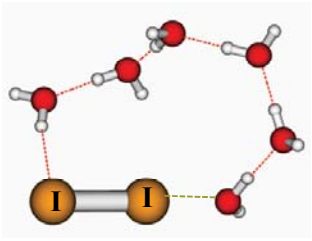

VIC

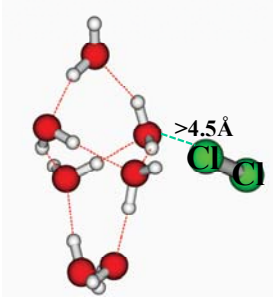

VIIA

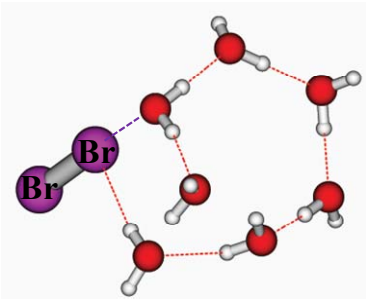

VIIB

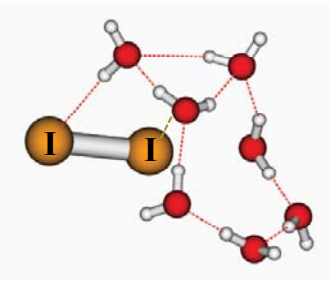

VIIC

Fig. 4.1 (Contd.)

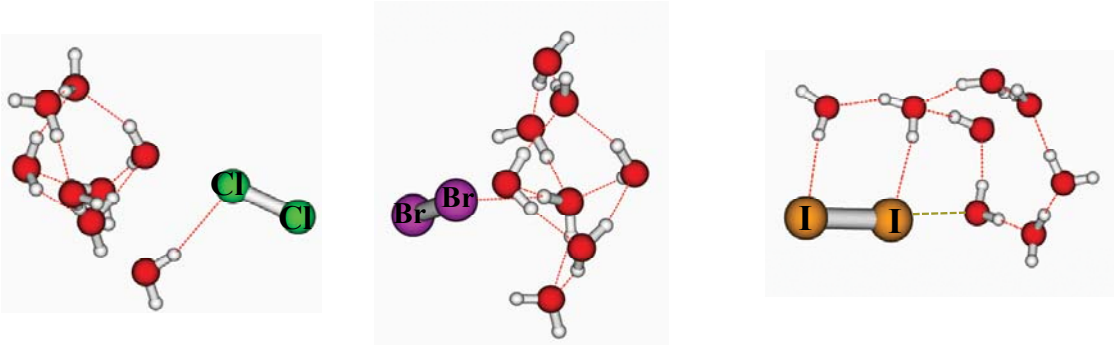

VIIIA VIIIB VIIIC

Fig. 4.1. The fully optimized most stable structures calculated applying BHHLYP functional with 6-311++G(d,p) set of split valence basis function (6-311 basis set is used for iodine) for (IA) $Cl_2.H_2O$; (IB) $Br_2.H_2O$, (IC) $I_2.H_2O$; (IIA) $Cl_2.2H_2O$; (IIB) $Br_2.2H_2O$ (IIC) $I_2.2H_2O$; (IIIA) $Cl_2.3H_2O$; (IIIB) $Br_2.3H_2O$, (IIIC) $I_2.3H_2O$; (IVA) $Cl_2.4H_2O$; (IVB) $Br_2.4H_2O$, (IVC) $I_2.4H_2O$; (VA) $Cl_2.5H_2O$; (VB) $Br_2.5H_2O$, (VC) $I_2.5H_2O$; (VIA) $Cl_2.6H_2O$; (VIB) $Br_2.6H_2O$, (VIC) $I_2.6H_2O$; (VIIA) $Cl_2.7H_2O$; (VIIB) $Br_2.7H_2O$, (VIIC) $I_2.7H_2O$; (VIIIA) $Cl_2.8H_2O$, (VIIIB) $Br_2.8H_2O$ and (VIIIC) $I_2.8H_2O$. Cl, Br and I atoms are shown by marked spheres, the smallest 'white' colour spheres refer to H atoms and the rest (red colour) corresponds to O atoms in each structure.

The structures of all these systems are widely different for the larger size clusters (n>6) though they are fairly similar in case of smaller clusters (n=1-6) except for n=2. The structure of $Br_2.nH_2O$ (n=7) cluster is quite different from that in the earlier reported work at a lower level of theory.[55]

4.3.2. Atomic Charge and Bond Order

The calculated Mulliken atomic charges over two Br atoms in $Br_2.H_2O$ cluster are about +0.04 and -0.08 a.u. A small variation of atomic charge over two Br atoms is observed for different size hydrated clusters, $Br_2.nH_2O$, and observed to be in the range of 0.04–0.14 a.u. This suggests that Br_2 exists as a charge-separated ion-pair species

($Br^{\delta+}$-$Br^{\delta-}$) in the studied hydrated clusters. For $I_2.H_2O$ cluster, the calculated Mulliken atomic charges over two I atoms are ~ +0.03 and -0.16 a.u. The variation on atomic charge over two I atoms for different size of hydrated clusters, $I_2.nH_2O$, is observed to be larger than that of Br atoms in $Br_2.nH_2O$ cluster. This suggests that I_2 does exist as a charge-separated ion-pair species ($I^{\delta+}$-$I^{\delta-}$) in the studied hydrated clusters like Br_2 in $Br_2.nH_2O$ systems. However, in contrary to I_2 and Br_2 systems, Cl_2 does not exist as a charge separated species in presence of solvent water molecules. The calculated Mulliken charges over two Cl atoms are fairly close (+0.01 and -0.04 a.u.). This may be due to the high electro negativity of Cl atom compared to Br and I atoms. This observation may be due to the fact that there is a competition between ion the solvation force, which favours a localized charge distribution and the chemical bond interaction, which tends to delocalize a charge. As one moves from Cl_2 to Br_2 to I_2, the bond gets longer and weaker. As a result, at some stage the charge-separated form becomes more stable than the delocalized form. In other words, the cost to form charge-separated ion pair is large in case of $Cl_2.nH_2O$ system compared to $Br_2.nH_2O$ or $I_2.nH_2O$ systems due to relatively large ionization potential and comparable electron affinity values. It is known that Mulliken charge is sensitive to basis function applied in the calculation. Thus, atomic charges are also calculated applying Atoms in Molecules (AIM) based procedure at BHHLYP/6-311G(d,p) level of theory. The predicted charge-separation between two halogen atoms is +0.09, +0.13 and +0.19 a.u.for $Cl_2.H_2O$, $Br_2.H_2O$ and $I_2.H_2O$ systems, respectively. The charge-separation values calculated by AIM procedure show a similar trend as calculated Mulliken charges do. Bond orders between the two halogen atoms for all the clusters ($X_2.nH_2O$; X=Cl & I; n=1-8) are also calculated following the definition

due to Mayer.[58] The calculated bond distance (r_{xx}) and bond order (B_{xx}) between two halogen atoms do not show any significant variation on addition of successive solvent water molecules. From the structural information it is noted that only a few water molecules are in close surrounding of halogen (X_2) moiety.

4.3.3. Solvent Stabilization and Interaction Energy

Solvent stabilization energy of these clusters $X_2.nH_2O$ (X=Cl, Br & I) may be expressed as

$$E^{solv} = E_{X2.\ nH2O} - (nE_{H2O} + E_{X2})$$

where $E_{X2.\ nH2O}$ refers to the energy of the cluster $X_2.nH_2O$ (X=Cl Br and I). E_{H2O} and E_{X2} refer to the energy of a single H_2O and X_2 (X=Cl, Br & I) system. Thus, the calculated solvent stabilization energy represents the solvent stabilization of the molecular cluster on addition of successive solvent water molecules accounting interaction of halogen atoms with water units as well as inter water H-bonding. The solvent stabilization energy of the $X_2.nH_2O$ (X=Cl, Br & I) clusters calculated at MP2/6-311++G(d,p) level of theory (for I 6-311 basis is used) are provided in Table 4.1. The variation of solvation energy (E^{solv}) *vs*. *n*, number of water molecules in $X_2.nH_2O$ cluster (X=Cl, Br & I) are displayed in Fig.4.2 (A-C), respectively, showing a continuous increase on addition of each solvent water unit. As expected, the calculated solvent stabilization energy is very small compared to the same calculated for charged systems, $X_2^{\bullet-}.nH_2O$ (as discussed in Chapter 2).

It is clearly seen from Table 4.1 that the solvent stabilization energy is the highest for $I_2.nH_2O$ system. But between $Cl_2.nH_2O$ and $Br_2.nH_2O$ systems the solvent

stabilization energy does not follow any systematic trend; variation is different for different cluster size (n) of $Cl_2.nH_2O$ and $Br_2.nH_2O$ systems. It is known that solubility of Br_2 gas is higher than Cl_2 gas in bulk water. Thus, the calculated solvent stabilization energy cannot explain the solubility trend of the halogen (Cl_2, Br_2 & I_2) in water. Let us introduce another energy term known as interaction energy.

The interaction energy (E^{int}) between the halogen (X_2) and water cluster in the hydrated cluster, $X_2.nH_2O$ (X=Cl, Br & I) may be defined as

$$E^{int} = E_{X2\ nH2O} - (E_{(H2O)n} + E_{X2})$$

where, $E_{X2\ nH2O}$ refers to the energy of the cluster $X_2.nH_2O$ (X=Cl & I). $E_{(H2O)n}$ and E_{X2} refer to the energy of $(H_2O)_n$ and X_2 (X=Cl, Br & I) systems respectively. The energy of the $(H_2O)_n$ system is calculated by removing halogen (X_2) part from the optimized geometry of the cluster followed by a single point energy calculation. E_{X2} is also evaluated in the similar way i.e. by removing the water part of the optimized structure of hydrated cluster followed by single point energy calculation. Thus, the interaction energy actually calculates the net interaction of X_2 with $(H_2O)_n$ systems in these hydrated clusters. The interaction energy of the $X_2.nH_2O$ (X=Cl, Br & I) clusters calculated at MP2/6-311++G(d,p) level of theory are listed in Table 4.1. As expected, the calculated interaction energy is very small compared to the same calculated for charged systems, $X_2^{\bullet-}.nH_2O$ (as discussed in Chapter 2). Moreover, it can be easily seen from Table 4.1 that the interaction energy for $Cl_2.nH_2O$ systems is quite small with respect to Br_2 and I_2 hydrated systems. This does support the presence of Br_2 and I_2 as charge separated ion-pair in the hydrated clusters. The plot of calculated interaction energy (E^{int}) *vs*. n, number of water molecules for $X_2.nH_2O$ (X=Cl, Br & I) clusters are displayed in Fig. 4.2 (A-C),

respectively. The interaction energy for the hepta- and the octa- hydrated clusters of Cl_2 systems is smaller than that of the hexa- hydrated cluster. This may be due to the specific geometry of the hydrated clusters where seven solvent water molecules form H-bonded cluster and remains far away from Cl_2 moiety. For $Br_2.nH_2O$ clusters, the calculated interaction energy profile shows saturation at n=7. In case of $I_2.nH_2O$ clusters, the calculated interaction energy profile shows a stepwise saturation nature at n=6 and 8.

Table 4.1: Calculated solvent stabilization and interaction energy in kcal/mol for $X_2.nH_2O$ systems (X=Cl, Br & I; n=1-8) at MP2/6-311++G(d,p) level of theory. 6-311 basis set is applied for I atom.

Species $X_2.nH_2O$	Solvent stabilization energy of $X_2.nH_2O$ clusters (kcal/mol)			Interaction energy of $X_2.nH_2O$ clusters (kcal/mol)		
	X=Cl	X=Br	X=I	X=Cl	X=Br	X=I
n = 1	2.85	3.86	4.57	3.07	4.11	4.88
n = 2	9.85	5.52	8.42	4.36	5.76	3.00
n = 3	9.88	13.53	16.31	3.91	7.74	10.80
n = 4	25.82	27.68	32.18	7.42	9.58	14.59
n = 5	28.24	30.23	33.69	8.49	11.02	15.76
n = 6	45.66	47.87	52.70	9.31	11.66	16.48
n = 7	65.00	60.03	67.40	4.55	11.32	23.40
n = 8	73.25	71.26	76.71	6.57	13.73	23.11

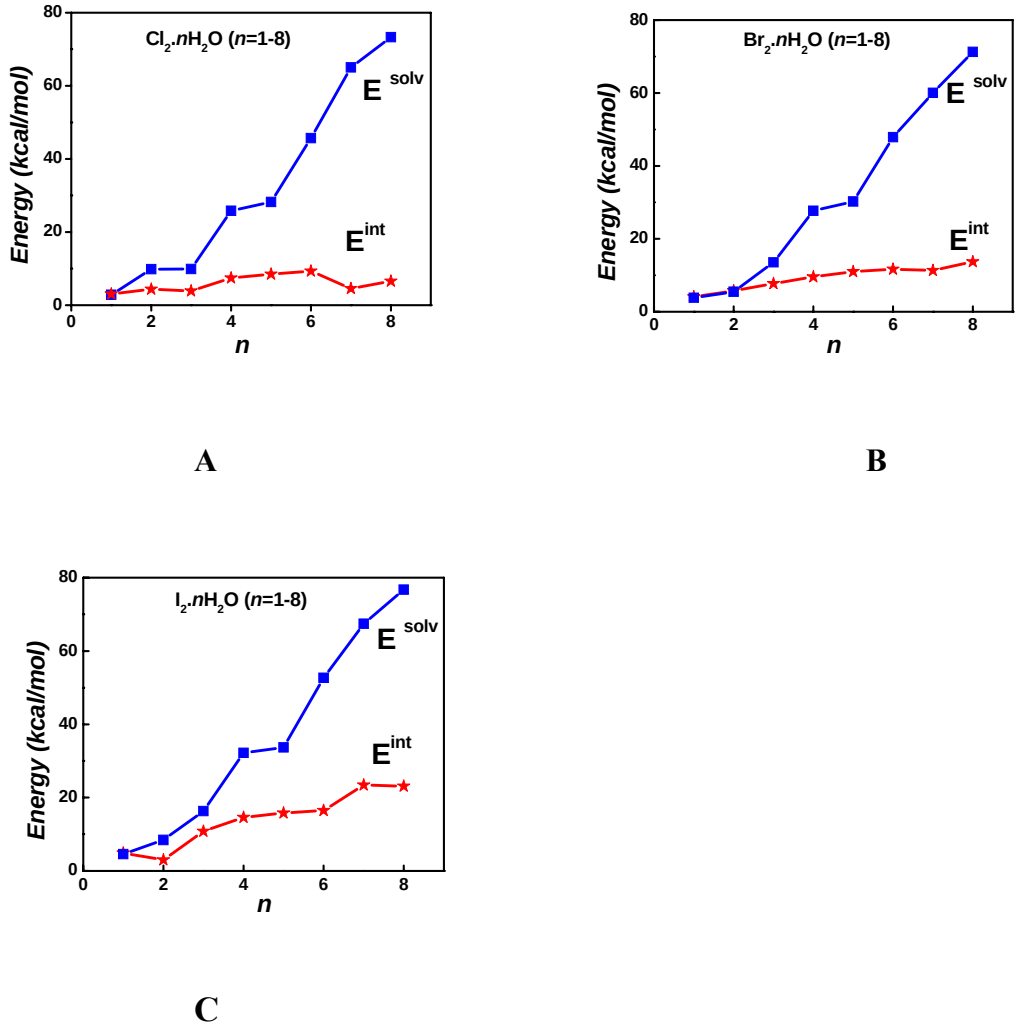

Fig. 4.2. Plot of calculated interaction energy, E^{int} and solvent stabilization energy, E^{solv} at MP2/6-311++G(d,p) level in kcal/mol *vs*. *n*, number of water molecules for (A) $Cl_2.nH_2O$, (B) $Br_2.nH_2O$ and (C) $I_2.nH_2O$ clusters.

The interaction energy (E^{int}) is the measure of the interaction between the halogen moiety and water units. Thus, a large value of E^{int} indicates the presence of a large number of water molecules in close surrounding of the halogen moiety. For the present systems, calculated E^{int} is small and does show only a small increase with the addition of water molecules. That explains the presence of only a few water molecules (2–3) in the

close vicinity of the halogen moiety. In case of hydrated clusters, $X_2.nH_2O$ (X=Cl, Br & I; n=1-8), the solvent stabilization and the interaction energies are very close for a few small size clusters. But when the inter molecular hydrogen bond among water molecules starts to build up; solvation energy surpasses the interaction energy. The variation of solvent stabilization energy with size of the cluster (n) for all the systems is similar. On the other hand, variation of the interaction energy with size of the cluster (n) is different for Cl_2 system compared to that of Br_2 and I_2 system.

Table 4.1 indicates that the interaction energy decreases from $I_2.nH_2O$ to $Cl_2.nH_2O$ systems for all sizes of the clusters except that for n=2. Thus the calculated interaction energy in these halogen-water clusters should be able to predict the solubility of X_2 in water. Calculated higher interaction energy for $Br_2.nH_2O$ clusters compared to that for $Cl_2.nH_2O$ cluster is able to explain the higher solubility of bromine in bulk water over chlorine. As $I_2.nH_2O$ posses highest interaction energy among these three systems, iodine in the gas phase is expected to have much higher solubility in the bulk water compared to bromine and chlorine gases. The overall solubility order of gaseous halogens in water is $I_2 > Br_2 > Cl_2$.

4.4. Conclusions

Both *ab initio* (MP2) and hybrid exchange-correlation density functional method have been applied to study microhydration of halogen gases with a split valence 6-311++G(d,p) basis function. It is concluded that both Br_2 and I_2 exist as a charge separated ($Br^{+\delta}$-$Br^{-\delta}$ and $I^{+\delta}$-$I^{-\delta}$) entity in the hydrated clusters. Though structures of $Cl_2.nH_2O$ clusters are similar to that of iodine system, Cl_2 does not exist as a charge

separated ion pair in presence of solvent water units. The interaction and solvent stabilization energies are calculated for $X_2.nH_2O$ clusters (X=Cl, Br & I; n=1-8). Calculated solvent stabilization energy increases on successive addition of solvent water molecules but the interaction energy saturates for all the three halogen-hydrated systems. The higher interaction energy and charge distribution over I atom in $I_2.nH_2O$ clusters compared to that of $Br_2.nH_2O$ and $Cl_2.nH_2O$ clusters suggests that solubility of gas phase I_2 is higher than Br_2 and Cl_2 gases. It is to be noted that first principle based study on the microhydration can also explain bulk phenomenon like the order of solubility of gases in a series.

CHAPTER 5

UV-Vis Spectra of Anionic Hydrated Clusters: Extrapolation to Bulk

5.1. Introduction

Recently, a few attempts are being made to reproduce the bulk properties, like detachment energies of the excess electron of bulk solute solution (aqueous) from the knowledge of finite size anionic hydrated cluster data applying size selected photoelectron spectroscopy.[9,33-35] UV-Vis spectra of many transients in aqueous solution (bulk) are widely applied to study complex chemical reaction. However, no effort is made to connect UV-Vis spectra of a solute in aqueous solution to that of its finite size hydrated clusters. In this regard, hydrated clusters of $Cl_2^{\bullet-}$, $Br_2^{\bullet-}$, $I_2^{\bullet-}$ and $CO_3^{\bullet-}$ are studied following *first principle* based theoretical methods to understand the origin of UV-Vis transition and to extract bulk optical absorption spectra of these radical anions in their respective aqueous solution. This study is very useful to those who practice radiation chemistry. In aqueous solution, hydroxyl radical ($^{\bullet}OH$) reacts with X^- (X=Cl, Br &I) to form a transient species, which has a broad and strong absorption in the UV-visible region.[3,59] This absorption maximum is assigned to the halogen dimer radical anion species, $X_2^{\bullet-}$(X=Cl, Br &I), a specific one electron oxidising species. It is reported that $Cl_2^{\bullet-}$, $Br_2^{\bullet-}$ and $I_2^{\bullet-}$ species absorb strongly in their respective aqueous solution with absorption maximum (λ_{max}) at 340, 360 and 380 nm, respectively. Similarly, hydroxyl

radical ($^{\bullet}OH$) reacts with HCO_3^- or CO_3^{2-} to form a transient species, which has a broad and strong absorption in the visible region with absorption maximum, λ_{max} at 600 nm. This absorption maximum is assigned to the carbonate radical anion species, $CO_3^{\bullet-}$, a specific one electron oxidising species.[60] In this chapter, results of chlorine dimer radical anion ($Cl_2^{\bullet-}$) and carbonate radical anion species ($CO_3^{\bullet-}$) are presented in detail. Simulated UV-Vis spectra of $Cl_2^{\bullet-}$ and $CO_3^{\bullet-}$ hydrated clusters are compared with the reported experimental transient optical absorption spectra of $Cl_2^{\bullet-}$ and $CO_3^{\bullet-}$ species in aqueous solution and electronic transitions responsible for the optical absorption spectra of $Cl_2^{\bullet-}$(aq) and $CO_3^{\bullet-}$ are also assigned based on studies of excited states.

5.2. Theoretical Approach

As it is discussed in chapter 2, quasi Newton Raphson based algorithm is applied to carry out geometry search in each of hydrated clusters with various initial structures designed systematically following bottom-up approach to find out the most stable equilibrium structure. This procedure involves the calculation of a multi-dimensional potential energy surface for these clusters and finding a minimum on the surface. The key issue in this search procedure is to guess a good initial geometry of the cluster, which might converge during the calculation to a local or the global minimum. It is to be noted that the adopted procedure for geometry search cannot guarantee to locate the global minimum. Thus simulated annealing combined with Monte-Carlo sampling method has also been applied to search for the global minimum energy structure for each size clusters.[36] In this method, molecular coordinates have been displaced by a random amount and the energy of the system has been evaluated at the new structure. The new

structure with lower in energy has been accepted while structures with higher energies have been accepted at a probability determined by the Boltzmann factor. Random structures have been generated by carrying out Monte Carlo steps at a high temperature (2,000 K) for more than 8000 steps. Both configuration interaction with single electron excitation (CIS) method and time dependent density functional theory (TDDFT) has been adopted for predicting a few low lying excited states of all the clusters, reported in this chapter.

5.3. Results and Discussion

5.3.1. Structure

Various possible initial structures of $Cl_2^{\bullet-}.nH_2O$ clusters (n=1-11) are considered for global geometry optimization and a number of minimum energy structures (conformers) are obtained. The global minimum energy structure of each size of hydrated cluster, $Cl_2^{\bullet-}.nH_2O$ (n=1-11) at BHHLYP/6-311++G(d,p) is displayed in Fig. 5.1. Structures of $Cl_2^{\bullet-}.nH_2O$ clusters (n=1-5) are also very close to the reported structures by Johnson and co-workers.[24] It is observed that the $Cl_2^{\bullet-}.nH_2O$ clusters are stabilized by double hydrogen bonding (DHB), single hydrogen bonding (SHB) and inter water hydrogen bonding (WHB). Conformation having H-bonded water network (WHB arrangements) are more stable over the other structures where H_2O units are connected to the anion moiety independently either by SHB or DHB for a particular size of cluster. H-bonded water network having two, three or four H_2O units are present in the different conformers of these clusters. Hydrated cluster having cyclic water network units is the

most stable conformer for each size cluster. These observations are very similar to that of $Cl_2^{\bullet-}.nH_2O$ clusters as discussed in Chapter 2 and 3. $Cl_2^{\bullet-}.nH_2O$ clusters (n=4-11) contain at least one four member water ring. In each case, the distance between the two Cl atoms is ~ 2.6 Å, the distance between Cl and H-bonded H atoms is 2.3-2.8 Å (SHB and DHB bond) and the distance between O and H atoms in inter water network is

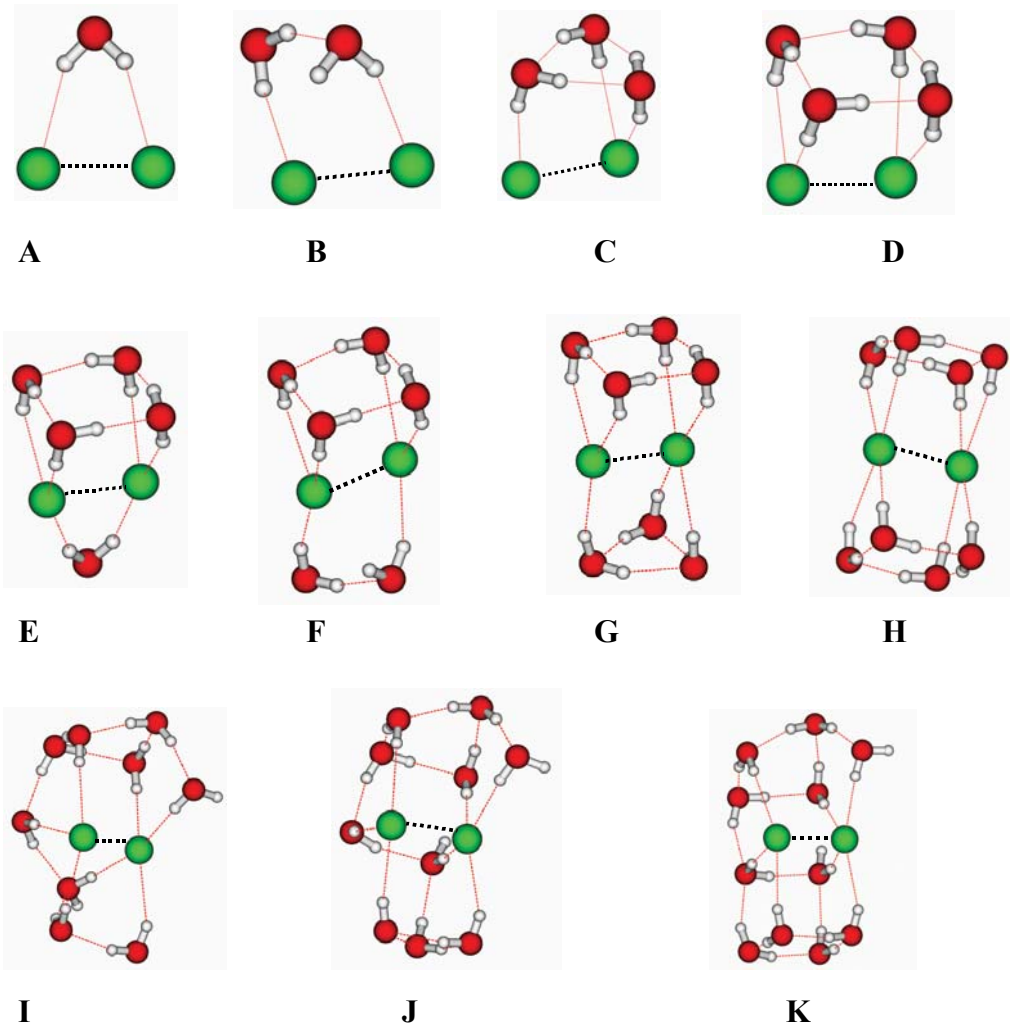

Fig. 5.1. Fully optimized global minimum energy structures at BHHLYP/6-311++G(d,p) level of theory for (A) $Cl_2^{\bullet-}.H_2O$, (B) $Cl_2^{\bullet-}.2H_2O$, (C) $Cl_2^{\bullet-}.3H_2O$, (D) $Cl_2^{\bullet-}.4H_2O$, (E) $Cl_2^{\bullet-}.5H_2O$, (F) $Cl_2^{\bullet-}.6H_2O$, (G) $Cl_2^{\bullet-}.7H_2O$, (H) $Cl_2^{\bullet-}.8H_2O$, (I) $Cl_2^{\bullet-}.9H_2O$, (J) $Cl_2^{\bullet-}.10H_2O$ and (K) $Cl_2^{\bullet-}.11H_2O$ clusters. Cl atoms are shown by the largest green colour spheres, the smallest spheres refer to H atoms and the rest (red in colour) corresponds to O atoms in each structure shown in the figure.

1.9-2.1 Å (WHB bond). It is also observed that the nature of σ type *hemi* bond (*2c-3e*) between two Cl atoms is remaining same as in case bare $Cl_2^{\bullet-}$. These observations are also similar for *hemi* bonded $Br_2^{\bullet-}.nH_2O$ and $I_2^{\bullet-}.nH_2O$ clusters.

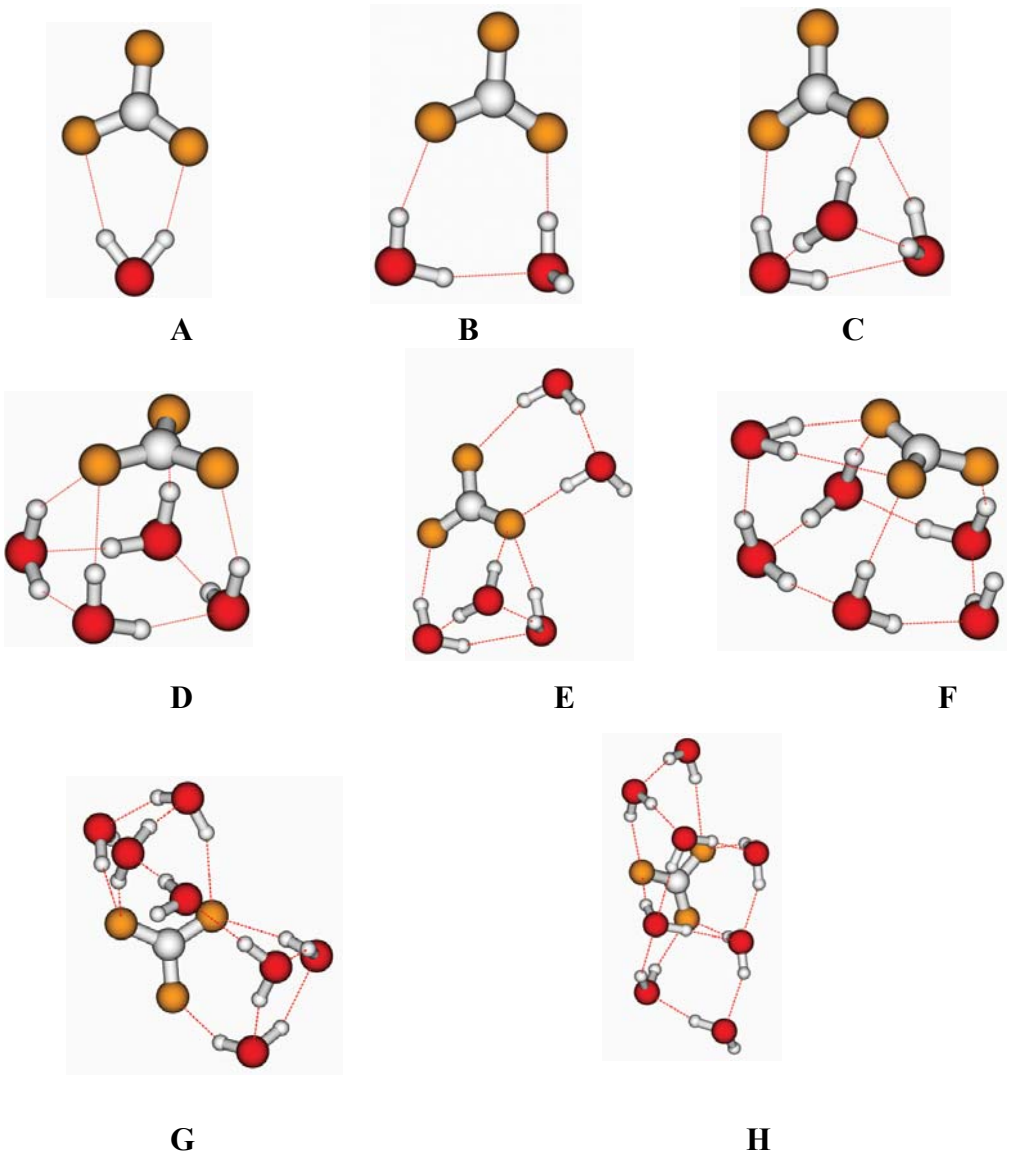

Fig.5.2. Fully optimized global minimum energy structures at B3LYP/6-311++G(d,p) level of theory for (A) $CO_3^{\bullet-}.H_2O$, (B) $CO_3^{\bullet-}.2H_2O$, (C) $CO_3^{\bullet-}.3H_2O$, (D) $CO_3^{\bullet-}.4H_2O$, (E) $CO_3^{\bullet-}.5H_2O$, (F) $CO_3^{\bullet-}.6H_2O$, (G) $CO_3^{\bullet-}.7H_2O$ and (H) $CO_3^{\bullet-}.8H_2O$. C atoms are shown by the grey colour spheres, the smallest spheres refer to H atoms and the rest corresponds to O atoms in each structure shown in the figure. Yellow colour spheres refer to the carbonate O atoms and rest (red in colour) for water O atoms.

The structures of the hydrated cluster, $CO_3^{\bullet-}.nH_2O$ (n=1-8) are calculated at B3LYP/6-311++G(d,p) level of theory and discussed in Chapter 2. Similarly various possible initial structures of $CO_3^{\bullet-}.nH_2O$ (n=1-8) clusters are considered for global geometry optimization and a number of minimum energy structures (conformers) are obtained. Fully optimized global minimum energy structure of each size of hydrated cluster, $CO_3^{\bullet-}.nH_2O$ (n=1-8) at B3LYP/6-311++G(d,p) level is displayed in Fig. 5.2. These structures of the hydrated cluster, $CO_3^{\bullet-}.nH_2O$ are very close to that discussed in Chapter 2.

It is observed that $CO_3^{\bullet-}.nH_2O$ clusters are stabilized by double hydrogen bonding (DHB), single hydrogen bonding (SHB) as well as inter water hydrogen bonding (WHB). In each case, the distance between the C and O atoms of carbonate moiety ($CO_3^{\bullet-}$) is ~ 1.3 Å. The calculated distance between O (of $CO_3^{\bullet-}$) and H-bonded H atoms is 1.8-2.2 Å (SHB and DHB bond) and the distance between O and H atoms in inter water network is 1.9-2.1 Å (WHB bond). It is worth to mention that the globally optimized structures for both the cases are very close to that of most stable structure as discussed in Chapter 2.

5.3.2. UV-Vis Spectra

Calculations are performed to find out a few low lying excited states for all the solvated clusters as well as for the isolated dimer radical anion ($Cl_2^{\bullet-}$) at both CIS and TDDFT level of theory to observe the shift in optical absorption wavelength (λ) of the dimer radical anion ($Cl_2^{\bullet-}$) with addition of solvent water molecules. The absorption maxima (λ_{max}) for isolated dimer radical anion ($Cl_2^{\bullet-}$) is found to be at 437 nm at CIS/6-

311++G(d,p) level of theory. The λ_{max} values of the $Cl_2^{\bullet-}.nH_2O$ clusters (n=1-11) calculated at same level of theory are listed in Table 5.1.

Excited state calculations at CIS/6-311++G(d,p) level of theory suggest that $Cl_2^{\bullet-}.nH_2O$ clusters (n=1-11) have absorption bands in UV-Vis region. Visualization of appropriate MOs indicates that the strong absorption is due to an electronic transition from the highest doubly occupied MO to the lowest singly occupied MO ($\sigma \rightarrow \sigma^*$) in all these hydrated clusters as in for bare $Cl_2^{\bullet-}$ system. This suggests that micro hydration does not change the bonding pattern in $Cl_2^{\bullet-}$ system. The optical absorption profiles for each of the $Cl_2^{\bullet-}.nH_2O$ systems (n=0-11) are generated using ten low lying excited states and the UV-Vis spectra for $Cl_2^{\bullet-}$ and $Cl_2^{\bullet-}.10H_2O$ systems are shown in Fig.5.3-I (a) and (b), respectively. There is an excellent agreement between the experimental aqueous phase optical absorption profile (see Fig.5.3-I c) and the present calculated one for $Cl_2^{\bullet-}.10H_2O$ cluster.[3,59] The calculated intensity is scaled with the measured molar extinction coefficient value for $Cl_2^{\bullet-}$(aq) following pulse radiolysis technique. It is worth to mention that λ_{max} values of the $Cl_2^{\bullet-}.nH_2O$ clusters calculated applying Time Dependent Density Functional Theory (TDDFT) are largely red shifted (~ 150 nm) in all these hydrated clusters.

The aqueous UV-Vis spectra of other similar radicals ($Br_2^{\bullet-}$ and $I_2^{\bullet-}$) are also studied. In these cases also the strong absorption is due to an electronic transition from the highest doubly occupied MO to the lowest singly occupied MO ($\sigma \rightarrow \sigma^*$). The simulated optical absorption profiles based on few low lying transitions for $Br_2^{\bullet-}.10H_2O$ and $I_2^{\bullet-}.8H_2O$ hydrated clusters are also in excellent agreement with experimental aqueous phase optical absorption profile.

Table 5.1. Calculated absorption maxima (λ_{max}) in nm at CIS/6-311++G(d,p) level of theory for $Cl_2^{\bullet-}.nH_2O$ (n=1-11) clusters and at TDDFT-B3LYP/6-311++G(d,p) level of theory for $CO_3^{\bullet-}.nH_2O$ (n=1-8) clusters.

Size	Absorption Maxima, λ_{max} (nm)	
	$Cl_2^{\bullet-}.nH_2O$	$CO_3^{\bullet-}.nH_2O$
$n = 1$	434	576
$n = 2$	434	560
$n = 3$	410	574
$n = 4$	418	559
$n = 5$	417	578
$n = 6$	415	580
$n = 7$	406	585
$n = 8$	417	595
$n = 9$	373	-
$n = 10$	346	-
$n = 11$	362	-

It is also interesting to study the change in optical absorption wavelength (λ) of the doublet carbonate radical anion ($CO_3^{\bullet-}$) with the successive addition of solvent water molecules. Excited state calculations are performed to find out a few low lying excited states for all the hydrated carbonate anion clusters, $CO_3^{\bullet-}.nH_2O$ as well as for the isolated radical anion ($CO_3^{\bullet-}$) applying time dependent density functional theory (TDDFT) with B3LYP hybrid density functional. The calculations are carried out for the most stable structure of each size hydrated cluster. The absorption maxima (λ_{max}) for isolated dimer

radical anion ($CO_3^{\bullet-}$) is found to be at 580 nm at TDDFT (B3LYP)/6-311++G(d,p) level of theory.

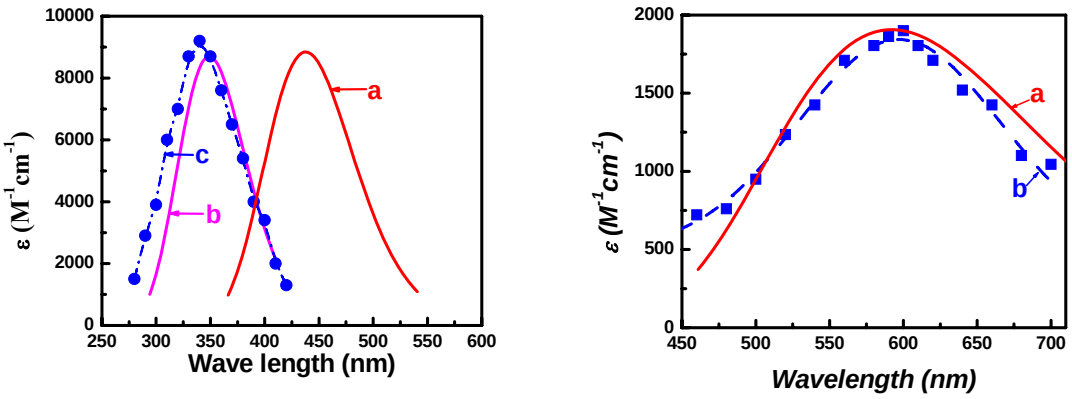

I **II**

Fig. 5.3. (I) Optical absorption profile for (a) $Cl_2^{\bullet-}$ and (b) $Cl_2^{\bullet-}.10H_2O$ at CIS/6-311++G(d,p) level of theory. (c) Experimental absorption profile for $Cl_2^{\bullet-}$ in aqueous solution. (II) Optical absorption profile for (a) the most stable structure of $CO_3^{\bullet-}.8H_2O$ at TDDFT/6-311++G(d,p) with B3LYP hybrid density functional and (b) experimental absorption profile for $CO_3^{\bullet-}$ in aqueous solution.

The λ_{max} values of the $CO_3^{\bullet-}.nH_2O$ clusters (n=1-8) calculated at the same level of theory are supplied in Table 5.1. Visualization of the appropriate molecular orbital (MO) indicates that the optical absorption is mainly due to an electronic transition from the highest doubly occupied bonding sigma MO to the lowest singly occupied antibonding sigma MO ($\sigma \rightarrow \sigma^*$) in all these hydrated clusters. The optical absorption profiles for each of the $CO_3^{\bullet-}.nH_2O$ systems (n=0-8) are generated based on ten low lying excited states and the UV-Vis spectra for $CO_3^{\bullet-}.8H_2O$ systems is shown in Fig. 5.3-II(a). There is an excellent agreement between the experimental aqueous phase optical absorption spectrum (see Fig. 5.3-II(b)) and the present calculated one for the most stable structure of $CO_3^{\bullet-}.8H_2O$ cluster.[60] The calculated absorbance is scaled with the reported experimental

molar extinction coefficient value for $CO_3^{\bullet-}$(aq) following pulse radiolysis technique. It is to be noted that λ_{max} values of the $CO_3^{\bullet-}.nH_2O$ clusters calculated by applying CIS (configuration interaction with single electron excitation) procedure is largely blue shifted (~ 350 nm) in all these hydrated clusters.

5.4. Conclusions

Global minimum energy structures of $Cl_2^{\bullet-}$ and $CO_3^{\bullet-}$ hydrated clusters are obtained applying simulated annealing with Monte Carlo sampling procedure. Based on a few calculated low lying excited states applying CIS procedure, UV-Vis spectra of these hydrated clusters are simulated. UV-Vis spectra of $Cl_2^{\bullet-}.10H_2O$ cluster is in excellent agreement with the measured aqueous phase spectra of $Cl_2^{\bullet-}$ system. Simulated UV-Vis spectra of $CO_3^{\bullet-}.8H_2O$ cluster at B3LYP-TDDFT/6-311++G(d,p) level is in excellent agreement with the measured aqueous phase spectra of $CO_3^{\bullet-}$ system. In all the cases the strong absorption is due to an electronic transition from the highest doubly occupied MO to the lowest singly occupied MO ($\sigma \rightarrow \sigma^*$).

CHAPTER 6

Structure, Energetics and Spectra of Ammonia Embedded Neutral Clusters

6.1. Introduction

Up to chapter 5, discussions have been carried about microhydration of neutral halogen molecule, X_2 (X=Cl, Br & I) and anionic non-spherical species, Y (Y= $Cl_2^{\bullet-}$, $Br_2^{\bullet-}$, $I_2^{\bullet-}$, $CO_3^{\bullet-}$, NO_3^- and CO_3^{2-}). This chapter describes about microsolvation of solute in a less polar medium like ammonia. In recent years, hydrogen bonded cluster of polar solvent molecules encapsulating a solute atom, small molecule or ion have been a subject of intense investigations for experimental as well as theoretical research. If a solute is immersed into a hydrogen bonded solvent medium, preexisting solvent network breaks up to accommodate the solute and a new hydrogen bonded network forms surrounding the solute. Ammonia is also an important solvent that can form hydrogen bonded network. The clusters of alkali metal atom and polar solvent molecules have been studied at length, often from the interests related to solvated electron. However, the detailed mechanism on the formation of solvated electron in this medium with alkali metal atom is not yet fully understood. Thus, solvated electron in polar solvents has been a subject of continued research. In this respect, a lot of research has been carried out to understand the structure and properties of singly negatively charged clusters of water and

ammonia.[61-62] Hydrogen bonded water clusters with alkali metal atom residing in the cluster cavity (M.$n$$H_2O$) have also been studied to a great extent.[63-67,17]

Solvated electrons can form rather readily with the alkali metals in polar solvent because of the relatively low energy requirement for ionization. The most familiar case occurs in the solvent stabilization of alkali metal atoms in bulk ammonia, where optical transitions involving these electrons are responsible for the strong colors of the resulting solutions. The formation of solvated electron in finite size clusters is also expected. A number of theoretical and experimental efforts have been put to gather knowledge on ammonia clusters in presence of Li, Na and Cs alkali metal atoms in the context of solvated electron.[16-17,66-72] In this chapter, structure, energy parameters and IR spectra of ammonia clusters in presence of a potassium metal atom (K.$n$$NH_3$, n=1-6) based on first principle electronic structure theory is presented to study the process of microsolvation in ammonia medium. Studies on these size selected clusters play a critical role to follow the evolution of molecular level properties with the size of the cluster in gas phase and to bridge the gap between the properties of single ammonia cluster (K-NH_3) to the bulk solution of K metal in ammonia solvent. The variation of calculated properties with size (n) of the clusters, K.$n$$NH_3$ is also reported. As a number of minimum energy structures are predicted for higher cluster, weighted average properties of the clusters are calculated based on the statistical population of different minimum energy structures at 150 K.

6.2. Theoretical Approach

Full geometry optimization of ammoniated clusters has been carried out without any symmetry restriction to locate minimum energy structures applying a nonlocal hybrid

density functional, namely, Becke's half-and-half (BHH) exchange and Lee-Yang-Parr (LYP) correlation functional (BHHLYP). Split valence basis set with diffusion and double polarization functions on all the atoms, 6-311++G(2d,2p) has been used in all calculations. Pseudo Newton Raphson based algorithm has been applied to look for the minimum energy structures for each K.nNH$_3$ cluster. The major concern in this algorithm is to guess a good starting geometry of the cluster, which might converge during the calculation to a local or the global minimum. In the present calculation, several possible starting geometries are generated based on different possible three-dimensional structures. Hessian calculations have been performed to check the nature of the optimized structures, to calculate thermodynamic parameters and to generate IR spectrum of the clusters. In a number of cases, first hand optimized minimum energy structures of these open shell systems have yielded one or more normal modes having imaginary frequency. In these cases, the structures have been reoptimized focusing attention on these normal modes till the structures generate no imaginary frequency. Population of the minimum energy configurations of each size clusters has been calculated based on free energy change (ΔG) at 150 K following Boltzmann population distribution.

6.3. Results and Discussion

6.3.1. Structure

Only one stable minimum energy structure is obtained through full geometry optimizations of small size (n=1-3) K.nNH3 clusters. It is to be noted that the geometries of clusters having different orientations of N atoms from NH$_3$ molecule with respect to K atom are considered as the initial guess structures in the present study and only the most

stable minimum energy structure is taken from different optimized configurations with small difference in dangling hydrogen orientations. All the stable configurations that are found for each size K.*n*NH_3 cluster are displayed in Fig. 6.1. The minimum energy structure of mono-ammoniated potassium cluster, K.NH_3 is shown in Fig. 6.1-I. It is clearly seen that N atom of NH_3 is directed towards the K atom and it is ~2.8 Å apart from the metal atom. It is worth to mention that two initial guess structures are considered for geometry optimization. In one case, the N atom of NH_3 is directed towards K atom and in the other case H atoms of NH_3 face towards the metal atom. Full geometry optimization generates exactly the same structure as shown in Fig. 6.1-I. Thus for the larger clusters, the initial thought structure is made where the N atom of NH_3 is oriented towards K atom. Only one minimum energy structure is predicted for di-ammoniated cluster, K.2NH_3 with ∠NKN of 180ºand the optimized structure is displayed in Fig. 6.1-II. Several initial guess structures are considered for the tri-ammoniated clusters, K.3NH_3 based on the minimum energy structure of K.2NH_3. But only one stable minimum energy structure displayed in Fig. 6.1-III is predicted having ∠NKN = 120º. In all these cases N and K atoms are in same plane. Two minimum energy structures are obtained for K.4NH_3 cluster and shown in Fig.6.1-IVA and IVB, respectively. The most stable structure (see Fig. 6.1-IVA) is a distorted tetrahedral with four N atoms in the corners keeping K atom at the center and more stable than structure IVB having square planar arrangement with four N atoms at the corners by 1.09 kcal/mol. Based on these minimum energy structures, initial guess structures for K.5NH_3 and K.6NH_3 are modeled. In each case, three stable minimum energy structures are found and displayed in Fig. 6.1-VA-VC and Fig.6.1-VIA-VIC, respectively. The most stable conformer of K.5NH_3 cluster is displayed in figure

Fig. 6.1-VA having distorted trigonal bipyramidal arrangement with five N atoms around K atom. The planar arrangement of five N atoms around K atom is least stable conformer among the three and shown in Fig. 6.1-VC. The solvent ammonia molecules are bound by each other with weak intermolecular hydrogen bonding. In structure 6.1-VB, the three NH_3 molecules in a plane approached to K from one side and two NH_3 molecules in approached to K from opposite side. The conformers shown in Fig. 6.1-VB and 6.1-VC is 3.20 and 0.89 kcal/mol, respectively less stable than the most stable conformer, VA. The most stable minimum energy structure of $K.6NH_3$ cluster is displayed in Fig. 6.1-VIA having distorted octahedral arrangement with six N atoms around the central K atom. Fig.6.1-VI B showing pentagonal pyramidal arrangement of N atoms around K atom and 0.36 kcal/mol less stable compare to the most stable structure. The least stable conformer of hexa ammoniated potassium cluster is shown in Fig. 6.1-VI C and having planar arrangement of six NH_3 molecules around K atom. The NH_3 molecules are connected by six weak intermolecular hydrogen bonds. This structure is 4.07 kcal/mol less stable than the most stable conformer.

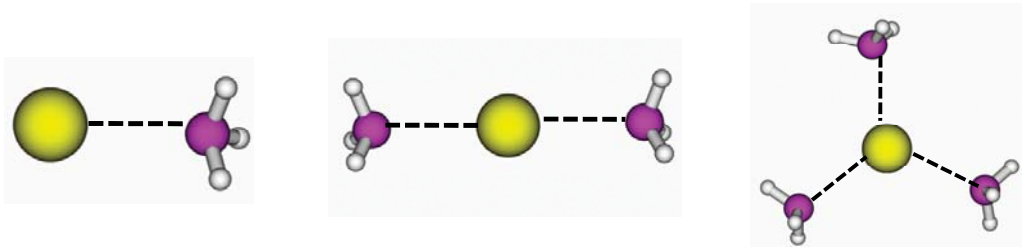

I **II** **III**

Fig. 6.1 (Contd.)

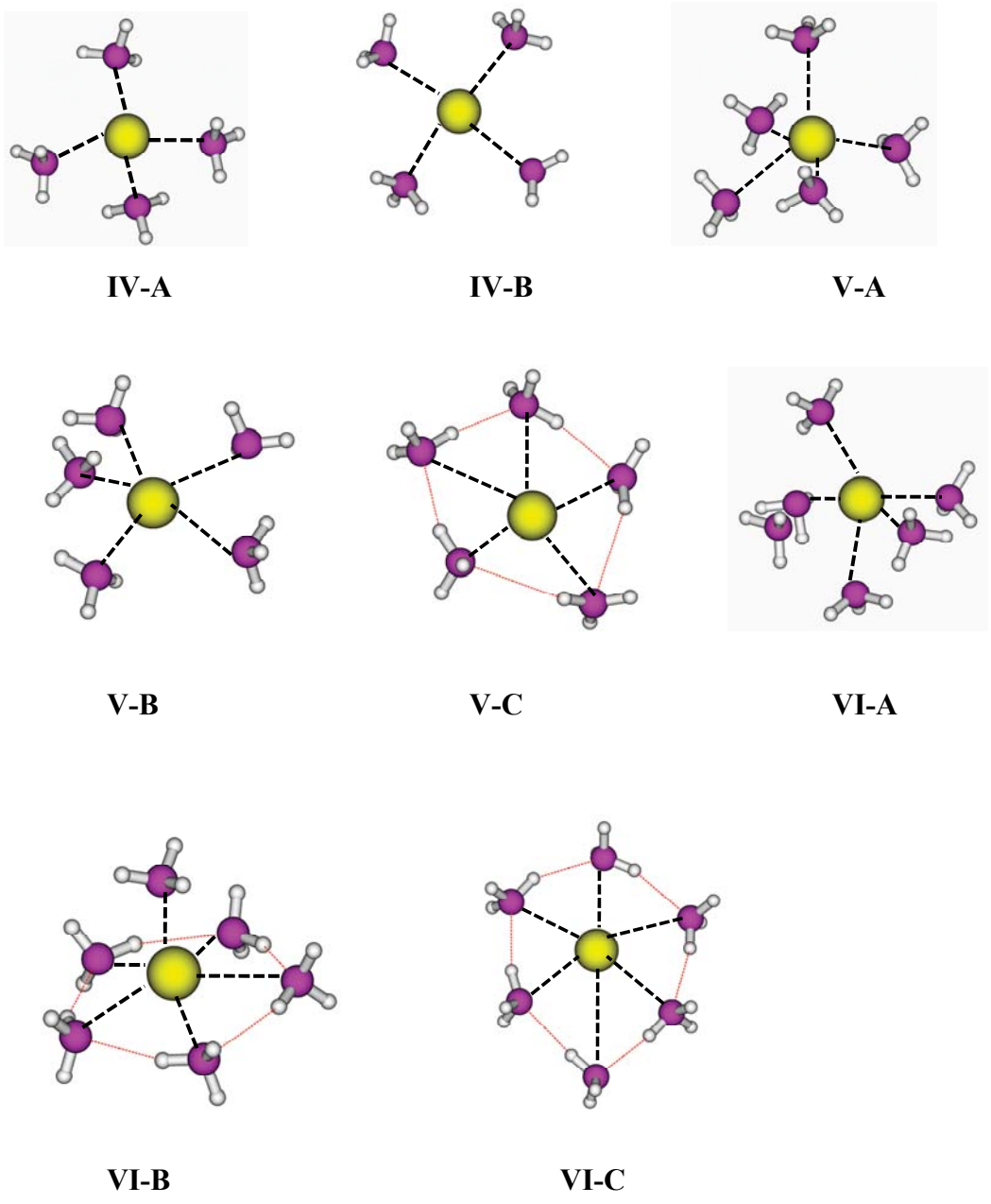

Fig. 6.1. The fully optimized structures calculated at BHHLYP/6-311++G(2d,2p) level of theory for (I) $K.NH_3$, (II) $K.2NH_3$, (III) $K.3NH_3$, (IV) $K.4NH_3$, (V) $K.5NH_3$, and (VI) $K.6NH_3$ clusters. K atoms are shown by the largest yellow colour spheres, the smallest white spheres refer to H atoms and the rest (pink colour) corresponds to N atoms in each structure shown in the figure. Marked alphabets in upper case are used to refer different minimum energy conformers for each hydrated cluster size arranged in order of stability showing 'A' as the most stable one.

In all the clusters, K.nNH$_3$ (n=1-6) the K-N distance varies from 2.8–3.0 Å. The energy of K..NH$_3$ interaction is calculated to vary from 5-6 kcal/mol and the energy due to hydrogen bonding between two NH$_3$ molecules is ~1 kcal/mol. Thus, the ammoniated cluster is dominantly stabilized by the solute-solvent interaction rather than solvent-solvent interaction. The solvent-solvent interaction energy plays significant role in the larger size clusters though.

6.3.2. Solvent Stabilization Energy

The solvent stabilization energy of K.nNH$_3$ clusters can be expressed as

$$E^{solv} = E_{K.nNH_3} - (nE_{NH_3} + E_K),$$

where $E_{K.nNH_3}$, E_{NH_3} and E_K refer to the total energy of the optimized cluster, K.nNH$_3$, the energy of a single NH$_3$ molecule at equilibrium geometrical and the energy of K atom, respectively. Thus, calculated E^{solv} essentially refers to the total interaction energy of the solute with n solvent NH$_3$ units around it in the ammoniated cluster of size n. The calculated weighted average solvent stabilization energy (E_w^{solv}) of the K.nNH$_3$ (n=1-6) clusters are supplied in Table 6.1. The plot for the variation of E_w^{solv} *vs*. n is shown in Fig. 6.2-A. The weight factor of a minimum energy structure within a particular size (n) of cluster is calculated based on the statistical population of the conformer at 150 K. The best-fitted linear plot having correlation coefficient greater than 0.99 is

$$E_w^{solv} = 2.06 + 5.35 \text{ n},$$

where E_w^{solv} is expressed in kcal/mol and n is the cluster size.

6.3.3. Vertical Ionization Potential

Vertical ionization potential (VIP) of the ammoniated clusters, K.nNH$_3$ can be calculated based on the relation,

VIP = E[K.nNH$_3$] - E^s[K$^+$.nNH$_3$],

where E[K.nNH$_3$] is the energy of the optimized K.nNH$_3$ cluster and E^s[K$^+$ nNH$_3$] is the single point energy of the K.nNH$_3$ obtained by removing one electron from the optimized K.nNH$_3$ cluster. VIP is the energy required to remove an electron from the neutral clusters. The weighted average VIP (VIP$_w$) values are also calculated and listed in Table 6.1. The plot for the variation of VIP$_w$ *vs*. *n* is displayed in Fig. 6.2-B showing gradual decrease in energy with the size of the cluster (*n*).

Table 6.1. Calculated weighted average energy parameter of K.nNH$_3$ clusters (*n*=1-6) at BHHLYP/6-311++G(2d,2p) level of theory.

Species	Weighted average solvent stabilization energy, E_w^{solv} (kcal/mol)	Weighted average vertical ionization potential, VIP_w (eV)
K.NH$_3$	6.21	3.75
K.2NH$_3$	12.41	3.28
K.3NH$_3$	19.22	2.94
K.4NH$_3$	25.52	2.76
K.5NH$_3$	28.74	2.75
K.6NH$_3$	32.6	2.60

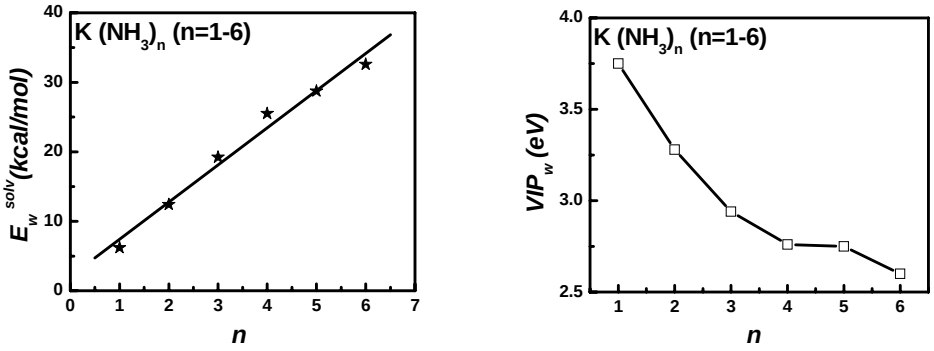

A B

Fig. 6.2. Plot of calculated weighted average (A) solvent stabilization energy (E_w^{solv}) in kcal/mol and (B) vertical ionization potential (VIP_w) in eV *vs*. number of ammonia molecules (*n*) in K.*n*NH_3 (*n*=1-6) cluster at BHHLYP/6-311++G(2d,2p) level of theory. To estimate E_w^{solv} and VIP_w the weight factor is calculated based on the statistical population of all the minimum energy structures of each size cluster at 150 K.

6.3.4. IR Spectra

As discussed in the previous sections, K.*n*NH_3 clusters are stabilized by the interaction between K and N (from NH_3) atoms as well as inter ammonia H-bonding interaction. Due to these interactions it is expected that bands due to stretching (N-H), bending and inversion modes of NH_3 in the ammoniated clusters K.*n*NH_3 (*n*=1-6) get shifted compared to that of free ammonia molecule. IR spectra for all the conformers of K.*n*NH_3 cluster (n ≤ 6) and free NH_3 are calculated. Lorentzian line shape has been applied with peak half-width of 20 cm^{-1} for all the IR spectra plots. Based on the literature data on the vibrational frequency of NH_3 (ν_{sym} = 3337 cm^{-1}, ν_{asym} = 3444 cm^{-1}, ν_{bend} = 1627 cm^{-1} and $\nu_{inversion}$ = 950 cm^{-1}) and the present calculated values (ν_{sym} = 3596 cm^{-1}, ν_{asym} = 3720 cm^{-1}, ν_{bend} = 1732 cm^{-1} and $\nu_{inversion}$ = 1061cm^{-1}) at BHHLYP/6-

311++G(2d,2p) level, the scaling factor is taken as 0.93 to account the anharmonic nature of vibration. The same scaling factor has been used for predicting IR spectrum in all these clusters. Calculated scaled frequencies for free NH_3 are 986, 1611, 3345 and 3460 cm^{-1}, respectively for inversion ($\nu_{inversion}$), bending (ν_{bend}), symmetrical stretching (ν_{sym}) and asymmetrical stretching (ν_{asym}) at BHHLYP/6-311++G(2d,2p) level of theory and the theoretical IR spectra is displayed in Fig.6.3-A. It is worth to mention that the peak in the N-H stretching region is due to asymmetric mode, and the symmetric mode is too weak to observe. Scaled IR spectra for mono ammoniated cluster, $K.NH_3$ with a strong sharp peak in the N-H stretching region is shown in Fig.6.3-B. It is interesting to observe that all the mode of ammonia compare to free molecule get red shifted ($\Delta\nu_{bend}$ = - 20 cm^{-1}, $\Delta\nu_{sym}$ = - 48 cm^{-1} and $\Delta\nu_{asym}$ = -59 cm^{-1}) except the inversion mode which is blue shifted compare to the same ($\Delta\nu_{inversion}$ = 100 cm^{-1}) in $K.NH_3$ cluster. It is also worth to mention that in the N-H stretching region the major contribution to the peak is from symmetric mode. The IR bands below 1000 cm^{-1} are due to librations of NH_3 in this cluster. Scaled IR spectra for di-ammoniated cluster, $K.2NH_3$ with a strong sharp peak in the N-H stretching region is shown in Fig.6.3-C. It is clear from the figure that the inversion mode gets blue shifted ($\Delta\nu_{inversion}$ = 105 cm^{-1}) compare to that free ammonia molecule, and the bending mode is vanished. The scaled IR spectra of $K.3NH_3$ cluster is displayed in Fig.6.3-D and similar in nature to that of $K.2NH_3$ cluster. From tetra-ammoniated cluster onwards (n>3) more than one conformer is found, so weighted average scaled IR spectra is generated based on the statistical population at 150 K. Weighted average scaled IR spectra of $K.4NH_3$ cluster with strong sharp peak in the N-H stretching region is displayed in Fig.6.3-E. It is clearly seen from the Fig.6.3-D, that the inversion band is vanished and the bending mode is

reappear. Both the bending and inversion mode is seen in the weighted average scaled IR spectra of $K.5NH_3$ cluster (see Fig.6.3-E). The IR spectra of $K.5NH_3$ cluster also consists of strong peak at N-H stretching region. The features of the weighted average scaled IR spectra of $K.6NH_3$ cluster (see Fig.6.3-F) is very similar to that of $K.6NH_3$ cluster. In all the IR spectra of $K.6NH_3$ cluster (n =1-6) the bending and stretching bands are red shifted ($\Delta\nu$ = -) and inversion band is blue shifted ($\Delta\nu$ = +) compare to that of free ammonia molecule. It is also interesting to observe that in the N-H stretching region the major contribution to the peak is from symmetric mode for all the ammoniated clusters, $K.6NH_3$ (n =1-6). On the other hand the major contribution to the peak due to N-H stretching for free NH_3 molecule is due to the asymmetric mode.

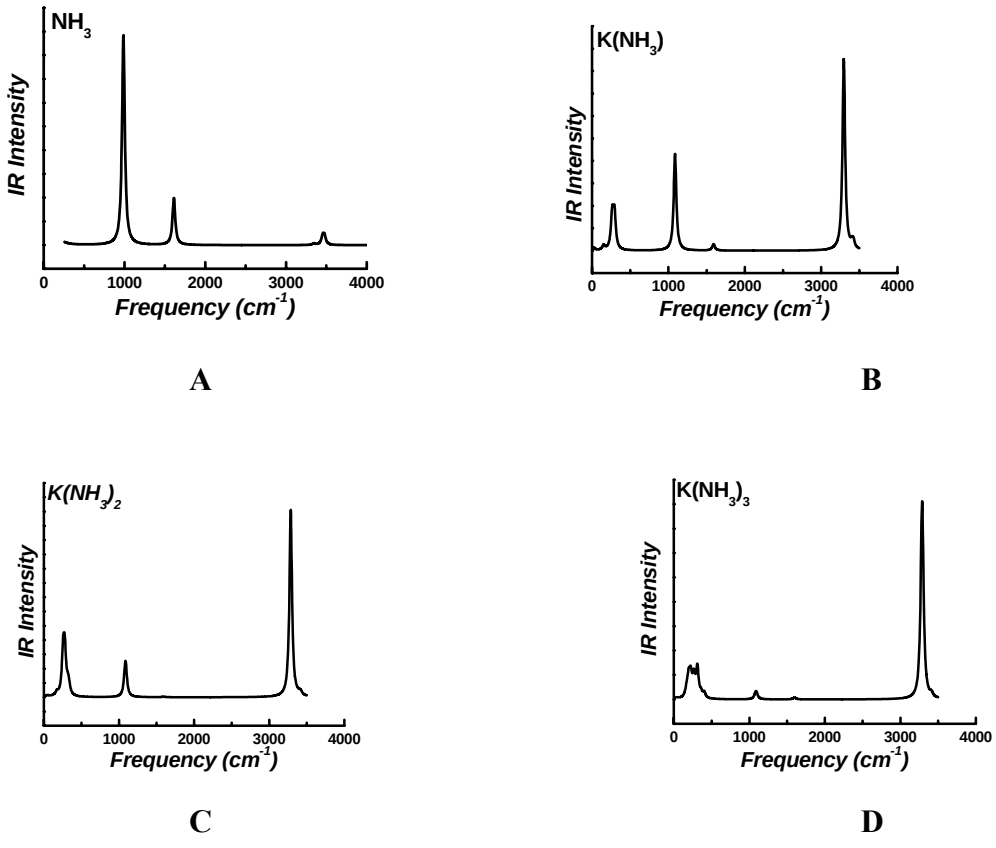

Fig. 6.3 (Contd.)

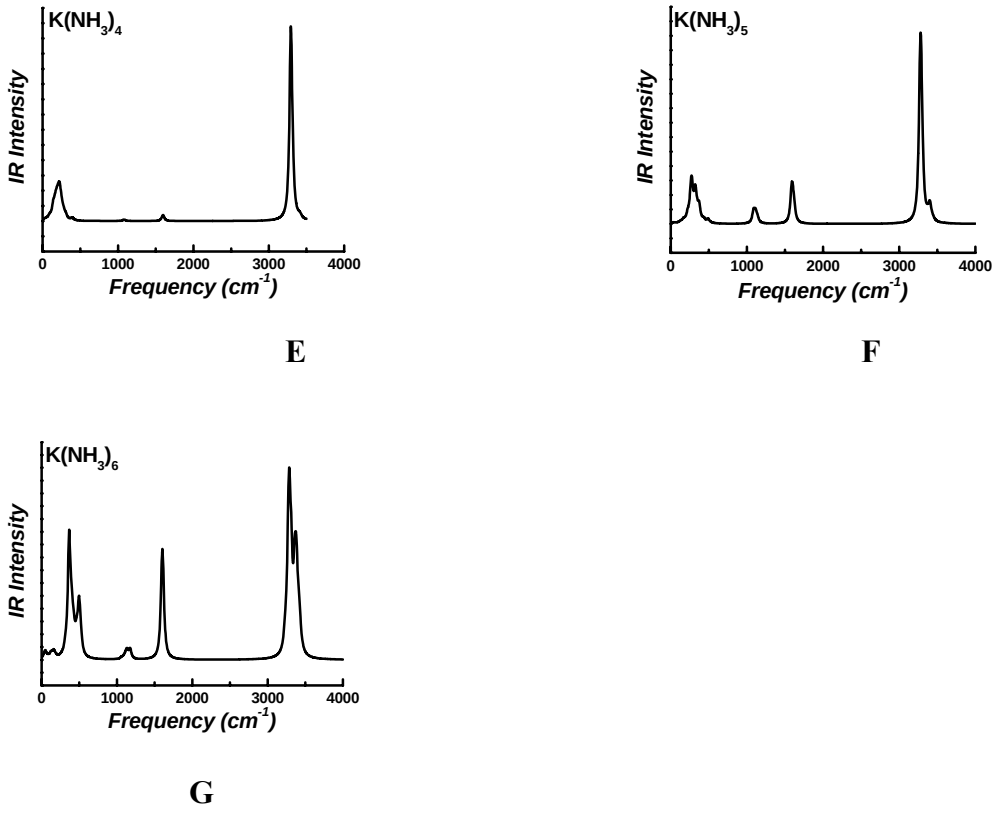

Fig. 6.3. Calculated scaled IR spectra at BHHLYP/6-311++G(2d,2p) level of theory for (A) free NH_3 molecule, and for the ammoniated cluster, K.*n*NH_3 (*n*=1-3), (B) K.NH_3; (C) K.2NH_3; (D) K.3NH_3. Calculated scaled weighted average IR spectra at same level for the ammoniated cluster, K.*n*NH_3 (*n*=4-6), (E) K.4NH_3; (F) K.5NH_3; (G) K.6NH_3. The scaling factor is taken as 0.93 to account the anharmonic nature of vibrations. The weight factor is calculated based on statistical population of individual conformer at 150 K. Lorentzian line shape has been considered with peak half-width of 20 cm^{-1} for all the IR plots.

6.4. Conclusions

Structure and energy of ammoniated clusters, K.*n*NH_3 (*n*=1-6) are reported to study the micro-solvent stabilization of potassium atom in ammoniated environment. Becke's half and half hybrid exchange-correlation functional (BHHLYP) has been applied to study the present systems with a Pople triple split valence 6-311++G(2d,2p) basis function. Various initial guess structures are taken for each size of cluster and full

geometry optimizations are carried without imposing any symmetry restriction. Several closely spaced minimum energy structures are predicted for larger size clusters (n>3) based on quasi-Newton search. It is observed that the ammoniated potassium cluster is stabilized by different types of interactions namely potassium–nitrogen interaction and hydrogen bonded interaction in ammoniated network. But structures having potassium–nitrogen interactions are more stable compared to those of hydrogen bonded structures. As several closely spaced minimum energy structures are obtained for larger clusters (n>3), weighted average energy parameters are also calculated based on the statistical population at 150 K. Linear variation of weighted average solvent stabilization energy with size of the cluster (n) is observed. Gradual decrease in VIP_w with the size of the cluster (n) is also observed. Hessian calculation is also carried out on each cluster to generate IR spectra. In all the IR spectra of K.$n$$NH_3$ cluster (n=1-6) the bending and stretching bands are red shifted and inversion band is blue shifted compare to that of free ammonia molecule. It is also interesting to observe that in the N-H stretching region the major contribution to the peak is from symmetric mode for all the ammoniated clusters, K.$n$$NH_3$ (n=1-6). On the other hand the major contribution to the peak due to N-H stretching for free NH_3 molecule is due to the asymmetric mode.

CHAPTER 7

Structure, Energetics and Spectra of CO_2 Embedded Anionic Clusters

7.1. Introduction

Up to chapter 6, discussions have been carried about microsolvation of various charged and neutral species in strongly polar solvent like water and less polar solvent like ammonia medium. To understand the microsolvation of solutes, studies have been carried out also in nonpolar medium like carbon dioxide and presented in this chapter. Small anionic clusters having negatively charged chromophore have considered as model systems for studying the influence of solvation on various fundamental molecular processes.[73-74] In this regard, iodine dimer radical anion ($I_2^{\bullet-}$) embedded in argon (Ar) and carbon dioxide (CO_2) cluster have been studied extensively by various researchers applying both experimental and theoretical techniques.[75-79] Photo induced dissociation and recombination dynamics of these clusters have been studied by femtosecond photoelectron spectroscopy, time-resolved absorption recovery experiments and molecular dynamics simulation. Molecular electronic structure theory has also been applied to study the geometry of the solvated monomer cluster, $I_2^{\bullet-}.CO_2$.[48] *First principle* based theoretical studies is interesting in such clusters for characterizing the specific interactions between solute $I_2^{\bullet-}$ and solvent CO_2 molecules as well as between two solvent CO_2 molecules. As CO_2 molecule is having centre of symmetry, vibrational IR

and Raman spectroscopic studies is also interesting to study the microsolvation of $I_2^{\bullet-}$ in CO_2. In what follows, a systematic theoretical study on structure, energetics (solvent stabilization, interaction and vertical detachment energy) and spectra (both IR and Raman) of $I_2^{\bullet-}.nCO_2$ clusters (n=1-10) is presented to elucidate the effect of microsolvation in this chapter.

7.2. Theoretical Approach

It is reported in the literature that BHHLYP functional performs well to describe such open shell doublet systems.[43-44] Energy parameters are further improved by single point energy calculations applying second order Moller-Plesset (MP2) perturbation theory adopting 6-311+G(d) basis sets. Quasi Newton Raphson based algorithm as well as Monte Carlo based simulated annealing procedures have been applied with the effective fragment solvent CO_2 molecules to find out the global minimum energy structure of different size molecular clusters.[36] Hessian calculations have been performed for all the optimized minimum energy structures to check the nature of the equilibrium geometry and to generate IR spectrum. Raman spectrum is also calculated for all the clusters. Basis sets 6-311G(d) for I is obtained from the Extensible Computational Chemistry Environment Basis Set Database, Pacific Northwest National Laboratory.

7.3. Results and Discussions

7.3.1. Structure

It is observed that, in this system the conformers of a particular size of cluster is very close in energy (within 0.3 kcal/mol) and have near equal statistical contribution.

Thus Monte Carlo based simulated annealing procedure is applied to find out the global minimum energy structures. The most stable structure of mono solvated cluster, $I_2^{\bullet-}.CO_2$ calculated at BHHLYP level of theory is shown in Fig. 7.1(A). It is interesting to note that the CO_2 moiety in the cluster is near perpendicular to I…I axis in the most stable structure. It is to be noted that an initial guess structure where the CO_2 moiety is parallel to I…I axis is also considered. However, geometry optimization leads to the same structure as shown in Fig. 7.1(A). It is clearly observed from Fig. 7.1(A) that the geometry of solvent CO_2 unit in the cluster is slightly distorted form isolated CO_2 structure in presence of $I_2^{\bullet-}$ system. Free CO_2 is having $D_{\alpha h}$ point group with r_{CO}= 1.14 Å and <OCO = 180º. But in the cluster, CO_2 unit has a lower symmetry (C_{2v}) with the calculated bond distance and bond angle of 1.14 Å and 176.4º respectively. The calculated geometrical parameters of the cluster suggests that the solvent CO_2 molecule in the solvated anion cluster is bent by ~ 3.6º, CO bond length remains unchanged though compared to free CO_2.

The most stable structures for $I_2^{\bullet-}.nCO_2$ (n=2-10) are displayed in Fig. 7.1(B-J). The calculated <OCO angles are varied from 176.8º to 177.3º in the most stable structure of $I_2^{\bullet-}.5CO_2$ cluster (structure shown in Fig. 7.1E). Similar variation in calculated <OCO angles is observed for $I_2^{\bullet-}.nCO_2$ clusters (n=6-10). It is observed that for clusters having more than five solvent CO_2 units, at least one solvent CO_2 unit is at a distance of > 4 Å from solute $I_2^{\bullet-}$ unit.

In contrast to the present observation, the previous theoretical prediction based on molecular dynamics simulation incorporating an empirical force field for solute-solvent as well as solvent-solvent interactions favors the successive addition of solvent CO_2

molecules in an asymmetric fashion.[74] This may be due to inaccurate treatment of solute-solvent and solvent-solvent interactions in these anionic clusters favoring induced dipole-induced dipole interaction between two solvent CO_2 molecules over ion-induced dipole interaction between the solute $I_2^{\bullet-}$ and solvent CO_2 molecules. To verify the influence of spin-orbit coupling in the equilibrium structure of these solvated clusters, geometry optimizations of the equilibrium structures are repeated including spin orbit interaction at the same level of theory for *n*=1 and 6 as test cases with no significant change in the optimized structures.

In summary, the calculated I…I bond distance is shorter than the isolated solute $I_2^{\bullet-}$ (3.334 Å) unit in all the solvated clusters, $I_2^{\bullet-}.nCO_2$ (*n*=1-10). On each successive addition of solvent CO_2 units, I…I distance decreases in all these solvated clusters. On the addition of ten solvent CO_2 molecules to the iodine dimer radical anion system, $I_2^{\bullet-}$ a decrease of ~ 0.3 Å in I…I bond distance is occurred. In all these cases, the structures obtained on full optimization applying Newton Raphson procedure are further optimized using Monte Carlo simulated annealing method to look for the global minimum energy structures. However, in all the cases the global structures predicted are very close to those obtained by applying Newton Raphson procedure. On refining these global minimum energy structures applying BHHLYP method, the same structures are obtained. This confirms that the predicted structures are truly global minimum energy structures.

To see the effect of solvation on the distribution of the excess electron in iodine dimer radical anion, $I_2^{\bullet-}$, Mulliken atomic spin ($\alpha-\beta$) population over different atoms is calculated in $I_2^{\bullet-}.nCO_2$ clusters (n=1-10). It is observed that the odd electron spin is mostly populated over two I atoms in case of mono solvated cluster, $I_2^{\bullet-}.CO_2$.

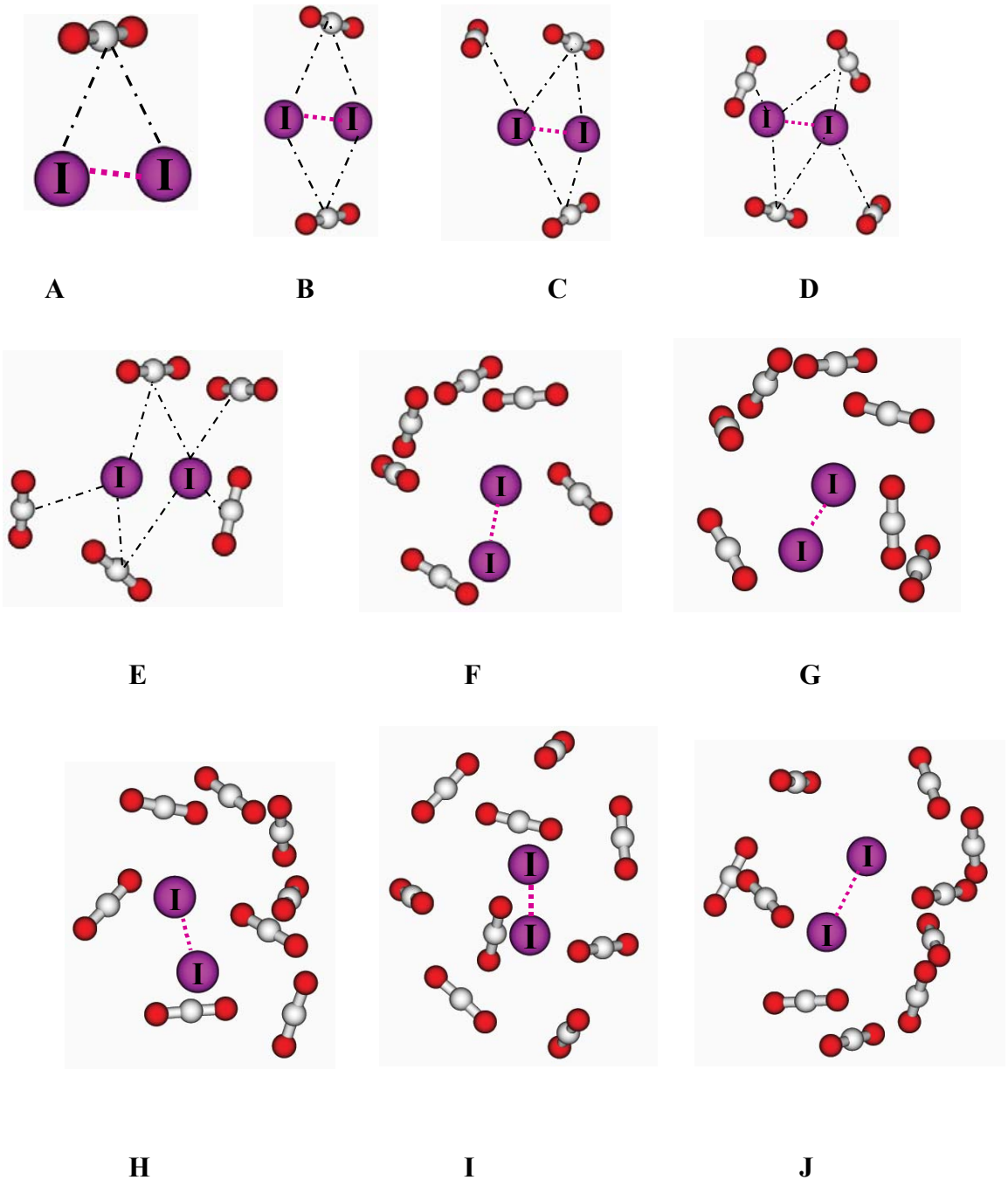

Fig. 7.1. Fully optimized global minimum energy structures calculated at BHHLYP/6-311+G(d) level of theory for (A) $I_2^{\bullet-}.CO_2$, (B) $I_2^{\bullet-}.2CO_2$, (C) $I_2^{\bullet-}.3CO_2$, (D) $I_2^{\bullet-}.4CO_2$, (E) $I_2^{\bullet-}.5CO_2$, (F) $I_2^{\bullet-}.6CO_2$, (G) $I_2^{\bullet-}.7CO_2$, (H) $I_2^{\bullet-}.8CO_2$, (I) $I_2^{\bullet-}.9CO_2$ and (J) $I_2^{\bullet-}.10CO_2$ clusters (I atom is treated by 6-311G(d) basis set). I atoms are shown by the largest violet spheres, the grey spheres correspond to C atoms and the red spheres refer to O atoms of solvent CO_2 units in each structure of the solvated cluster. In each case, the distance between the two I atoms is ~ 3.3 –3.0 Å, the distance between C and I atoms is ~ 3.9-4.9Å.

It is also noticed that the spin distribution of the odd electron changes marginally on successive addition of solvent CO_2 molecules in $I_2^{\bullet-}.nCO_2$ clusters (n=2-10). Mulliken and Lowdin population analysis also suggests that a major part of the excess charge is distributed mainly over the solute moiety in all the solvated clusters, $I_2^{\bullet-}.nCO_2$ (n=1-10).

7.3.2. Solvent Stabilization and Ion-Solvent Interaction Energy

The solvent stabilization energy of $I_2^{\bullet-}.n\ CO_2$ clusters can be expressed as

$$E^{stab} = E_{I_2^-.nCO_2} - (nE_{CO_2} + E_{I_2^-}),$$

where $E_{I_2^-.nCO_2}$, E_{CO_2} and $E_{I_2^-}$ refer to the total energy of the cluster $I_2^{\bullet-}.nCO_2$, the energy of a single solvent CO_2 molecule and the energy of bare $I_2^{\bullet-}$ system, respectively. The calculated E^{solv} values are tabulated in Table 7.1. Thus, E^{solv} essentially evaluates to the total interaction energy (ion-solvent interaction + solvent-solvent interaction) of the solute $I_2^{\bullet-}$ with n solvent CO_2 units around the solute in the solvated cluster of size n. The plot for the variation of E^{solv} *vs*. n (cluster size) is displayed in Fig. 7.2-I(a) to show that E^{solv} varies linearly with the number of solvent CO_2 molecules in the solvated clusters and the variation of E^{solv} is best fitted by the following linear relation:

$E^{solv} = -0.072 + 0.243.n$,

when E^{solv} is expressed in eV and n is the number of solvent CO_2 molecules. This linear fitted plot has correlation coefficient greater than 0.999. Stabilization energy for solvated cluster, $I_2^{\bullet-}.nCO_2$ (n=1-10) calculated by applying such discrete model corresponds to the internal energy of the molecular clusters. The stabilization energy of the clusters (E^{solv}) increases with the increase in the number of solvent molecules accounting ion-solvent

interaction as well as solvent-solvent interaction. In other words, solvent stabilization energy does not saturate because it remains favorable to attach additional CO_2 molecules to the existing CO_2 network. The linear relationship between solvent stabilization energy (E^{solv}) and cluster size (n) suggests that on an average the total interaction energy between anionic solute $I_2^{\bullet-}$ and solvent CO_2 molecule is ~ 243 meV for small size clusters at MP2 level of theory.

The interaction between the solute iodine dimer radical anion, $I_2^{\bullet-}$ and the solvent CO_2 cluster, $(CO_2)_n$ known as interaction energy between ion and solvent ($E^{int\text{-}is}$) may be calculated by the following relation,

$$E^{\text{int}-is} = E_{I_2^-.nCO_2} - (E_{(CO_2)_n} + E_{I_2^-})$$

where $E_{I_2^-.nCO_2}$, $E_{(CO_2)_n}$ and $E_{I_2^-}$ refer to the energy of the cluster $I_2^{\bullet-}.nCO_2$, the energy of $(CO_2)_n$ system and the energy of $I_2^{\bullet-}$ system respectively. The energy of the $(CO_2)_n$ system ($E_{(CO_2)_n}$) is calculated by removing the solute part from the fully relaxed structure of the solvated cluster followed by single point energy calculation at the same level of theory. $E_{I_2^-}$ is also evaluated in the same way i.e. by removing the solvent CO_2 units from the optimized structure of the cluster followed by single point energy calculation. The definition suggests that the interaction energy accounts the net interaction of solute $I_2^{\bullet-}$ and the solvent CO_2 molecules eliminating inter solvent interactions. The calculated ion-solvent interaction energy for $I_2^{\bullet-}.nCO_2$ (n=1-10) is tabulated in Table 7.1. The plot for the variation of $E^{int\text{-}is}$ *vs*. n (cluster size) is depicted in Fig. 7. 2-I(b). It is observed that $E^{int\text{-}is}$ also varies linearly with the number of solvent CO_2 molecules in the solvated clusters and the variation of $E^{int\text{-}is}$ is best fitted by the following linear relationship.

$E^{int\text{-}is} = 0.171 + 0.129.n$,

when $E^{int\text{-}is}$ is expressed in eV and n is the number of solvent CO_2 molecules. This linear fitted plot has correlation coefficient > 0.99. The linear relation suggests that the average interaction energy between the anionic solute and a solvent CO_2 molecule is ~ 129 meV at MP2 level.

On subtracting the ion-solvent interaction ($E^{int\text{-}is}$) from the solvent stabilization energy (E^{stab}) of each cluster, the solvent-solvent interaction energy ($E^{int\text{-}ss}$) can be evaluated. The calculated solvent-solvent interaction energy ($E^{int\text{-}ss}$) of $I_2^{\bullet-}.nCO_2$ (n=1-10) is tabulated in Table 7.1. The variation of $E^{int\text{-}ss}$ with size of the cluster (n) is also shown in Fig. 2-I(c).

As the solvent CO_2 molecules are far apart, the calculated solvent-solvent interaction energy is close to zero for $I_2^{\bullet-}.nCO_2$ clusters ($n \leq 4$). For higher clusters the same increases asymptotically. In the present case, the solvent-solvent interaction energy has dispersion nature and originated from dipole induced dipole-dipole interaction of solvent CO_2 molecules. It is worth to mention that the calculated interaction energy between two solvent CO_2 molecules is ~ 85 meV in case of neutral $(CO_2)_n$ clusters (n=1-3) at MP2/6-311+G(d) level of theory. The energy parameters for mono- and di- solvated clusters are also calculated applying CCSD(T) method and the values are listed in Table 7.1. It is worth to mention that basis set superposition error (BSSE) calculated for di-solvated cluster, $I_2^{\bullet-}.2CO_2$ following counterpoise method is less than 5% and the same for mono-solvated cluster, $I_2^{\bullet-}.CO_2$ is about 12%.[45]

Table 7.1. Various energy parameters in eV of the most stable conformer for each size cluster of $I_2^{\bullet-}.nCO_2$ (n=1-10) at MP2/6-311+G(d) level of theory.

Species, $I_2^{\bullet-}.nCO_2$	E^{solv} in eV[$]	$E^{int\text{-}is}$ in eV[$]	$E^{int\text{-}ss}$ in eV	VDE^n in eV			
				Experimental Measurement[‡]	MP2/6-311+G(d)[†]	CCSD(T)/6-311+G(d)[†]	MP2/6-311+G(d) + SOC[†]
n=0	-	-	-	3.24	3.41 (5)	3.12 (4)	3.33 (3)
n=1	0.224, (0.232)	0.224, (0.232)	-	3.38	3.56 (5)	3.29 (3)	3.49 (3)
n=2	0.430, (0.442)	0.422, (0.435)	0.008, (0.008)	3.49	3.71 (6)	3.44 (2)	3.66 (5)
n=3	0.648	0.574	0.074	3.59	3.79 (6)	-	3.75 (4)
n=4	0.838	0.753	0.085	3.67	3.92 (7)	-	3.87 (5)
n=5	1.052	0.842	0.211	3.74	3.97 (6)	-	3.93 (5)
n=6	1.424	0.976	0.448	3.82	4.02 (5)	-	3.99 (4)
n=7	1.636	1.099	0.537	3.90	4.08 (5)	-	4.06 (4)
n=8	1.866	1.219	0.647	3.99	4.15 (4)	-	4.11 (3)
n=9	2.225	1.300	0.925	-	-	-	-
n=10	2.298	1.427	0.872	-	-	-	-

[$]Values in the parentheses are at CCSD(T)/6-311+G(d) level of theory.

[‡]Values are corresponding to 'X' band data taken from ref. 48.

[†]Values in the parentheses are the maximum % error with respect to the experimental measurement. I atom is treated by 6-311G(d) basis set in all the calculations.

7.3.3. Vertical Detachment Energy

Vertical detachment energy (VDE) of $I_2^{\bullet-}.nCO_2$ (n=1-8) clusters are reported by Neumark and co-workers.[48] Vertical detachment energy (VDE) is the energy required to remove an electron from the anionic solvated clusters. VDE of the solvated clusters, $I_2^{\bullet-}.nCO_2$ can be defined by the relation:

$$VDE^n = E[I_2^{\bullet-}.nCO_2] - E^s[I_2.nCO_2],$$

where $E[I_2^{\bullet-}.nCO_2]$ is the energy of the optimized $I_2^{\bullet-}.nCO_2$ cluster and $E^s[I_2.nCO_2]$ is the single point energy of the $I_2.nCO_2$ obtained by removing the extra electron from the optimized $I_2^{\bullet-}.nCO_2$ cluster. The VDE for the minimum energy structures (most stable structure) of the cluster, $I_2^{\bullet-}.nCO_2$ (n=1-8) is calculated following post Hartree-Fock second order Moller-Plesset (MP2) perturbation theory with 6-311+G(d) set of basis functions (for I 6-311G(d) basis set is taken). The VDE values calculated without and with spin-orbit coupling are tabulated in Table 7.1. The variation of VDE with the size of the cluster (n) is shown in Fig. 7.2-II (a) and II (b), respectively without and with spin-orbit coupling (SOC) with relativistic corrections.[80] It is clearly seen that the VDE values is blue-shifted with increasing cluster size and this is consistent with the previous report (the experimental data is also shown in Fig. 7.2-II-c).[48] Increasing VDE with size signifies that the stability of the neutral cluster decreases with size. The calculated values of VDE and the variation of present theoretical values on VDE of solvated clusters with size is in excellent agreement with the VDE value corresponding to the X band measured by Neumark and coworker (see Table 7.1).[48] The X band is only surviving band for highest cluster (n=8) in their study. It is worth to mention that the weighted average VDE is also calculated for the $I_2^{\bullet-}.8CO_2$ cluster (taking 6 minimum energy structures) and no

change in VDE is observed. This is due to the fact that all the minimum energy structure are very close in energy and all having nearly same VDE. As calculation of VDE at CCSD(T) level for higher cluster is beyond our scope at present so VDE for the two lower cluster are calculated at CCSD(T) level of theory with same basis set and are systematically lower than the MP2 values by 0.27 eV (see Table 7.1).

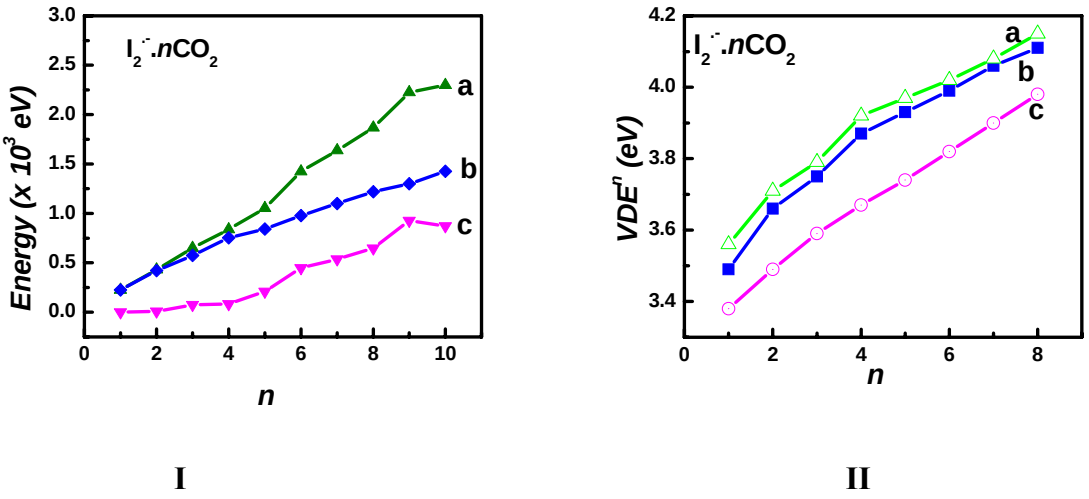

Fig. 7.2. (I) Variation of calculated (a) solvent stabilization energy (E^{solv}), (b) ion-solvent interaction energy (E^{int-is}) and (c) solvent-solvent interaction energy (E^{int-ss}) in kcal/mol with the number of solvent CO_2 molecules (n) in $I_2^{\bullet-}.nCO_2$ cluster at MP2/6-311+G(d) level of theory .(II) Plot of vertical detachment energy, (VDE^n) in eV *vs.* number of CO_2 molecules (n) of $I_2^{\bullet-}.nCO_2$ cluster (n=1-8) (a) at MP2/6-311+G(d) level without SOC corrections , (b) at MP2/6-311+G(d) level with SOC corrections and (c) at experimental level. (I is treated by 6-311G(d) basis set).

7.3.4. IR and Raman Spectra

As discussed in the earlier section, $I_2^{\bullet-}.nCO_2$ (n=1-10) clusters are stabilized by the interaction between $I_2^{\bullet-}$-CO_2 (solute-solvent) as well as CO_2-CO_2 (solvent-solvent) interactions. Due to these interactions, it is expected that the normal modes of solute and

solvent units in $I_2^{\bullet-}.nCO_2$ (n=1-10) clusters get modified compared to that of free solute $I_2^{\bullet-}$ and solvent CO_2 units. Normal mode analysis for all the $I_2^{\bullet-}.nCO_2$ clusters (n=1-10) and isolated $I_2^{\bullet-}$ and CO_2 systems has been carried out. IR and Raman spectra of these systems have been simulated. Lorentzian line shape has been applied with peak half-width of 10 cm^{-1} for all the vibrational spectral plots. Based on the literature data on the stretching and bending frequency modes of CO_2 (ν_{bend} = 667 cm^{-1}, ν_{sym} = 1388 cm^{-1} and ν_{asym} = 2349 cm^{-1}) and the present calculated values (ν_{bend} = 703 cm^{-1}, ν_{sym} = 1466 cm^{-1} and ν_{asym} = 2547 cm^{-1}) at BHHLYP/6-311+G(d) level of theory, the scaling factor is considered as 0.93 to account the anharmonic nature of vibrations. The same scaling factor has been used for predicting vibrational spectrum in all these clusters. Calculated scaled frequencies for free CO_2 are 653, 1363 and 2369 cm^{-1}, respectively for bending (ν_{bend}), symmetrical stretching (ν_{sym}) and asymmetrical stretching (ν_{asym}) and the theoretical IR and Raman spectra are displayed in Fig. 7. 3(A) and 3(B), respectively.

As CO_2 is having center of symmetry, the symmetric stretching mode is only Raman active, and other modes are IR active as shown in Fig. 7.3(A) and Fig. 7.3(B). The only vibrational mode (91 cm^{-1}) of $I_2^{\bullet-}$ is also Raman active and shown in Fig. 7.3(C). It is to be noted that symmetric stretching mode of CO_2 in these solvated clusters remains insensitive. Scaled IR and Raman spectra for mono solvated cluster, $I_2^{\bullet-}.CO_2$ is shown in Fig. 7.3(D) and 7.3(E) respectively. The IR spectrum is characterized by a strong peak at 2332 cm^{-1} in asymmetric stretching region of C-O bond and a relatively weak band at ~650 cm^{-1} in the bending region of C-O bond. The Raman spectra is characterized by a strong band at ~90 cm^{-1} (corresponding to symmetric I-I stretch) and two weak bands at ~ 650 cm^{-1} (corresponding to bending mode of CO_2) and 1346 cm^{-1} (corresponding to

symmetric C-O stretching mode of CO_2). The interesting feature of this Raman spectrum is band at ~ 650 cm^{-1} (bending region of CO_2 molecule) and a very weak band at ~ 2330 cm^{-1} (asymmetric C-O stretching region of CO_2), which are absent in the free CO_2 Raman spectrum(see Fig. 7.3). The $I_2^{\bullet-}.CO_2$ cluster is stabilized by $I_2^{\bullet-}$ and CO_2 interaction, and some amount of negative charge is also transferred to solvent CO_2 moiety from the solute $I_2^{\bullet-}$ unit. As a result, the symmetry of CO_2 molecule is distorted compared to the free solvent molecule and the symmetric bending mode becomes Raman active. Symmetric C-O stretching mode remains IR inactive as in case of free CO_2 system. Both the stretching modes of CO_2 are red shifted compared to the free molecule ($-\Delta\nu_{sym}$ = 17 cm^{-1} and $-\Delta\nu_{asym}$ = 37 cm^{-1}) but the bending mode is both red and blue shifted compared to the free molecule ($\Delta\nu_{bend}$ = + 5 and -6 cm^{-1}) in this cluster. The degeneracy of bending vibrational mode of CO_2 is lost in this anionic mono solvated cluster, $I_2^{\bullet-}.CO_2$. Two bands at 647 and 658 cm^{-1} are observed in the vibrational analysis, and appeared as small broad peak ~650 cm^{-1} in both IR and Raman spectra compared to free CO_2 molecule spectra. IR spectra of the larger solvated anionic clusters, $I_2^{\bullet-}.nCO_2$ (n=2-10) show more or less similar features as their smaller counter parts. However, marked differences are observed in Raman spectra of these clusters on successive addition of solvent CO_2 molecules. The relative intensity of the Raman band corresponding to symmetric stretching region of C-O bond continuously increases on successive addition of solvent CO_2 units; the position of the band is insensitive to the number of solvent molecules though. The weak Raman band at ~ 2330 cm^{-1} is most intense in case of $I_2^{\bullet-}.9CO_2$ cluster (see Fig. 7.3F). This may be due

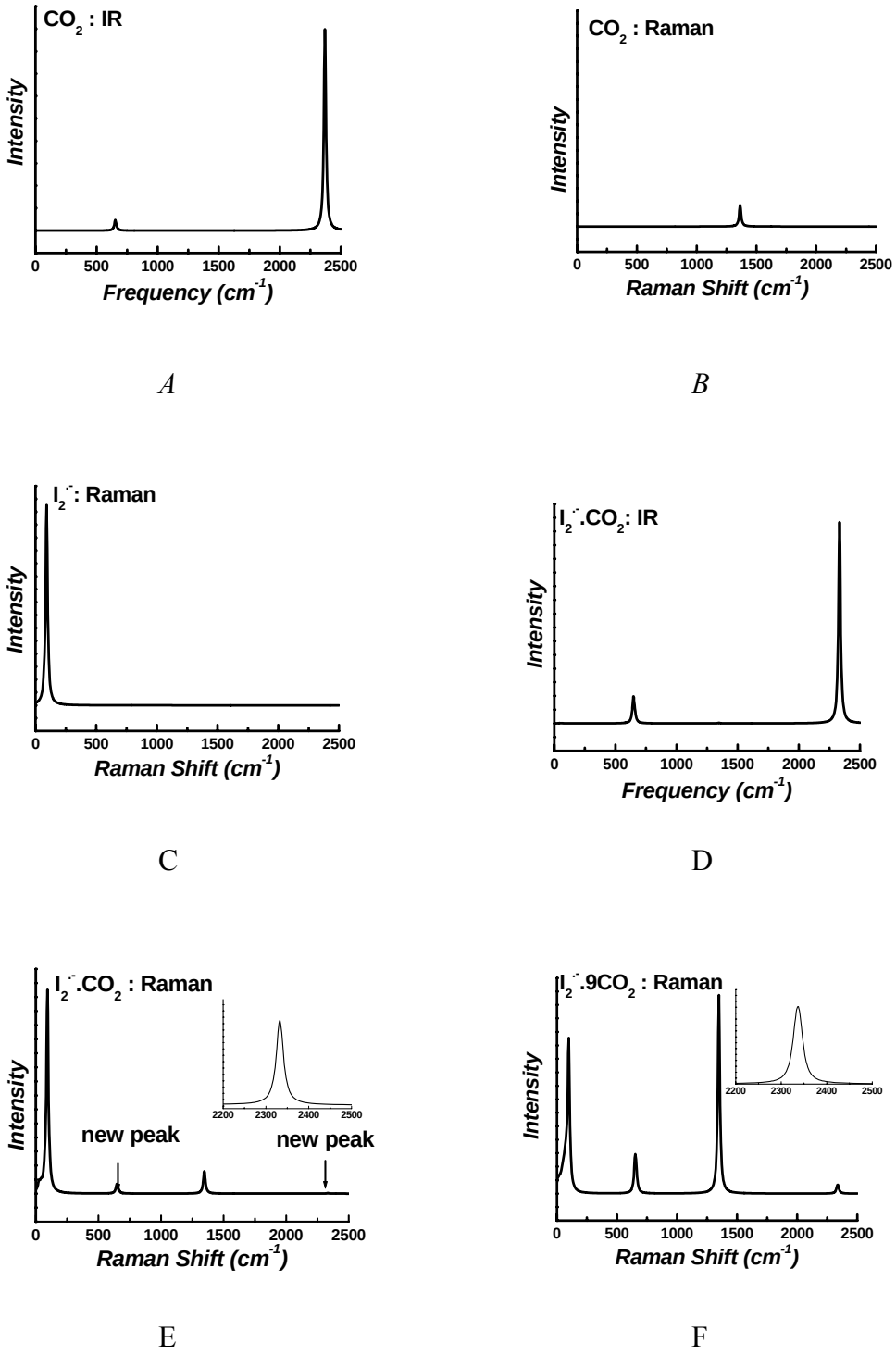

Fig. 7.3. Scaled (A) IR and (B) Raman spectra of CO_2 molecule. Scaled (C) IR and (B) Raman spectra of $I_2^{\bullet-}.CO_2$ and (D) Raman spectra $I_2^{\bullet-}.9CO_2$ cluster. A scaling factor of 0.93 is applied to account the anharmonic nature of vibration. Lorentzian line shape has been applied with peak half-width of 10 cm^{-1} for all the vibrational spectra plots.

to the maximum charge transfer of the excess electron to the solvent CO_2 units in this particular cluster.

In summary, degeneracy of bending mode of free solvent CO_2 unit is lost when it interacts with charged solute $I_2^{\bullet-}$ to form a molecular cluster. Two vibrational bands are observed at the bending region (~ 650 cm^{-1}) of CO_2 in normal mode analysis. Both the stretching modes of CO_2 are red shifted compared to the free molecule but the bending mode is both red and blue shifted compared to the free molecule in these solvated clusters. IR spectra plot of $I_2^{\bullet-}$ nCO_2 (*n*=1-10) clusters show similar features. Vibrational band at the bending region of CO_2 (~ 650 cm^{-1}) in Raman spectra is a characteristic feature for the formation of $I_2^{\bullet-}.CO_2$ cluster. A weak band in the asymmetric stretching region (~ 2330 cm^{-1}) of CO_2 vibration appears in the Raman spectra in these solvated clusters and the band is most intense for $I_2^{\bullet-}$ 9CO_2 cluster.

7.4. Conclusions

Structure, energy and spectra of $I_2^{\bullet-}.nCO_2$ clusters (*n*=1-10) are reported to study the process of microsolvation of the negatively charged solute, $I_2^{\bullet-}$ in carbon dioxide. Hybrid density functional (BHHLYP) is applied to study the structural aspects of the present solvated clusters with a split valence 6-311+G(d) basis function. Monte Carlo based simulated annealing procedure is also applied to find out the global minimum energy structure. Solvent stabilization and interaction energies are calculated applying MP2 as well as CCSD(T) theory. It is observed that both the solvent stabilization as well as interaction energy continuously increases with the successive addition of solvent CO_2 units. It is clearly seen that the VDE values is blue-shifted with increasing cluster size

and this is consistent with the previous report. Increasing VDE with size signifies that the stability of the neutral cluster decreases with size. The calculated values of VDE and the variation of present theoretical values on VDE of solvated clusters with size are in excellent agreement with the measured VDE value corresponding to the X band. Simulated IR and Raman spectra of all the solvated $I_2^{\bullet-}$ $n$$CO_2$ clusters (n=1-10) show similar features. When solvent CO_2 unit interacts with the charged solute $I_2^{\bullet-}$ to form a molecular cluster the linearity of CO_2 unit is lost and as a result degeneracy of the bending mode of free solvent CO_2 unit is lifted. Vibrational band at the bending region of CO_2 and asymmetric C-O stretching region of CO_2 in Raman spectra shows characteristic feature for the formation of $I_2^{\bullet-}.CO_2$ cluster.

CHAPTER 8

A Generalized Microscopic Theory of Photodetachment Energy of Electron for Finite size Solvated Anionic Cluster: A Step Towards Bulk

8.1. Introduction

During the last few decades, several attempts have been made to extract bulk properties of a chemical species in a solvent from the knowledge of the properties of the small size solvated cluster. Bulk properties like solubility and UV-Vis spectra in aqueous solution are successfully extracted from the results based on microhydration study and presented in the previous chapters. Recently, with the advent of the supersonic expansions and nozzle beam techniques, solvation in small size ion embedded clusters has been amenable to the experimental observation[7-10, 23-32]. These experiments provide molecular level information on microsolvation and dependence of the vertical detachment energy (VDE) and adiabatic detachment energy (ADE) on the number of solvent molecules. Computer simulation based investigations also provide useful information on the solvation of the cluster of finite size as well as the cluster having sufficiently large size[81]. However, in many cases, the exact form of the interaction potential is not known for the complex hetero cluster. Therefore, the calculation of the solvation energy for finite as well as infinite size clusters (bulk) becomes problematic. Although *ab initio*

quantum mechanics based approaches bypass this problem, investigations based on this approach are limited only to clusters of small size[82-83]. More importantly, simulation or quantum mechanics based study does not provide any explicit analytical expression for the dependence on the number of solvent molecules. Work in this direction was earlier initiated by Jortner and coworkers[33]. Theoretical considerations of the ion solvation in clusters of finite size predict that the detachment energies of a solvated anion should scale as 1/R linearly, where R is the radius of the solvated clusters and is proportional to the solvent number, *n*. In this model, the solvent number dependent detachment energy (both $\Delta E_{VDE}(n)$ and $\Delta E_{ADE}(n)$) of the cluster expressed as[9],

$$\Delta E_{\vartheta}(n)=\Delta E_{\vartheta}(\infty) +A_{\vartheta}(n+\delta)^{-1/3} \quad (1)$$

Where, ϑ refers to ADE or VDE, $\Delta E_{\vartheta}(\infty)$ is the bulk detachment energy and A_{ϑ} is the proportionality constant. Here δ is an equivalent solvent number corresponding to the solute and accounts for the contribution of the solute to the cluster volume. However, the extrapolation results obtained from this simple model are found to be in poor agreement with the experimental results [9, 35].

Dixon and coworkers raised an important question concerning whether the exponent (1/3) is constant for all anionic clusters of different charges or not and argued that the exponent should be dependent on the nature of the ion.[35] Accordingly, another empirical law was proposed, written as

$$\Delta E_{\vartheta}(n) = \Delta E_{\vartheta}(\infty) + A_{\vartheta}\ (n+\delta)^{-p} \quad (2)$$

The calculated results based on this model were better than the earlier models but the error was still quite significant, particularly for the di-anion hydrated clusters. Most importantly, the variation of p from system to system is not properly defined. The

possible breakdown of these laws may be due to the fact that all these empirical laws are proposed by including two or three unknown parameters in an arbitrary way which is based on the continuum theory wherein the microscopic details are not considered. However, if solute-solvent and solvent-solvent motions are strongly correlated, the continuum theory breaks down and one needs to have a microscopic theory in order to understand the solvent number (n) dependence of ΔE_{VDE} (n) and ΔE_{ADE} (n).

Hence, in the present chapter, the objective has been to address an important issue in obtaining the proper n-dependence of the expressions for the solvation energy in a generalized manner.

8.2. Theoretical Methodology

The system that is considered here consists of a single negative ion of charge –q and n number of polar solvent molecules surrounding it. The solvation energies of the negative ion and its mono ionized form with charge –(q-1) are respectively defined as

$$U_1 = \rho \iint U_1(\boldsymbol{r}, \boldsymbol{\omega})\, \mathbf{g_1}(\boldsymbol{r}, \boldsymbol{\omega}, n) d\boldsymbol{r}\, d\boldsymbol{\omega} \qquad (3)$$

$$U_2 = \rho \iint U_2(\boldsymbol{r}, \boldsymbol{\omega})\, \mathbf{g_2}(\boldsymbol{r}, \boldsymbol{\omega}, n) d\boldsymbol{r}\, d\boldsymbol{\omega} \qquad (4)$$

Where, $U_1(\boldsymbol{r}, \boldsymbol{\omega})$ and $U_2(\boldsymbol{r}, \boldsymbol{\omega})$, respectively, represent the interaction potential energy between the ions with charge –q and –(q-1) with the polar solvent molecules and g_i **(r, ω, *n*)** (i=1,2) represents the static pair distribution function between the ion and solvent molecules for the system containing a finite number (n) of solvent molecules. Here, ρ represents the bulk density of the solvent molecules. The quantities of interest are the

vertical detachment energy (VDE) and adiabatic detachment energy (ADE), defined respectively as

$$\Delta E_{VDE}(n) = A + \iint [U_2(\boldsymbol{r}, \boldsymbol{\omega}) - U_1(\mathbf{r}, \boldsymbol{\omega})] \, \mathbf{g_1}(\boldsymbol{r}, \boldsymbol{\omega}, n) d\boldsymbol{r} \, d\boldsymbol{\omega} \quad (5a)$$

$$\Delta E_{ADE}(n) = A + \iint [U_2(\boldsymbol{r}, \boldsymbol{\omega}) \mathbf{g_2}(\boldsymbol{r}, \boldsymbol{\omega}, n) - U_1(\boldsymbol{r}, \boldsymbol{\omega}) \, \mathbf{g_1}(\boldsymbol{r}, \boldsymbol{\omega}, n)] d\boldsymbol{r} \, d\boldsymbol{\omega} \quad (5b)$$

Where, A is the electron affinity of the ion $\mathbf{A^{q-}}$ in gas phase. In order to have an explicit expression for VDE and ADE of the system containing finite number of solvent particles, what is needed is a relation between the pair distribution function g_i **(r, ω)** of the infinite system and its finite system counterpart g_i **(r, ω,** n**).** Such a relation may be derived by following the approach of Salacuse et.al. by means of Taylor-series expansion in powers of $1/n$.[84] Here, the derivation is extended from the nonpolar system to the case of ion-polar system. Semi-grand canonical ensemble is considered where only the number of solvent molecules is allowed to fluctuate but the single negative ion is kept fixed in each member of the ensemble.[85] In this semi grand canonical ensemble, the two-particle distribution function may be expressed as

$$\boldsymbol{P}(\boldsymbol{r_s}, \boldsymbol{r_d}, \boldsymbol{\omega}) = \sum_{\boldsymbol{n=0}}^{\infty} P_{\boldsymbol{eq}}(n) P \quad (\boldsymbol{r_s}, \boldsymbol{r_d}, \boldsymbol{\omega}, n) \quad (6)$$

Where, $P_{\boldsymbol{eq}}(n)$ is the probability that in equilibrium the system contains n solvent molecules and a single ion and P $(\boldsymbol{r_s}, \boldsymbol{r_d}, \boldsymbol{\omega}, n)$ is the pair distribution function for a system containing a single anion and n solvent molecules. Here, $\boldsymbol{r_s}$, $\boldsymbol{r_d}$ and $\boldsymbol{\omega}$ represent the position vector of the ion, and the position vector and orientation of the solvent molecule, respectively. Now expanding $\boldsymbol{P}(\boldsymbol{r_s}, \boldsymbol{r_d}, \boldsymbol{\omega}, \boldsymbol{n})$ in the number of particles around the average number of particles, one get

$$\bar{n} = \sum_{n=0}^{\infty} n \mathrm{P}_{eq}(n) \tag{7}$$

$$\mathrm{P}(\boldsymbol{r_s}, \boldsymbol{r_d}, \boldsymbol{\omega}) = \mathrm{P}\ (\boldsymbol{r_s}, \boldsymbol{r_d}, \boldsymbol{\omega}, \overline{n}) + \frac{1}{2}\overline{(n-\overline{n})^2}\frac{\partial^2}{\partial \overline{n}^2}\mathrm{P}\ (\boldsymbol{r_s}, \boldsymbol{r_d}, \boldsymbol{\omega}, \overline{n})$$

$$+ \frac{1}{6}\overline{(n-\overline{n})^3}\frac{\partial^3}{\partial \overline{n}^3}\mathrm{P}\ (\boldsymbol{r_s}, \boldsymbol{r_d}, \boldsymbol{\omega}, \overline{n})$$

$$+ \ldots\ldots\ldots\ldots\ldots\ldots\ldots \tag{8}$$

where, the averages of fluctuation of the number of solvent particles are defined as

$$\sum_{n=0}^{\infty}(n-\overline{n})\mathrm{P}_{eq}(n) = 0 \tag{9a}$$

$$\sum_{n=0}^{\infty}(n-\overline{n})^m \mathrm{P}_{eq}(n) = \overline{(n-\overline{n})^{\mathrm{m}}}\ \text{for}\ \mathrm{m} > 1 \tag{9b}$$

In the homogeneous limit, one can write

$$\mathrm{P}(\boldsymbol{r_s}, \boldsymbol{r_d}, \boldsymbol{\omega}) = \frac{\rho_s \rho}{\Omega}\mathrm{g_i}(\mathbf{r},\boldsymbol{\omega});\ \mathrm{P}(\boldsymbol{r_s}, \boldsymbol{r_d}, \boldsymbol{\omega}, \overline{n}\ ) = \frac{\rho_s \rho}{\Omega}\mathrm{g_i}(\mathbf{r},\boldsymbol{\omega}) \tag{10}$$

where, ρ_s and ρ represent the ion and solvent density, respectively, and $\mathbf{r} = \mathbf{r_d} + \mathbf{r_s}$. Approximating the average density ($=\overline{n}/\mathrm{V}$) to be equal to the solvent density, Eq.(6) can be reduced to

$$\mathrm{g_i}(\mathbf{r}, \boldsymbol{\omega}) = \mathrm{g_i}(\mathbf{r}, \boldsymbol{\omega}, \overline{n}) + \frac{1}{2}\frac{\overline{(n-\overline{n})^2}}{\overline{n}}\frac{\rho}{\overline{\mathrm{n}}}\frac{\partial^2}{\partial \rho^2}\left(\rho \mathrm{g_i}(\mathbf{r}, \boldsymbol{\omega}, \overline{n})\right)$$

$$+ \frac{1}{6}\frac{\overline{(n-\overline{n})^3}}{\overline{n}}\frac{\rho^2}{\overline{n}^2}\frac{\partial^3}{\partial \rho^3}\left(\rho \mathrm{g_i}(\mathbf{r}, \boldsymbol{\omega}, \overline{n})\right). \tag{11}$$

The effect of a single ion on $\mathrm{g_i}(\mathbf{r}, \boldsymbol{\omega})$ enters through the fluctuation of the number of solvent particles and pair distribution $\mathrm{g_i}(\mathbf{r}, \boldsymbol{\omega}, \overline{n})$ for the finite system. For simplicity, the effect of a single ion on the fluctuation of the number of solvent particles is neglected. This approximation is a reasonably good one if the system contains an appreciable

number of solvent molecules. In this approximation, one may relate these quantities to the compressibility defined along the lines of Salacuse et. al. [84] as

$$\frac{\overline{(n-\overline{n})^2}}{\overline{n}} = \mathrm{S}(0), \quad \frac{\overline{(n-\overline{n})^3}}{\overline{n}} = \left[\mathrm{S}(0)^2 + \frac{\partial \mathrm{S}(0)}{\partial(\beta\mu)}\right] \tag{12}$$

where $\mathrm{S}(0) = 1 + 4\pi\rho \int_0^\infty r^2\, dr[g(r) - 1]$ and $g(r) = <\mathrm{g_i}(\mathbf{r}, \boldsymbol{\omega})>_\omega$, where the latter represents the angular average of the pair distribution function $\mathrm{g_i}(\mathbf{r}, \boldsymbol{\omega})$, $\beta = 1/\mathrm{kT}$ (k and T represent Boltzmann constant and absolute temperature, respectively) and μ is the chemical potential of the solvent molecules**.** Now substituting Eq.(11) in Eq.(10) and for simplicity relabeling $\overline{n}$ by *n* and retaining the terms up to $1/n^2$

$$\mathrm{g_i}(\mathbf{r}, \boldsymbol{\omega}, n) = \mathrm{g_i}(\mathbf{r}, \boldsymbol{\omega}) + \frac{C_i^1(\mathrm{r},\omega)}{n} + \frac{C_i^2(\mathrm{r},\omega)}{n^2} \tag{13}$$

is obtained, where, $\mathrm{C_1}(\mathrm{r}, \omega)$ and $\mathrm{C_2}(\mathrm{r}, \omega)$ are respectively defined as

$$\mathrm{C_i^1}(\mathrm{r}, \omega) = \mathrm{S}(0)\frac{\rho}{2}\frac{\partial^2}{\partial\rho^2}(\rho \mathrm{g_i}(\boldsymbol{r}, \boldsymbol{\omega}) \tag{14}$$

$$\mathrm{C_i^2}(\mathrm{r}, \omega) = \frac{\mathrm{S}(0)^2}{4}\rho\frac{\partial^2}{\partial\rho^2}\left[\rho\frac{\partial^2}{\partial\rho^2}(\rho \mathrm{g_i}(\boldsymbol{r}, \boldsymbol{\omega}))\right] \frac{\rho^2}{6}\left[S(0)^2\, \frac{\partial S(0)}{\partial(\beta\mu)}\right]\frac{\partial^3}{\partial\rho^3}(\rho \mathrm{g_i}(\boldsymbol{r}, \boldsymbol{\omega})) \tag{15}$$

Now substituting Eq.(13) in Eqs.(5a) and (5b)

$$\Delta \mathrm{E_{VDE}}(\mathrm{n}) = \Delta \mathrm{E_{VDE}}(\infty) + \frac{M_1^{VDE}}{n} + \frac{M_2^{VDE}}{n^2} \tag{16}$$

$$\Delta \mathrm{E_{ADE}}(\mathrm{n}) = \Delta \mathrm{E_{ADE}}(\infty) + \frac{M_1^{ADE}}{n} + \frac{M_2^{ADE}}{n^2} \tag{17}$$

is obtained, where

$$\Delta \mathrm{E_{VDE}}(\infty) = \rho \iint [U_2(\boldsymbol{r}, \boldsymbol{\omega}) - U_1(\boldsymbol{r}, \boldsymbol{\omega})\mathrm{g_1}(\boldsymbol{r}, \boldsymbol{\omega}) d\boldsymbol{r}\, d\boldsymbol{\omega} + \boldsymbol{I} \tag{18}$$

$$\mathrm{M_1^{VDE}} = \rho \iint [U_2(\mathbf{r}, \boldsymbol{\omega}) - U_1(\mathbf{r}, \boldsymbol{\omega})]\, \boldsymbol{C_1}(\boldsymbol{r}, \boldsymbol{\omega}) d\boldsymbol{r}\, d\boldsymbol{\omega} + I \tag{19}$$

$$\mathrm{M_2^{VDE}} = \rho \iint [U_2(\mathbf{r}, \boldsymbol{\omega}) - U_1(\mathbf{r}, \boldsymbol{\omega})]\, \boldsymbol{C_2}(\boldsymbol{r}, \boldsymbol{\omega}) d\boldsymbol{r}\, d\boldsymbol{\omega} \tag{20}$$

$$\Delta \mathrm{E_{ADE}}(\infty) = \rho \iint [U_2(\boldsymbol{r}, \boldsymbol{\omega})\, \mathrm{g_2}(\boldsymbol{r}, \boldsymbol{\omega}) - U_1(\boldsymbol{r}, \boldsymbol{\omega})\, \mathrm{g_1}(\boldsymbol{r}, \boldsymbol{\omega})]\, d\boldsymbol{r}\, d\boldsymbol{\omega} + I \tag{21}$$

$$M_1^{ADE} = \rho \iint [U_2(\mathbf{r}, \boldsymbol{\omega}) C_1^{ADE}(\boldsymbol{r}, \boldsymbol{\omega}) - U_1(\mathbf{r}, \boldsymbol{\omega}) C_2^{ADE}(\boldsymbol{r}, \boldsymbol{\omega})] \, d\boldsymbol{r} \, d\boldsymbol{\omega} + I \quad (22)$$

$$M_2^{ADE} = \rho \iint [U_2(\mathbf{r}, \boldsymbol{\omega}) C_3^{ADE}(\boldsymbol{r}, \boldsymbol{\omega}) - U_1(\mathbf{r}, \boldsymbol{\omega}) C_4^{ADE}(\boldsymbol{r}, \boldsymbol{\omega})] \, d\boldsymbol{r} \, d\boldsymbol{\omega} + I \quad (23)$$

$$C_1^{ADE}(\boldsymbol{r}, \boldsymbol{\omega}) = S(0) \frac{\rho}{2} \frac{\partial^2}{\partial \rho^2} (\rho g(\mathbf{r}, \boldsymbol{\omega})) \; ; \; C_2^{ADE}(\boldsymbol{r}, \boldsymbol{\omega}) = S(0) \frac{\rho}{2} \frac{\partial^2}{\partial \rho^2} (\rho g_2(\mathbf{r}, \boldsymbol{\omega})) \quad (24)$$

$$C_3^{ADE}(\boldsymbol{r}, \boldsymbol{\omega}) = S(0)^2 \rho \frac{\partial^2}{\partial \rho^2} \left[\rho \frac{\partial^2}{\partial \rho^2} (\rho g_1(\mathbf{r}, \boldsymbol{\omega})) \right] - \frac{\rho^2}{6} \left[S(0)^2 + \frac{\partial S(0)}{\partial (\beta \mu)} \right] \frac{\partial^3}{\partial \rho^3} (\rho g_1(\mathbf{r}, \boldsymbol{\omega})) \quad (25)$$

$$C_4^{ADE}(\boldsymbol{r}, \boldsymbol{\omega}) = S(0)^2 \rho \frac{\partial^2}{\partial \rho^2} \left[\rho \frac{\partial^2}{\partial \rho^2} (\rho g_2(\mathbf{r}, \boldsymbol{\omega})) \right] - \frac{\rho^2}{6} \left[S(0)^2 + \frac{\partial S(0)}{\partial (\beta \mu)} \right] \frac{\partial^3}{\partial \rho^3} (\rho g_2(\mathbf{r}, \boldsymbol{\omega})) \quad (26)$$

Equations (16) and (17) are derived based on some approximations including truncation of higher order terms, and the accuracy of these expressions can be tested if experimental results are available for the systems with large and wide range of values of *n*. However, the results are available for the systems clusters of small size, since experimentally, it is difficult to prepare the clusters of desired size. Therefore, to obtain the bulk values of $\Delta E_{VDE}(\infty)$ and $\Delta E_{ADE}(\infty)$ from the knowledge of experimental results of $\Delta E_{VDE}(n)$ and $\Delta E_{ADE}(n)$ for few clusters of finite size is problematic. So what is needed are expressions for $\Delta E_{VDE}(n)$ and $\Delta E_{ADE}(n)$ valid for small size clusters that converge to the respective equations (16) and (17) valid for large size clusters. Motivated by the derived Eqs.(16) and (17), the more general expressions similar to those equations defined as is proposed

$$\Delta E_{VDE}(n) = \Delta E_{VDE}(\infty) + \frac{M_1^{VDE}}{(n+\sigma)} + \frac{M_2^{VDE}}{(n+\sigma)^2} \quad (27)$$

$$\Delta E_{ADE}(n) = \Delta E_{ADE}(\infty) + \frac{M_1^{ADE}}{(n+\sigma)} + \frac{M_2^{ADE}}{(n+\sigma)^2}, \quad (28)$$

by introducing a parameter σ representing the contribution from the solute volume as well as the charge on the solute ion. It is assumed here that the parameter σ to be given by

$\sigma = qV_R$ based on the assumption that as the solute and solvent size ratio V_R or numerical value of the charge q becomes very large, only then solvent molecules near to the surface mainly contribute to the solvation energy. In this limit i.e. $\lim(q, V_R) \rightarrow \infty$, $\Delta E_{VDE}(n)$ or $\Delta E_{ADE}(n) \rightarrow \Delta E_{VDE}(\infty)$ or $\Delta E_{ADE}(\infty)$. It is thus very clear from Eqs.(27) and (28) that when $n >> \sigma$, they respectively converge to Eqs.(16) and (17) valid for clusters of large size. Eqs. (16), (17), (27) and (28) are the main new results of the present work.

It is worthwhile to obtain a relation between the coefficients M_1^{VDE} and M_2^{VDE} as well as M_1^{ADE} and M_2^{ADE}. In order to derive an expression, let us assume that in the asymptotic limit i.e. say at $n = n_m$, $\Delta E_{VDE}(n_m+1) = \Delta E_{VDE}(n_m)$ and $\Delta E_{ADE}(n_m+1) = \Delta E_{ADE}(n_m)$, and obtain thereby the relations

$$\frac{M_1^{VDE}}{M_2^{VDE}} = -\frac{2(n_m+\sigma)+1}{(n_m+\sigma)(n_m+\sigma)+1)} < 0 \quad (29)$$

$$\frac{M_1^{ADE}}{M_2^{ADE}} = -\frac{2(n_m+\sigma)+1}{(n_m+\sigma)(n_m+\sigma+1)} < 0 \quad (30)$$

which show that the coefficients M_1^{VDE} and M_2^{VDE} are of opposite sign and similarly M_1^{ADE} and M_2^{ADE} are also opposite in sign. Equations (16)-(17) and (27)-(28) are new results and will be used to find out $\Delta E_{VDE}(\infty)$ and $\Delta E_{ADE}(\infty)$ by the extrapolation method.

8.3. Results and Discussion

In order to study the dependence of the vertical detachment energy $\Delta E_{VDE}(n)$ and adiabatic detachment energy $\Delta E_{ADE}(n)$ on the finite solvent number, what is needed is a microscopic evaluation of the quantities M_1^{VDE}, M_2^{VDE}, M_1^{ADE} and M_2^{ADE}. These quantities can be evaluated using simulation results, provided accurate inter-particle potentials are

known. However, for most of the complex systems, accurate inter-particle potentials are not known, and hence the evaluation of these quantities becomes difficult. The present study focuses mainly on the *n*-dependence of the derived expressions and therefore treats the coefficients as unknown parameters.

Now the results of numerical calculations carried out using the present formalism is presented. The procedure to be adopted is to find out the optimum values of $M_1^{VDE}$and M_2^{VDE} using calculated values of σ, Eq.(16) or Eq.(27) depending on the range of n, and the experimental values of $\Delta E_{VDE}(n)$ so that the calculated results are very close to the experimental values. Using these values of $M_1^{VDE}$and M_2^{VDE}, $\Delta E_{VDE}(n)$ or ΔE_{ADE} (n) is calculated based on Eq.(16) or Eq.(27) and plotted in the graph as a function of $1/n$ or $1/(n+\sigma)$ depending on the range of *n* along with experimental results. On extrapolation of $\Delta E_{VDE}(n)$ to cluster of infinite size ($n=\infty$), the bulk detachment energy *viz*. $\Delta E_{VDE}(\infty)$ is obtained. Similar procedures are to be adopted to calculate $\Delta E_{ADE}(n)$. As an illustrative example, uni-negative and doubly negative anionic hydrated clusters are considered *viz*. $I^-.nH_2O$, $Br^-.nH_2O$, $Cl^-.nH_2O$, $NO_3^-.nH_2O$, and $SO_4^{-2}.nH_2O$ and $C_2O_4^{-2}.nH_2O$, respectively. Let us first calculate the volume ratio (V_R) which are 3, 2.5, 2, 2.5, 4 and 4 for the systems, $I^-.nH_2O$, $Br^-.nH_2O$, $Cl^-.nH_2O$, $NO_3^-.nH_2O$, $SO_4^{-2}.nH_2O$ and $C_2O_4^{-2}.nH_2O$, respectively. Then $I^-.nH_2O$ cluster is considered, for which experimental values of $\Delta E_{VDE}(n)$ are available for n=20 to 60.[86] Since the clusters are medium in size, Eq.(16) is used to calculate $\Delta E_{VDE}(n)$. The calculated results of $\Delta E_{VDE}(n)$ are plotted against $1/n$ for these systems along with experimental results in Fig.8.1(A). The best fitted plot (see Fig. 8.1A) has a correlation coefficient (R) greater than 0.98, showing an excellent agreement of the calculated values with the experimental results.

Table 8.1. Bulk vertical detachment ($\Delta E_{VDE}(\infty)$) and adiabatic detachment ($\Delta E_{ADE}(\infty)$) energy for $I^-.nH_2O$, $Br^-.nH_2O$, $Cl^-.nH_2O$, $NO_3^-.nH_2O$, $SO_4^{2-}.nH_2O$ and $C_2O_4^{2-}.nH_2O$ systems.

Systems	Calculated $\Delta E_{ADE}(\infty)$ or $\Delta E_{VDE}(\infty)$in eV based on extrapolation using new derived relations [a]	Calculated $\Delta E_{ADE}(\infty)$ or $\Delta E_{VDE}(\infty)$in eV based on extrapolation using Eq.1[a]	Experimental $\Delta E_{ADE}(\infty)$ or $\Delta E_{VDE}(\infty)$ in eV[a]
$I^-.nH_2O$	7.08[b] (**4**)	8.34 [d] (**13**)	7.40 [f]
$Br^-.nH_2O$	7.56[c] (**7**)	10.17 [d] (**25**)	8.15 [f]
$Cl^-.nH_2O$	9.18[c] (**3**)	12.47 (**40**)	8.90 [f]
$NO_3^-.nH_2O$	7.28 [c] (**2**)	10.92 (**46**)	7.46 [g]
$SO_4^{2-}.nH_2O$	8.07 [c] (**7**)	12.3 [e] (**42**)	8.65 [g]
$C_2O_4^{2-}.nH_2O$	6.83 [c] (**7**)	11.5 [e] (**57**)	7.32 [g]

[a] $\Delta E_{VDE}(\infty)$ values for $I^-.nH_2O$, $Br^-.nH_2O$ and $Cl^-.nH_2O$ systems and $\Delta E_{ADE}(\infty)$ values for $NO_3^-.nH_2O$, $SO_4^{2-}.nH_2O$ and $C_2O_4^{2-}.nH_2O$ systems. Bold values in the parentheses refers to % of error with respect to the experimental value.

[b] Calculated values are based on Eq. (12).

[c] Calculated values are based on Eq. (16).

[d] Ref. 35 (calculated based on Eq. 1).

[e] Ref. 9 (calculated based on Eq. 1).

[f] Ref. 87.

[g] Ref. 88.

The calculated bulk detachment energy $\Delta E_{VDE}(\infty)$ is shown in Table 8.1 along with the experimentally measured value. It is clear from Table1 that the results of $\Delta E_{VDE}(\infty)$ obtained from the expression derived here based on microscopic theory are in very good agreement with experimental results in comparison to the calculated results obtained from the empirical law given by Eq(1). $\Delta E_{VDE}(\infty)$ using Eq.(27) is also calculated and obtained the same value $\Delta E_{VDE}(\infty)$ based on Eq.(16). This happens because σ is 3 and is not large enough in comparison to the average sizes (n) of the cluster. However, in the case of small size hydrated clusters [86,32] viz. $Cl^-.nH_2O$ (n= 1 to 6), $Br^-.nH_2O$ (n=1 to 15), and $NO_3^-.nH_2O$ (n=1 to 5), it is found that the calculated results of $\Delta E_{VDE}(\infty)$ based on Eq.(27) are in much better agreement than the same quantity calculated based on Eq.(16). The reason is very obvious, since σ values of $Cl^-.nH_2O$, $Br^-.nH_2O$ and $NO_3^-.nH_2O$ systems are 2, 2.5 and 2.5, respectively, and these values are significant in comparison to the sizes of the clusters. The calculated values of $\Delta E_{VDE}(\infty)$ along with the same calculated values based on empirical relation given by Eq.(1) for these three systems, are shown in Table 8.1. Here also, the calculated results of $\Delta E_{VDE}(\infty)$ based on Eq.(27) are found to be in much better agreement than the same calculated values based on the empirical Eq(1) (see Table 8.1).

Now the doubly negatively charged ionic clusters *viz*. $SO_4^{-2}.nH_2O$ and $C_2O_4^{-2}.nH_2O$ are considered. The size of the hydrated clusters for these systems for which experimental data are available cover the range from n= 4 to 13 (for VDE) and from n= 4 to 40 (for ADE) for $SO_4^{-2}.nH_2O$ clusters [9,30-31] and n= 4 to 40 for $C_2O_4^{-2}.nH_2O$ clusters (ADE).[9] Since the sizes of the clusters are small here, $\Delta E_{VDE}(n)$ is calculated and $\Delta E_{ADE}(n)$ for $SO_4^{-2}.nH_2O$ system and $\Delta E_{ADE}(n)$ for $C_2O_4^{-2}.nH_2O$ system

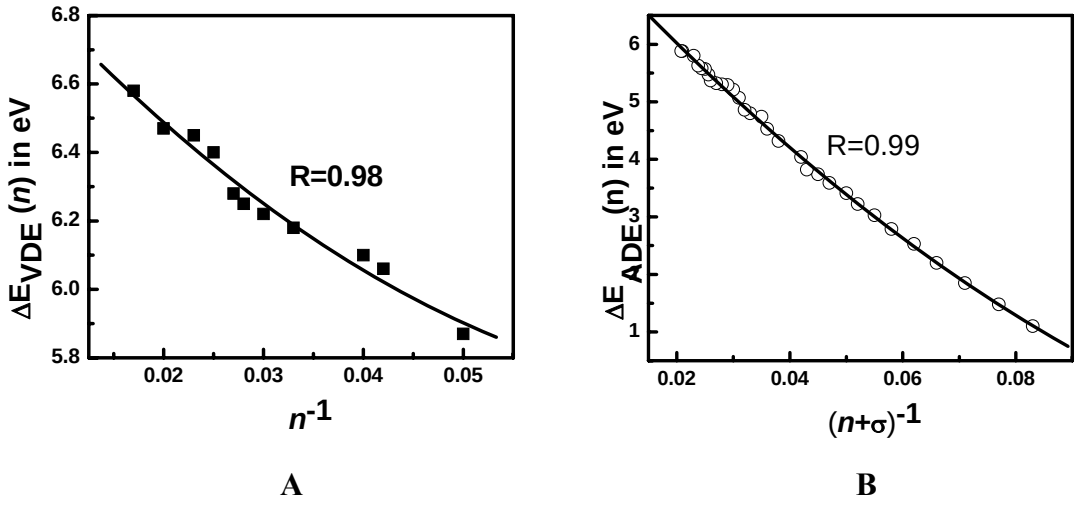

Fig. 8.1. (A) Plot of $\Delta E_{VDE}(n)$ *vs.* $(n)^{-1}$ for I^-. nH_2O systems. The result based on new relation are shown by solid line, and the solid squares (■) represent the experimental values taken from ref. 86. (B) Plot of $\Delta E_{ADE}(n)$ *vs* $(n+\sigma)^{-1}$ (σ=8) for $SO_4^{-2}.nH_2O$. The result based on new relation are shown by solid line, and the open circle (○) represent the experimental values taken from ref. 31

based on Eqs (27) and (28) and the results are tabulated in Table 8.1. Here also, the calculated results of $\Delta E_{VDE}(\infty)$ and $\Delta E_{ADE}(\infty)$ based on Eq.(27) are found to show much better agreement than the same calculated values based on Eq(1). The σ value of these systems is taken as 8, which is large in comparison to the size of the clusters and thus justifies the use of Eq.(27) rather than Eq.(16). The results of $\Delta E_{VDE}(n)$ and $\Delta E_{ADE}(n)$ are calculated for the system $SO_4^{-2}.nH_2O$ using the value of $\sigma = 8$ and the optimized values of M_1^{VDE}, M_2^{VDE}, $M_1^{ADE}$and M_2^{ADE}. The calculated results are plotted along with available experimental results in Fig.8.2(B). The $\Delta E_{ADE}(\infty)$ value is also calculated for the $C_2O_4^{-2}.nH_2O$ system based on Eq. (28) and shown in Table 8.1. The correlation coefficient for all the plots (R) is greater than 0.99, indicating that there is very good correspondence between the theory and the experiment. It is clear from the Table 8.1 that the maximum error in bulk values based on present theoretical calculation is 7% with

respect to experimentally measured values compared to 57% based on the previous model.

8.4. Conclusions

A new general relation connecting the finite size dependent vertical detachment energy and adiabatic detachment energy of the solvated anionic clusters of finite size is derived based on a microscopic theory. The *n*-dependence of the detachment energy is independent of the solute solvent interaction energy. The derived expressions are valid for system containing large number of solvent molecules. This relation is tested for cluster of medium size *viz*. $I^-.nH_2O$ and the calculated $\Delta E_{VDE}(\infty)$ value is found to be in very good agreement with the experimental $\Delta E_{VDE}(\infty)$ value. However, the experimental results are available mainly for small finite size clusters. To obtain the bulk values of $\Delta E_{VDE}(\infty)$ and $\Delta E_{ADE}(\infty)$ from the knowledge of $\Delta E_{VDE}(n)$ and $\Delta E_{ADE}(n)$ for small finite size cluster, general expressions given by Eqs. (27) and (28) have been proposed. It is worthwhile to mention that Eqs. (27) and (28) converge to Eqs. (16) and (17), respectively in large *n* limit. Using these expressions, (Eqs. (27) and (28)), $\Delta E_{VDE}(\infty)$ and $\Delta E_{ADE}(\infty)$ values are obtained from the knowledge of clusters of small size and are found to be in very good agreement with the available experimental results. The *n*-dependent expressions for $\Delta E_{VDE}(n)$ and $\Delta E_{ADE}(n)$ do not change from system to system in contrast to the expression proposed by Dixon and coworkers (Eq.2) where the exponent p varies from system to system. The calculated results based on the microscopic expressions (Eqs. (16) and (17) for cluster of large size and Eqs (27) and (28) for cluster of small size are found to be in very good agreement with the experimental results in

comparison to the onebased on empirical expression (Eq.(1)). These derived new relations are tested for hydrated cluster of simple spherical anions (Cl^-, Br^- and I^-) to complex non-spherical anions (NO_3^-, SO_4^{-2} and $C_2O_4^{-2}$). The maximum error in bulk values based on present theoretical calculation is 7% with respect to experimentally measured values compared to 57% based on the previous model. More importantly, the robust scheme proposed here provide a route to obtain $\Delta E_{VDE}(\infty)$ and $\Delta E_{ADE}(\infty)$ from the knowledge of $\Delta E_{VDE}(n)$ and $\Delta E_{ADE}(n)$ for finite and complex systems whose inter particle potentials are unknown.

References

1. Ohtaki, H.; Radani, T. *Chem. Rev.* **199**3, *93*, 1157.

2. Delahay, P. *Acc. Chem. Res.* **1982**, *15*, 40.

3. Nagarajan, V.; Fessenden, R. W. *J. Phys. Chem.***1985**, *89*, 2330.

4. Onsager, L. *J. Am. Chem. Soc.***1936**, *58*, 1486.

5. Kirkwood, J. G. *J. Chem. Phys.* **1939**, *7*, 911.

6. Cramer, C. J.; Truhlar, D. G. *Chem. Rev.* **199**9, *99*, 2161.

7. Ayotte, P. G.; Weddle, H.; Kim, J.; Johnson, M. A. *J. Am. Chem. Soc.* **1998**, *120*, 12361.

8. Robertson, W. H.; Diken, E. G.; Price, E. A.; Shin, J. W.; Johnson, M. A. *Science* **2003**, *299*, 1367.

9. Wang, X. B.; Yang, X.; Nicholas, J. B.; Wang, L. S. *Science*, **2001**, *294*, 1322.

10. (a) Lehr, L.; Zannai, M. T.; Frischkorn,C.; Weinkauf, R.; Neumark, D. M. *Science*, **1999**, *284***,** 635. (b) Ehrler, O. T.; Neumark, D. M. *Acc. Chem. Res.* **2009**, *42*, 769.

11. Ignaczak, A.; Gomes, J.A. N. F.; Cordeiro, M. N. D. S. *Eletrochimica Acta*. **1999**, *45*, 659.

12. Vaughn, S. J.; Akhmatskaya, E. V.; Vincent, M. A.; Masters, A. J.; Hillier, I. H. *J. Chem. Phys*. **1999**, *110*, 4338.

13. Faeder, J.; Parson, R. *J. Chem. Phys*. **1998**, *108*, 3909.

14. (a) Chen, H-Y.; Shew, W-S. *J. Am. Chem. Soc*.**2000**, *122*, 7534. (b) Masamura, M. *J. Chem. Phys.* **2003**, *118*, 6336. (c) Majumdar, D.; Kim, J.; Kim, K. S. *J. Chem. Phys.* **2000**, *112*, 101.

15. Xantheas, S. S. *J. Am. Chem. Soc.* **1995**, *117*, 10373.

16. Hashimoto, K.; Morokuma, K. *J. Am. Chem. Soc*. **1995**, *117*, 4151.

17. Hertel, I. V., Huglin, C. N.; Psculz, C. P. *Phys. Rev. Lett*. **1991**, *67*, 1767.

18. (a) Park, M.; Shin, I.; Singh, N. J.; Kim, K. S. *J. Phys. Chem. A* **2007**, *111*,10692. (b) Iyengar, S. S. *J. Chem. Phys.* **2005**, *123*, 084310. (c) Iyengar, S. S.; Petersen, M. K.; Day, T. J. F.; Burnham, C. J. ; Teige, V. E. ; Voth, G. A. *J. Chem. Phys*. **2005**, *123*, 084309.

19. (a) Marx, D.; Tuckerman, M. E.; Hutter, J.; Parrinello, M. *Nature*, **1999**, *397*, 601. (b) Kim. J.; Schmidt, U. W.; Gruetzmacher, J.A.; Voth, G. A.; Scherer, N. E. *J. Chem. Phys*. **2002**, *116*, 737. (c) Geissler, P. L.; Dellago, C.; David Chandler, D.; Hutter, J.; Parrinello, M. *Science*, **2001**, *291*, 2121.

20. Schatteburg, G. N.; Bondybey, V. E. *Chem. Rev*. **2000,** *100*, 4059.

21. Gomez, H.; Taylor,T. R. Neumark, D. M. *J. Chem. Phys.* **2002**,*116*, 6111.

22. Greenblatt, B. J.; Zanni, M. T.; Neumark, D. M. *Science* **1997**, *276*, 1675.

23. Weber, J. M.; Kelley, J. A.; Nielson, S. B.; Ayotte, P.; Johnson, M. A. *Science* **2000**, *287*, 2461.

24. Price, E. A.; Hammeer, N. I.; Johnson, M. A. *J. Phys. Chem. A* **2004**, *108,* 3910.

25. Myshakin, E. M.; Jordan, K. D.; Robertson, W. H.; Weddle, G. H.; Johnson, M. A. *J. Chem. Phys*. **2003**, *118*, 4945.

26. Bush, M.F.; Saykally, R. J.; Williams, E. R. *J. Am. Chem Soc.* **2007**, *129*, 2220.

27. Bragg, A.E.; Verlet, J.R.R.; Kammrath, A.; Cheshnovsky, O.; Neumark, D.M. *Science* **2004**, *306*, 669.

28. Verlet, J.R.R.; Bragg, A.E.; Kammrath, A.; Cheshnovsky, O.; Neumark, D.M. *Science* **2005** *307,*93.

29. Turi, L.; Sheu, W.; Rossky,P.J. *Science* **2005**, *309*, 914.

30. Wang, X. B.; Nicholas, J. B.; Wang, L. S.; *J. Chem. Phys*. **2000**, *113*, 10837.

31. Yang, X.; Wang, X. B.; Wang, L. S.; *J. Phys. Chem. A* **2002,** *106,* 7607.

32. Wang, X. B.; Yang, X.; Wang, L. S.; Nicholas, J. B. *J. Chem. Phys*. **2002**,*116*, 561,

33. Barnett, R. N.; Landman, U.; Clevelend, C. L.; Jortnar, J. *J. Chem. Phys.* **1988**, *88*, 4429.

34. Coe, J. V. *Int. Rev. Phys. Chem.* **2001**, *20*, 33

35. Zhan, C. G.; Zheng, F.; Dixon, D. A. *J. Chem. Phys.* **2003**, *119*, 781.

36. Day, P. N.; Pachter, R.; Gordon, M. S.; Merrill, G. N. *J. Chem. Phys.* **2000,** *112***,** 2063.

37. Cramer, C. J. *Essentials of Computational Chemistry: Theories and Models*, John Wiley & Sons, Ltd, **2002**.

38. Levine, I. N. *Quantum Chemistry*, Prentice Hall of India Pvt. Ltd. **2001**.

39. Bonini, M. G.; Miyamoto, S.; Di Mascio, P.; Augusto, O. *J. Biol. Chem*. **2004**, *279*, 51836.

40. Wayne, R. P. *Chemistry of Atmospheres*; Oxford University Press: Oxford, **2000**.

41. C. D. Cappa, M. J. Elrod *Phys. Chem. Chem. Phys*. **2001**, *3*, 2986.

42. Becke, A. D. J. Chem. Phys. **1993**, *98*, 1372.

43. Maity, D. K. *J. Phys. Chem. A* **2002**, *106*, 5716.

44. Braïda, B.; Hiberty, P. C.; Savin, A. *J. Phys. Chem. A* **1998**, *102*, 7872.

45. Boys, S.F.;Bernardi, F. *Mol. Phys*, **1990**, *19*, 553.

46. Schmidt,M. W.; Baldridge, K. K.; Boatz, J. A.; Elbert, S. T.; Gordon, M. S.; Jensen , J. H.; Koseki, S.; Matsunaga, N.; Nguyen, K. A.; Su, S. J.; Windus, T. L.; Dupuis, M.; Montgomery, J. A. *J. Comput. Chem.* **1993**, *14*, 1347.

47. Schaftenaar, G.; Noordik, J. H. *J. Comp.-Aided Mol. Des*. **2000**, *14*, 123.

48. Gomez, H.; Taylor, T. R.; Neumark, D. M. *J. Chem. Phys.* **2002**, *116*, 6111.

49. Nandi, S.; Sanov, A.; Delaney, N.; Faeder, J.; Parson, R.; Lineberger, W. C. *J. Phys. Chem. A* **1998**, *102*, 8827.

50. Hutter, J.; Alavi, A.; Deutsch, T.; Bernasconi, M.; Focher, P.; Fois,E.; Goedecker, S.; Marx, D.; Tuckerman, M.; Parinello, M. et al. *CPMD* version 3.9.2; IBM Research Division, MPI Festkoerperforschung: Stuttgart, Germany, 1990-2005.

51. (a) Trouiller, N.; Martins, J. L. *Phys. Re*V. *B: Condens. Mater.***1991**, *43*, 1993. (b) Sprik, M.; Hutter, J.; Parrinello, M. *J. Chem. Phys.***1996**, *105*, 1142.

52. Martyna, G. J.; Tuckerman, M. E. *J. Chem. Phys.* **1999**, *110*, 2810.

53. Nose, S. *J. Chem. Phys*. **1984**, *81*, 511(b) Nose, S. *Mol. Phys*.**1984**, *52*, 255. (c) Hoover, W. G. *Phys. ReV. A: At., Mos., Opt. Phys.* **1985**,*31*, 1695.

54. Park, M.; Shin, I.; Singh, N. J.; Kim, K. S. *J. Phys. Chem. A* **2007**, *111*,10692.

55. Ramondo, F.; Sodeau, J. R.; Roddis, T. B.; Williams, N. A. *Phys. Chem. Chem. Phys.* **2000**, *2*, 2309.

56. Engdahl, A.; Nelander, B. *J. Chem. Phys.* **1986**, *84*, 1981.

57. Johnsson, K.; Engdahl, A.; Ouis, P.; Nelander, B. *J. Phys. Chem.* **1992**, *96*, 5778.

58. Mayer, I. *Chem. Phys. Lett.* **198**, *97*, 270.

59. Grossweiner, L. I.; Matheson, M. S. *J. Phys. Chem*. **1957**, *61*, 1089.

60. Weeks, J. L.; Rabani, J. *J. Phys. Chem.***1966**, *70*, 2100.

61. (a) Ehrler, O. T.; Neumark, D. M. *Acc. Chem. Res.* **2009**, *42*, 769. (b) Kevan, L. *Acc. Chem. Res.* **1981**, 14, 138. (c) Coe, J. V.; Lee, G. H.; Eaton, J. G.; Arnold, S. T;, Sarkas, H. W; Bowen, K. H., Ludewigt, C.; Haberland, H.; Worsnop, D. R. *J. Chem. Phys*. **1990**, *92***,** 3980.

62. (a) Weyl, W. *Pogg. Ann.* **1984**, *199*, 350. (b) Sarkas, H. W; Arnold, S. T; Eaton, J. G.; Lee, G. H.; Bowen, K. H. *J. Chem. Phys.* **2002**, *116*, 5731.

63. Schulz, C. P.; Haugstatter, R.; Tittes, H. U.; Hertel, I. V. *Phys. Rev. Lett.* **1986**, *57***,** 1703.

64. Schulz, C. P.; Haugstatter, R.; Tittes, H. U.; Hertel, I. V. *Z. Phys. D* **1988**, *10*, 279.

65. Hashimoto; K.; Morokuma, K. *J. Am. Chem. Soc.* **1994**,*116*, 11436.

66. Hashimoto; He, S.; K.; Morokuma, K. *Chem. Phys. Lett.* **1993**, *206*, 297.

67. Misaizi, F.; Tsukamoto, K.; Sanekata, M.; Fuke, K. *Chem. Phys. Lett.* **1992**, *188*, 241.

68. Schulz, C. P.; Gerber, A.; Nitsch, C.; Hertel, I. V. *Z. Phys. D* **1991**, *20*, 65.

69. Nitsch, C.; Schulz, C. P.; Gerber, A.; Zimmermann-Edling, W.; Hertel, I. V. *Z. Phys. D: At., Mol. Clustres* **1992**, *22*, 651.

70. Takasu, R.; Hashimoto, K.; Fuke, K. *Chem. Phys. Lett.* **1996**, *258*, 94.

71. Takasu, R.; Misaizu, F.; Hashimoto, K.; Fuke, K. *J. Phys. Chem A* **1997**, *101*, 3078.

72. Stenbach, C.; Buck, U. *J. Chem. Phys.* **2005**, *122*, 134301.

73. Parson, R.; Faeder, J.; Delaney, N. *J. Phys. Chem. A* **2000,** *104*, 9653.

74. Sanov, A.; Lineberger, W. C. *Phys. Chem. Comm*. **2002**, *5*, 165.

75. Papanikolas, J.M.; Vorsa, V.; Nedal, M. E.; Campagnola, P.J.; Gord, J. R.; Lineberger, W. C. *J. Chem. Phys.* **1992**, *97*, 7002.

76. Papanikolas, J.M.; Vorsa, V.; Nedal, M. E.; Campagnola, P.J.; Buchenau, H. K; Lineberger, W. C. *J. Chem. Phys*. **1993**, *99*, 8733.

77. Davis. A. V.; Wester, R.; Bragg, A. E.; Neumark, D. M. *J. Chem. Phys*. **2003**, *119*, 2020.

78. Margulis, C. J.; Coker, D. F. *J. Chem. Phys*. **1999,** *110***,** 5677.

79. Delaney, N.; Faeder, J.; Maslen, P. E.; Parson, R. *J. Phys. Chem. A* **1997,** *101*, 8147.

80. Nakajima, T.; Hirao, K. *Chem. Phys. Lett*. **1999**, *302*, 383.

81. Perera, L.; Berkowitz, M. L. **1994**, *100*, 3085.

82. (a) Pathak, A. K.; Mukherjee, T.; Maity, D. K. *J. Chem. Phys*. **2006**, *124*, 024322. (b) Pathak, A. K.; Mukherjee, T.; Maity, D. K. *J. Phys. Chem. A* **2008**, *112,* 744. (c) Pathak, A. K.; Mukherjee, T.; Maity, D. K. *J. Chem. Phys.* **2007**, *127*, 044304.

83. (a) Pathak, A. K.; Mukherjee, T.; Maity, D. K. *Chem. Phys. Lett.* **2008**, *454*, 17. (b) Pathak, A. K.; Mukherjee, T.; Maity, D. K. *ChemPhysChem* **2008**, *9*, 2259.

84. Salacuse, J. J.; Denton, A. R.; Egelstaff, P. A. *Phys. Rev. E* **1996***, 53*, 2382.

85. Lynch, G. C.; Pettitt, B. M. *Chem. Phys*. **2000,** *258*, 405.

86. Markovich, G.; Pollack, S.; Giniger, R.; Cheshnovsky, O. *J. Chem. Phys.* **1994,** *101*, 9344.

87. Delahay, P.; Dziedzic, A. *Chem. Phys. Lett*. **1986**, *128*, 372.

88. Delahay, P. *Acc. Chem. Res.* **1982,** *15*, 40.

LIST OF PUBLICATIONS

***1**. "σ/σ*and π/π* two-center three-electron bonding in complexes formed between charged thiocyanate and X radical (X=Cl, Br, I and SCN)"

A. K. Pathak, T. Mukherjee and D. K. Maity

J. Mol. Str.: THEOCHEM, 755, p. 241-245, 2005.

2. "A comparative *ab initio* study of $Br_2^{\bullet-}$ and Br_2 water clusters"

A. K. Pathak, T. Mukherjee and D. K. Maity

J. Chem. Phys. v. 124, p. 024322 (1-7), 2006.

3. "Microhydration shell structure in $Cl_2^{\bullet-}.nH_2O$ clusters: A theoretical study"

A. K. Pathak, T. Mukherjee and D. K. Maity

J. Chem. Phys. v. 125, p. 074309 (1-13), 2006.

4. "Structure, energy and IR spectra of $I_2^{\bullet-}.nH_2O$ clusters (n=1-8): A theoretical study"

A. K. Pathak, T. Mukherjee and D. K. Maity

J. Chem. Phys. v.126, p. 034301 (1-14), 2007.

5. "Theoretical studies on photoelectron and IR spectral properties of $Br_2^{\bullet-}.nH_2O$ clusters"

A. K. Pathak, T. Mukherjee and D. K. Maity

J. Chem. Phys. v.127, p. 044304 (1-8), 2007.

6. " Structure, energy and IR spectra of K-nNH_3 cluster: A theoretical study"

A. K. Pathak, T. Mukherjee and D. K. Maity

Ind. J. Phys. v. 81, p. 901-913, 2007.

7. "IR Spectra of Small Carbonate-Water Clusters, $CO_3^{-2}(H_2O)_n$: A Theoretical Study"

A. K. Pathak, T. Mukherjee and D. K. Maity

Syn. React. Inorg. MetOrg. Nano Met. Chem. v. 38, p. 76-83, 2008.

***8**. "A theoretical study on SCN^- + XH reactions (X=O, S): Hemi bonded *vs* H-bonded intermediates"

A. K. Pathak, T. Mukherjee and D. K. Maity

J. Mol. Str.THEOCHEM v. 851, p. 158-166, 2008.

9. "A microhydration study of X_2-water clusters (X=Cl, Br and I): A theoretical study on X_2. nH_2O clusters (n=1-8)"

A. K. Pathak, T. Mukherjee and D. K. Maity

J. Phys. Chem. A v. 112 p. 744-751, 2008.

10. "Microhydration of NO_3^-: A Theoretical Study on Structure, Stability and IR Spectra"

A. K. Pathak, T. Mukherjee and D. K. Maity

J. Phys. Chem. A v. 112, p. 3399-3408, 2008.

11. "Photodetacment and UV-Vis spectral properties of $Cl_2^{\bullet-}.nH_2O$ clusters: Extrapolation to bulk"

A. K. Pathak, T. Mukherjee and D. K. Maity

Chem. Phys. Lett. v. 454, p. 17-23, 2008.

12. "Theoretical Study on Spectroscopic Properties of $CO_3^{\bullet-}.nH_2O$ Clusters: Extrapolation to Bulk"

A. K. Pathak, T. Mukherjee and D. K. Maity

ChemPhysChem v. 9, p. 2259-2264, 2008.

13. "Vibrational analysis of $I_2^{\bullet-}.nCO_2$ clusters (n=1-10): A first principle study on microsolvation"

A. K. Pathak, T. Mukherjee and D. K. Maity

J. Phys. Chem A v. 112, p. 12037-12044, 2008.

14. "Vertical detachment energy of $I_2^{\bullet-}.nCO_2$ clusters (n=1-8): Experiment vs. Theory"

A. K. Pathak, T. Mukherjee and D. K. Maity

J. Chem. Phys. v. 129, p. 246101 (1-2), 2008.

15. "Distinctive IR Signature of CO3•- and CO3 2- Hydrated Clusters: A Theoretical Study"

A. K. Pathak and D. K. Maity

J. Phys. Chem A (Lett.) v. 113, p. 13443-13447, 2009.

16. "Global Minimum-Energy Structure and Spectroscopic Properties of $I_2^{\bullet-}{\cdot}nH_2O$ Clusters: A Monte Carlo Simulated Annealing Study"

A. K. Pathak, T. Mukherjee and D. K. Maity

ChemPhysChem v. 11, p. 220-228, 2010.

17. "Quantum Chemical Study on UV-vis Spectra of Microhydrated Iodine Dimer Radical Anion"

A. K. Pathak, T. Mukherjee and D. K. Maity

J. Phys. Chem A v. 114, p. 721-724, 2010.

18. "Generalized Microscopic Theory for the Detachment Energy of Solvated Negatively Charged Ions in Finite Size Clusters: A Step toward Bulk"

A. K. Pathak, A. K. Samanta, D. K. Maity, T. Mukherjee and S. K. Ghosh

J. Phys. Chem. Lett. v. 1, p. 886-890, 2010.

19. “IR spectra of $Cl_2^{\bullet-}$ hydrated clusters”

A. K. Pathak and D. K. Maity

Manuscript under preparation (2009).

* Not included in the thesis

****